Program and Abstract Book

Berlin 5 - 7 July 2023

JULIUS WOLFF INSTITUT

CHARITÉ UNIVERSITÄTSMEDIZIN BERLIN

BIH Berlin Institute of Health @Charité

Wednesday, July 5th	Thursday, July 6th	Friday, July 7th
10:00–13:00 **Registration** Coffee & Snack	8:00–10:00 **Session 3** Lumbar Spine: Shape and Kinematics	8:30–10:30 **Session 7** Spinal Loads IV: Validation / Sensitivity / Developments
	10:00–10:30 **Coffee Break**	10:30–11:30 **Session 8: Poster Session** **"Coffee to Poster"**
	10:30–12:30 **Session 4** Spinal Loads I: Effects of Load, Posture, Exoskeleton and Belt	11:30–13:15 **Session 9** Trunk Stabilization and Control / Muscle Mechanics
13:10–13:30 **Welcome**	12:30–13:30 **Lunch Break**	13:15–13:30 **Final Words**
13:30–15:15 **Session 1** Intervertebral Disc: Tissue Mechanics	13:30–15:15 **Session 5** Spinal Loads II: Novel Technologies	13:30–14:30 **Lunch**
15:15–15:45 **Coffee Break**	15:15–15:45 **Coffee Break**	
15:45–18:00 **Session 2** Motion Segments: Load Sharing	15:45–17:30 **Session 6** Spinal Loads III: Scoliosis / Pain	
18:00 **Happy Hour**	19:00 **Dinner**	

Table of Contents

Scientific Committee

Navid Arjmand
Sharif University of Technology, Tehran, Iran

Babak Bazrgari
University of Kentucky, Lexington, USA

Daniel Belavy
University of Applied Sciences, Bochum, Germany

Marwan El-Rich
Khalifa University, Abu Dhabi, UAE

Fabio Galbusera
Schulthess Klinik, Zurich, Switzerland

Idsart Kingma (Organizer)
Dept. of Human Movement Sciences Vrije Universiteit Amsterdam, The Netherlands

Jude Meakin
University of Exeter, UK

Sandra Reitmaier
Berlin Institute of Health, Charité – Universitätsmedizin Berlin, Germany

Hendrik Schmidt (Organizer)
Berlin Institute of Health, Charité – Universitätsmedizin Berlin, Germany

Saeed A. Shirazi-Adl (Organizer)
Department of Mechanical Engineering Polytechnique Montréal, Canada

Coordinator: **Friedmar Graichen**

Administration: **Barbara Schiller, Theresa Ahnert**

Location: Julius Wolff Institute, Charité – Universitätsmedizin Berlin
Institutsgebäude Süd, Föhrer Straße 15, 13353 Berlin

Contact: ws2023@spine-biomechanics.com

Welcome Note of the Congress Participants

Dear colleagues and friends,

after 3 successful meetings and an imposed pandemic intermission, we are pleased to welcome you to our **4th International Workshop on Spine Loading and Deformation** in Berlin on July 5 - 7, 2023.

It has become increasingly evident that the key to providing the most effective care for patients suffering from spinal disorders lies in cross communications and collaborations between all those working in imaging, statistics, health care, epidemiology, physiology, ergonomics, biomedical industry, and related experimental and computational environments; in other words and as elegantly phrased by the late Alf Nachemson, "by interspecialty migrations".

Our workshop brings together researchers active in different disciplines to share, discuss, and re-examine the potentials of their recent studies on the spine. The research topics cover trunk loads, postures and motions (imaging, sensors, video camera, machine learning), tissue mechanical tolerance, biological responses to mechanical load, failure and pain generation and chronicity, measurements and model studies in sports, occupational and daily living tasks, with focus on the spino-pelvic, lumbar, thoracic and cervical regions of the spine. In addition, a Virtual Special Issue in the Journal of Biomechanics has been coordinated similar to previous workshops (see: J Biomech 49 (6) (2016), J Biomech 70 (2018) and J Biomech 102 (2020)). The Virtual Special Issue (Guest Editors: I. Kingma, H. Schmidt and S. Shirazi-Adl) aims to present up-to-date progresses in spine biomechanics using state-of-the-art, existing and novel measurement and computational techniques.

We cordially welcome you all to this **4th International Workshop on Spine Loading and Deformation** and wish you again an enriching scientific meeting and a pleasant stay in Berlin.

Yours,
Hendrik Schmidt
Idsart Kingma
Saeed A. Shirazi-Adl

10:30-13:00	**Registration / Coffee & Snack**
13:10-13:30 Lecture Hall	**Welcome and Workshop Opening Remarks** Hendrik Schmidt, Saeed A. Shirazi-Adl & Idsart Kingma
13:30-15:15 Lecture Hall	**Session 1: Intervertebral Disc – Tissue Mechanics** Moderators: Judith Meakin, Nicolas Newell
13:30	The effect of enzymatic denaturation vs. excessive fatigue loading degeneration on the time-dependent responses of the intervertebral disc Mohammad Nikkhoo (Taoyuan City, Taiwan)
13:45	A model of intervertebral disc degeneration using combined cyclic overloading and enzyme digestion David Rivera Tapia (Exeter, UK)
14:00	Contribution of the nucleus pulposus to viscoelastic recovery of the intervertebral disc Kay Raftery (Guildford, UK)
14:15	Acute effects of stab lesion on mechanical properties of the L4/L5 intervertebral disc in the rat Fangxin Xiao (Amsterdam, The Netherlands)
14:30	Load informed kinematic evaluation (LIKE) protocols for the simulation of daily activities in the intervertebral disc (IVD) Daniela Lazaro Pacheco (Exeter, UK)
14:45	Open Discussion
15:15-15:45	**Coffee Break**
15:45-18:00 Lecture Hall	**Session 2: Motion Segments – Load Sharing** Moderators: Fabio Galbusera, Luigi La Barbera
15:45	Biomechanical responses of adjacent segments post lumbar fusion surgery for osteoporotic patients: the effect of cement-augmentation Kinda Khalaf (Abu Dhabi, UAE)
16:00	Numerical investigation of healing process in ovine lumbar spine after nucleotomy Maxim Bashkuev (Magdeburg, Germany)

16:15	The influence of intervertebral disc geometry on spinal motion segment stiffness: a human 9.4T MRI study Nicolas Newell (London, UK)
16:30	Decreasing spinal implant load indicates progression of posterolateral fusion when measured continuously – in vivo proof of concept in sheep Maximilian Heumann (Davos, Switzerland)
16:45	Biomechanical alterations after spinal fusion treatment and their relation to cage subsidence Siddarth Ananth Swaminathan (Berlin, Germany)
17:00	In-silico modelling of the sacroiliac joints is sensitive to ligament pre-tension Mark Heyland (Berlin, Germany)
17:15	Multilevel contribution of passive structures in the spine – a cadaveric stepwise reduction study on the torso Moritz Jokeit (Zurich, Switzerland)
17:30	Open Discussion
18:00	**Happy Hour** Beer, Pretzel, Snacks and Live Jazz Music

08:00-10:00 Lecture Hall	**Session 3: Lumbar Spine – Shape and Kinematics** Moderators: Jaap van Dieën, Hendrik Schmidt
08:00	Trunk postures of surgical staff during surgical procedures measured using inertial measurement units Idsart Kingma (Amsterdam, The Netherlands)
08:15	Investigating concurrent validity of inertial sensors to evaluate multiplanar spine movement Kristen Beange (Ottawa, Canada)
08:30	Dynamic assessment of spine movement patterns using an RGB-D camera and deep learning Ryan Graham (Ottawa, Canada)
08:45	Comprehensive assessment of global spinal sagittal alignment and related normal spinal loads in a healthy population Florian Rieger (Zurich, Switzerland)
09:00	Is the healthy range of sagittal spinal curvature optimal for biomechanical loading? A finite element study Brittany Stott (Montréal, Canada)
09:15	Effect of personalized spinal profile on biomechanical response in an EMG-assisted optimization musculoskeletal model of the trunk Christian Larivière (Montréal, Canada)
09:30	Open Discussion
10:00-10:30	**Coffee Break**
10:30-12:30 Lecture Hall	**Session 4: Spinal Loads I – Effects of Load, Posture, Exoskeleton and Belt** Moderators: Idsart Kingma, Christian Larivière
10:30	The effect of a soft active exosuit on extensor muscle forces during lifting tasks determined by musculoskeletal models Dennis Anderson (Boston, USA)
10:45	Comparison of different back-supporting exoskeletons regarding musculoskeletal loading Jasper Johns (Sankt Augustin, Germany)

11:00	Numerical investigation of intra-abdominal pressure and spinal load-sharing upon the application of an abdominal belt Emeric Bernier (Montréal, Canada)
11:15	Effect of obesity on spinal loads during load-handling activities; a subject- and kinematics-specific musculoskeletal modeling approach Mohamad Parnianpour (Tehran, Iran)
11:30	In vivo load on knee, hip, and spine during manual materials handling with two lifting techniques Philipp Damm (Berlin, Germany)
11:45	Lumbar spine loads in repetition-to-failure deadlifts, with and without body armor Vanessa Ramirez (Natick, USA)
12:00	Open Discussion
12:30-13:30	**Lunch Break**
13:30-15:15 Lecture Hall	**Session 5: Spinal Loads II – Novel Technologies** Moderators: Tim Holsgrove, Tito Basani
13:30	Integrating novel technologies for spine biomechanics: opportunities and challenges Farshid Ghezelbash (Montréal, Canada)
13:45	Estimations of spinal loads using musculoskeletal models driven by measured or neural-network predicted postures during dynamic lifting activities Navid Arjmand (Tehran, Iran)
14:00	Development of an integrated spine biomechanics framework combining in-vivo, in-silico and in-vitro methods Isabelle Ebisch (Exeter, UK)
14:15	A pipeline for automated generation of individualized musculoskeletal spine models reveals substantial differences in spinal loading depending on curvature in large patient cohorts Tanja Lerchl (Garching, Germany)
14:30	Assessment of a fully-parametric thoraco-lumbar spine model with articulated ribcage Luigi La Barbera (Milan, Italy)
14:45	Open Discussion

15:15-15:45 **Coffee Break**

15:45-17:30 **Session 6: Spinal Loads III – Scoliosis / Pain**
Lecture Hall
Moderators: Saeed Shirazi-Adl, Marwan El-Rich

15:45 Estimating trunk muscle forces in adolescent idiopathic scoliosis patients during functional activities: a personalized experimentally controlled musculoskeletal modeling approach
Stefan Schmid (Bern, Switzerland)

16:00 Asymmetry of trunk muscle activation in adolescent idiopathic scoliosis during the simulation of forward flexion by musculoskeletal modelling
Tito Bassani (Milan, Italy)

16:15 Does low back pain influence spinal loads during waking in persons with unilateral transtibial amputation?
Courtney Butowicz (Bethesda, USA)

16:30 Effect of low back pain on the biomechanical kinetics/kinematics of the lumbar spine; a combined in vivo and in silico investigation
Ali Firouzabadi (Berlin, Germany)

16:45 On lumbar loading during dynamic flexion and return to the standing posture. effect of lumbo-pelvic rhythm and the range of motion in different age and sex groups
Rizwan Arshad (Kingston, Canada)

17:00 Open Discussion

19:00 **Departure for the Social Event: Dinner**

08:30-10:30 Lecture Hall	**Session 7: Spinal Loads IV – Validation / Sensitivity / Developments** Moderators: Navid Arjmand, Denis Anderson
08:30	Accuracy of AnyBody Modeling System in predicting ground reaction forces and centers of pressure in lifting activities and effect of the prediction errors on spinal loads Marwan El-Rich (Abu Dhabi, UAE)
08:45	Comparison of the loads at L4-L5 predicted by the AnyBody and OpenSim full musculoskeletal models Fabio Galbusera (Zurich, Switzerland)
09:00	Validity of evaluating dynamic spine loads without participant-specific measured kinematics Dennis Anderson (Boston, USA)
09:15	Variation in cervical spine loads during isometric extension in a neutral posture Rizwan Arshad (Kingston, Canada)
09:30	Integrated subject-specific Finite Element Musculoskeletal Model of trunk with ergonomic and clinical applications Saeed Shirazi-Adl (Montréal, Canada)
09:45	On the use of normalisation for group-level analysis of spine loads Samuel Howarth (Toronto, Canada)
10:00	Open Discussion
10:30-11:30 Entrance Hall	**Session 8: "Coffee to Poster" – Poster Session** Moderators: Saeed Shirazi-Adl, Idsart Kingma, Hendrik Schmidt All Poster Presenters of P1 - P18
11:30-13:15 Lecture Hall	**Session 9: Trunk Stabilization and Control / Muscle Mechanics** Moderators: Mohamad Parnianpour, Farshid Ghezelbash
11:30	Comparative evaluation of different spinal stability metrics Amir Eskandari (Burnaby, Canada)
11:45	Low-back pain and associated anxiety may increase the gain but reduce the precision of feedback in control of trunk posture and movement Jaap van Dieën (Amsterdam, The Netherlands)

12:00	Can intermittent changes in muscle length delay back muscle fatigue development? Niels Brouwer (Amsterdam, The Netherlands)
12:15	Can multi-body spine models predict muscle antagonism? A methodological and validation study Alice Caimi (Zurich, Switzerland)
12:30	The assessment of paraspinal muscle epimuscular fat in participants with and without low back pain: A case-control study Maryse Fortin (Montréal, Canada)
12:45	Open Discussion
13:15-13:30	**Final Words**
13:30-14:30	**Lunch**

Abstracts Podium

The effect of enzymatic denaturation vs. excessive fatigue loading degeneration on the time-dependent responses of the intervertebral disc

Khalaf K[a], Wang J L[b], Cheng C H[c,d], Nikkhoo M[c,d]

[a]Dept. of Biomed. Eng., Khalifa Univ. and Health Eng. Innovation Center, Abu Dhabi, UAE.
[b]Institute of Biomedical Engineering, National Taiwan University, Taipei, Taiwan.
[c]School of Physical Therapy and Graduate Institute of Rehabilitation Science, College of Medicine, Chang Gung University, Taoyuan, Taiwan.
[d]Bone and Joint Research Center, Chang Gung Memorial Hospital, Linkou, Taiwan.

The hydrostatic function of the intervertebral disc (IVD) (distributing loads/storing energy/restraining excessive motion) is significantly compromised in degenerated discs [1]. Simulation of IVD degeneration is relevant towards exploring potential regenerative protocols and therapies. The two main techniques currently used are enzymatic denaturation and mechanical fatigue loading [2]. This study compared their effects on time-dependent biomechanical IVD responses using a validated FE methodology.

Forty fresh-porcine thoracic IVDs were dissected from 6-month-old-juvenile pigs and equally assigned to 5-groups (intact, denatured, low-level, medium-level, high-level fatigue loading) (Fig. 1). Upon preloading (0.1 MPa compression/10min), a sinusoid cyclic load (Peak-to-peak/0.1-to-0.8 MPa) was applied [0.01-10 Hz] using a material testing apparatus (ElectroForce®3510), and dynamic-mechanical-analyses (DMA) was performed. A validated-inverse-poroelastic FE methodology [3] and in-vitro tests were used to identify the material properties. The intradiscal pressure (IDP), total fluid loss (TFL), and axial stress were calculated.

The storage modulus increased with frequency but decreased with enzymatic denaturation and high-level-fatigue loading. The loss modulus of the denatured IVD was smaller than intact and fatigued IVDs but was not affected by the fatigue loading magnitude. Both enzymatic denaturation and fatigue loading resulted in decreased phase angles at low frequencies. Denaturation decreased the IDP and TFL but did not significantly change the axial stress. A significant decrease in IDP and TFL during fatigue loading was only observed at low frequencies (Fig 2).

Enzymatic denaturation decreases the resistive strength and shock attenuation of IVDs, most likely due to the simultaneous breakage of collagen fibers and water-proteoglycan bonds. Fatigue loading also reduces the resistive strength and shock attenuation but only at low frequencies. Increasing fatigue loading further compromises the collagen network and decreases the resistive strength. Compared to fatigue loading, enzymatic denaturation reduces the IVD's hydrostatic capabilities in resisting external loads and absorbing energy to a greater extent.

[1] Kuo et al., Spine, 2010 (35); [2] Chan et al., Spine J., 2013 (13); [3] Nikkhoo et al., J. Biomech, 2018 (70).

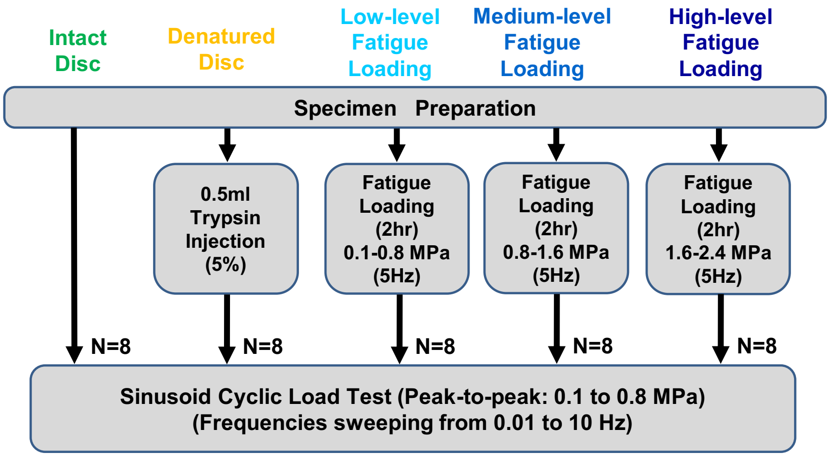

Figure 1: Procedure of the in-vitro experimental protocol for five IVD groups.

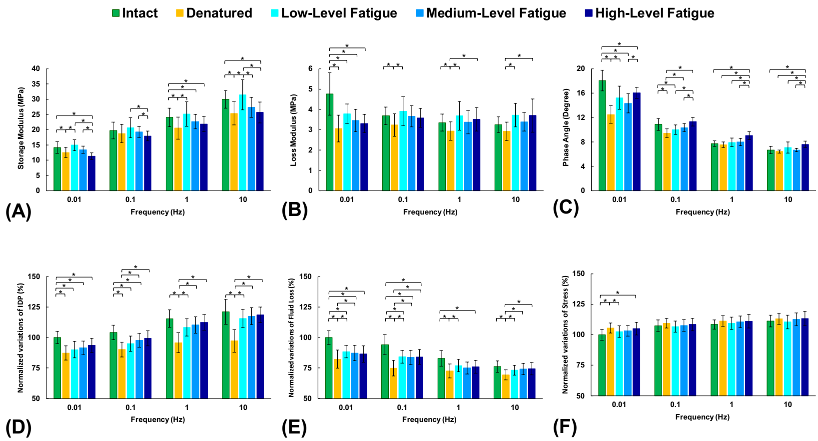

Figure 2: Measured IVD viscoelastic properties including (A) storage modulus, (B) loss modulus, and (C) phase angle from dynamic mechanical analysis (DMA). The effect of cyclic loading frequency on the (D) intradiscal pressure, (E) total fluid loss, (F) axial stress for IVDs in different groups (the results were normalized to the average response of intact IVDs at 0.01Hz).

A model of intervertebral disc degeneration using combined cyclic overloading and enzyme digestion

Rivera Tapia, ED[a], Meakin, JR[b], Holsgrove, TP[a]

[a]*Department of Engineering, Faculty of Environment, Science and Economy, University of Exeter, Exeter, UK.*

[b]*Department of Physics and Astronomy, Faculty of Environment, Science and Economy, University of Exeter, Exeter, UK.*

Intervertebral disc (IVD) degeneration is common and has been identified as a source of low back pain [1],[2]. This study aims to design a novel in-vitro method that combines overloading and enzyme degradation of the extracellular matrix to replicate clinically relevant characteristics of IVD degeneration.

Bovine tail specimens were allocated into groups (n=6 for each group): control; overload; overload+immersion in trypsin (hybrid); unloaded+trypsin injection; and unloaded+trypsin immersion. The control loading comprised equilibration followed by 8 loading/recovery periods in a 2-hour (sinusoidal loading):1-hour (static recovery) ratio. The overload and hybrid groups included hyperphysiological loading in the 4th period (Figure 1); at this time, trypsin was introduced into the test chamber (hybrid). Unloaded groups were immersed in saline for 11 hours; then trypsin was introduced via injection or immersion. Disc height and compressive stiffness were measured in loaded groups, and polarised light microscopy assessed microstructural disruption in all groups.

Overload and hybrid groups exhibited a significantly greater disc height loss than the control group (Figure 1), but there was no lasting difference in stiffness, corresponding to clinical cases of mild and moderate degeneration [3],[4]. Unloaded groups showed significantly greater microstructural disruption than control, overload, and hybrid groups, but there was no difference between them. The study resulted in three key findings: i) in unloaded groups, immersion in trypsin caused similar damage to injection; ii) the hybrid group did not have the damage observed in the unloaded+immersion group, suggesting that loading reduced the effect of trypsin; iii) trypsin in the unloaded groups led to cavities in the nucleus pulposus, which is not a common characteristic of IVD degeneration.

The hybrid model has excellent potential for future research, as increased cycles and/or higher trypsin exposure may provide a tuneable model of IVD degeneration for evaluating treatments using IVDs that reflect the target patient population.

[1] G. Livshits et al., Ann. Rheum. Dis., vol. 70, no. 10, pp. 1740–5, Oct. 2011, doi: 10.1136/ard.2010.137836.

[2] J. P. G. Urban and J. C. T. Fairbank, J. Biomech., vol. 102, p. 109573, Mar. 2020, doi: 10.1016/j.jbiomech.2019.109573.

[3] E. D. Rivera Tapia, J. R. Meakin, and T. P. Holsgrove, J. Biomech., vol. 142, no. August, p. 111260, Sep. 2022, doi: 10.1016/j.jbiomech.2022.111260.

[4] J. P. Thompson, R. H. Pearce, M. T. Schechter, M. E. Adams, I. K. Y. Tsang, and P. B. Bishop, Spine (Phila. Pa. 1976)., vol. 15, no. 5, pp. 411–415, May 1990, doi: 10.1097/00007632-199005000-00012.

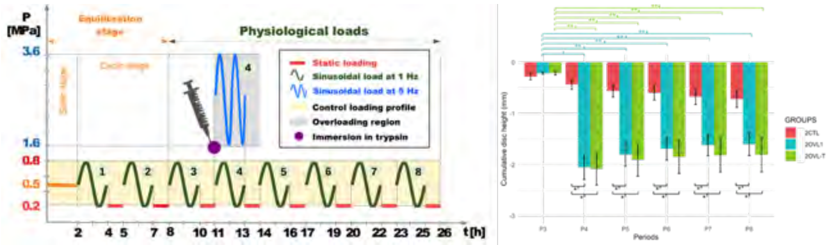

Figure 1: Loading profile of the control (2CTL), overload (2OVL1) and overload+trypsin (2OVL-T) groups (left) and resulting cumulative disc height (right).

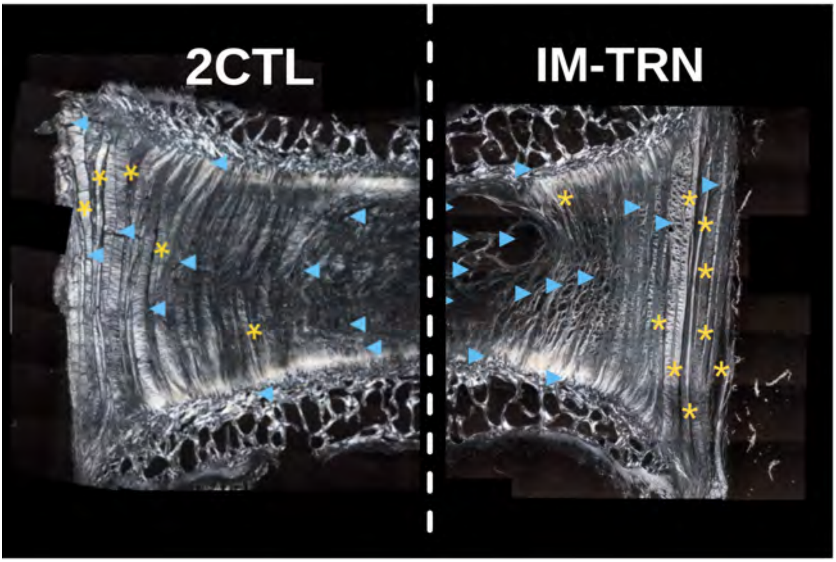

Figure 2: Imaging characterisation by polarised light microscopy of the control (2CTL) and immersed in trypsin (IM-TRN) groups showing greater disruption to the disc structure in the IM-TRN group, including large cavities in the nucleus pulposus. * Highlights delamination, ▸ highlights tears and ⧫ highlights distortions.

Contribution of the nucleus pulposus to viscoelastic recovery of the intervertebral disc

Raftery K[a], Rahman T[a,b], Newell N[a]

[a]*Department of Bioengineering, Imperial College London, UK*

[b]*Biomechanics group, Department of Mechanical Engineering, Imperial College London, UK*

Nucleus replacement devices (NRDs) have potential to treat degenerated or herniated intervertebral discs (IVDs). However, IVD height loss is a post-treatment complication [1,2]. IVD height recovery involves the nucleus pulposus [3], but the mechanism of this in response to physiological loads is not fully elucidated.

To characterise non-linear recovery behaviour of intact, nucleotomised, and NRD-treated bovine IVDs, under three physiological loading protocols.

36 bovine tail IVDs (12 intact, 12 nucleotomised, 12 NRD) and nine unconfined NRD samples underwent creep-recovery protocols simulating 1 hour of Sitting, Walking or Running, followed by 12 hours of recovery. A rheological model decoupled the fluid-independent (elastic, fast) and fluid-dependent (slow) recovery phases (Fig.1). In nucleotomised and NRD groups, nucleotomy efficiency (ratio of NP removed to remaining NP) was quantified following post-test sectioning.

Relative to intact, nucleotomised recovery at 12 hours decreased in Walking (-31.39%, $P<0.001$), but there was no significant change in Running (+4.72%) (Fig.2). In all protocols, changes to recovery significantly correlated with changes to the slow response ($P<0.0001$, $\rho=0.84$). In nucleotomised discs, the fast and slow responses negatively correlated with nucleotomy efficiency ($P<0.05$). In NRD-treated discs, recovery at 12 hours and the slow response were significantly lower relative to intact ($P<0.05$) (Fig.2). Non-linear recovery was not observed for unconfined NRDs.

The NP mainly facilitates slow-phase recovery, which is linearly dependent on the amount of NP material present. Nucleotomy may need to surpass a threshold to prevent redistribution of remaining NP and thus, restoration of recovery behaviour. Failure of this NRD to recover is attributed to poor fluid imbibition, and unconfined NRD performance cannot be extrapolated to the in vitro response. This knowledge informs both NRD design criteria to provide high osmotic pressure, and their testing standards, which may require confinement and incorporate a long-term recovery period.

[1] Berlemann U and Schwarzenbach O. An injectable nucleus replacement as an adjunct to microdiscectomy: 2-year follow-up in a pilot clinical study. Eur Spine J. 2009;18(11):1706–12. DOI: 10.1007/s00586-009-1136-0
[2] Zhang Z, Zhao L, Qu D, et al. Artificial nucleus replacement: surgical and clinical experience. Orthop. Surg. 2009;1(1):57-7. DOI: https://doi.org/10.1111/j.1757-7861.2008.00010.x
[3] Emanuel K, van der Veen A, Rustenburg C, et al. Osmosis and viscoelasticity both contribute to time-dependent behaviour of the intervertebral disc under compressive load: A caprine in vitro study. J Biomech. 2018; 70:10-5. DOI: 10.1016/j.jbiomech.2017.10.010

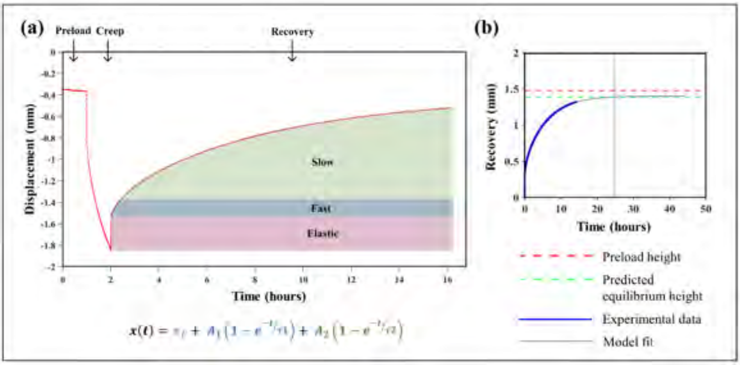

Figure 1: (A) Experimental data from one specimen (Sitting protocol). 0mm represents displacement at initial contact with the actuator. Pink, blue and green regions denote approximations of the elastic, fast and slow responses, with respect to the rheological model (equation 1). x(t) denotes recovery displacement, xE the elastic displacement, A1 and A2 the fast and slow displacement constants, and τ1 and τ2 the fast and slow time constants. (B) Recovery was normalised to the height at preload. The experimental data were fit to the visco-elastic model, which predicted the equilibrium height and time (vertical black line).

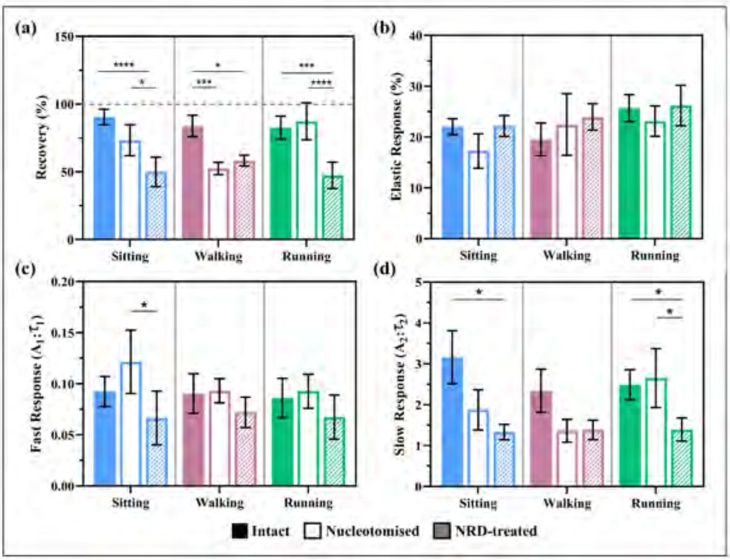

Figure 2: (A) Overall recovery at 12 hours, (B) elastic response, (C) fast response and (D) slow response between intact, nucleotomised, and NRD-treated groups. 100% recovery (dashed line) indicates a complete restoration of the height prior to loading. The fast and slow responses were defined as a function of the displacement and time constant ratio (represented as A:τ). * P < 0.05, *** P < 0.001, **** P < 0.0001.

Acute effects of stab lesion on mechanical properties of the L4/L5 intervertebral disc in the rat

Xiao F[a,b], van Dieën J[a], Han J[c,d], Maas H[a]

[a]*Department of Human Movement Sciences, Faculty of Behavioural and Movement Sciences, Vrije Universiteit Amsterdam, Amsterdam Movement Science, The Netherlands*
[b]*School of Exercise and Health, Shanghai University of Sport, Shanghai, China*
[c]*College of Rehabilitation Sciences, Shanghai University of Medicine and Health Sciences, Shanghai, China*
[d]*Faculty of Health, Arts and Design, Swinburne Univ. of Technology, Hawthorn, VIC, Australia*

Low back pain (LBP) is one of the most common musculoskeletal problems [1]. LBP may affect motor behaviour due to mechanical changes of the spine resulting from injury or degeneration, or due to effects of nociception on neuromuscular control. The relative importance of these mechanisms, and their possible interaction, are unknown [2]. Our overall objective is to assess the effects of nociception and spine instability, and their interaction on trunk muscles activity and body movement in a rat model. As a first step, we aimed to assess the acute effects of IVD lesion on the mechanical properties of the L4/L5 IVD.

27 L4/L5 spinal segments were collected from Wistar rats (male/female=14/13, body weight 345.6 ± 85.8 gram, age 12.7 ± 0.7 weeks) within 2 hours after sacrifice, stored at -20°C. Following thawing, bending tests were performed to assess the intersegmental angle-moment characteristics. Specimens were loaded in three target directions (right bending, left bending, flexion) before and after IVD lesion.

SPM analysis indicated that in right bending, no significant changes in angle-moment relationships were found (Fig. 1A), but in left bending and flexion, significantly lower angle-moment curves were found after IVD lesion (Fig. 1B,C). Peak stiffness, peak moment, and hysteresis were significantly decreased (between 6%-11%, effect size: 0.13-0.26) after IVD lesion in all directions (Fig. 1D-F).

Stab lesion of the L4/L5 IVD in the rat caused small to moderate acute changes in IVD mechanical properties. We have previously shown the timing of the histological response of the IVD to this lesion [3], but the relationship between IVD structure and mechanical function has not yet been established. Our next step will be to evaluate the long-term effects of IVD lesion on spine mechanics and the neural control of trunk muscles.

[1] Hoy D, March L, Brooks P, et al. The global burden of low back pain: estimates from the Global Burden of Disease 2010 study. Ann Rheum Dis 2014;73(6):968-74. doi: 10.1136/annrheumdis-2013-204428 [published Online First: 2014/03/26]
[2] van Dieën J JH, Reeves NP, Kawchuk G, et al. Motor Control Changes in Low Back Pain: Divergence in Presentations and Mechanisms. J Orthop Sports Phys Ther 2019;49(6):370-79. doi: 10.2519/jospt.2019.7917 [published Online First: 2018/06/14]
[3] Maas H, Noort W, Hodges PW, et al. Effects of intervertebral disc lesion and multifidus muscle resection on the structure of the lumbar intervertebral discs and paraspinal musculature of the rat. J Biomech 2018;70:228-34. doi: 10.1016/j.jbiomech.2018.01.004 [published Online First: 2018/02/06]

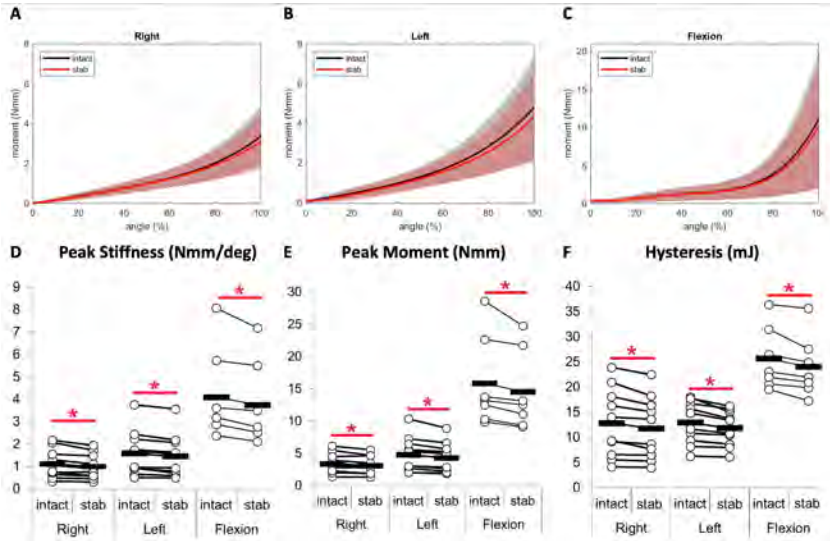

Figure 1: (First row) Comparison of angle-moment curves in (A) Right bending (B) Left bending (C) Flexion. Angle-moment curve for intact disc in black and stabbed disc in red. Moments are plotted as a function of normalized bending angle, and presented as mean with 95% confidence interval. (Second row) Mechanical properties of segments before and after IVD lesion. (D) Peak Stiffness (E) Peak Moment (F) Hysteresis. Hollow circles represent individual data of each specimen, black bars represent the mean of the group. *: $p < 0.05$, significant difference between intact and stabbed segments. (sample size: Right bending=10, Left bending=10, Flexion=7)

			mechanical parameter		
	n (m/f)		Peak Stiffness (Nmm/deg)	Peak Moment (Nmm)	Hysteresis (mJ)
Right bending	10 (5/5)	intact	1.113 (0.644)	3.370 (1.589)	12.815 (6.853)
		stab	0.988 (0.566)	3.112 (1.446)	11.814 (6.235)
	reduction (%)		11.2	7.7	7.8
Left bending	10 (5/5)	intact	1.585 (1.008)	4.787 (2.725)	12.943 (4.223)
		stab	1.455 (1.0.965)	4.318 (2.352)	11.827 (3.527)
	reduction (%)		8.2	9.8	8.6
Flexion	7 (4/3)	intact	4.095 (2.072)	15.850 (7.031)	25.652 (6.238)
		stab	3.747 (1.889)	14.541 (6.201)	24.045 (6.114)
	reduction (%)		8.5	8.3	6.3

Data are presented as mean (SD).

Table 1: Mechanical properties of IVD before and after IVD lesion

Load informed kinematic evaluation (LIKE) protocols for the simulation of daily activities in the intervertebral disc (IVD)

Lazaro Pacheco D, Holsgrove TP

Department of Engineering, Faculty of Environment, Science and Economy, University of Exeter, Exeter, UK

Current spine test standards simplify loads (e.g. ASTM F2789-10, ISO 18192), and IVD culture systems generally focus on axial compression, despite research showing that multi-axis loading effects cell viability [1]. In-vivo load data from instrumented vertebral replacements (IVBR) [2] combined with spine simulators could help understand how different activities, populations and lifestyles affect IVD health. However, the load-coupling and large range in load rates across different activities make the real-time replication of these complex loads in-vitro extremely challenging.

This study outlines the development of a Load Informed Kinematic Evaluation (LIKE) protocol for the replication of 20 unique activities to represent the average daily activity profile of a UK young adult population (25-44y) based on the Harmonised European Time Use Surveys (HETUS) [3]. A six-axis bioreactor was used to replicate Orthoload data obtained from IVBRs in a bovine IVD specimen (n=1), with loads scaled based on cross-sectional area (Figure 1). All activities were slowed down to allow for a stable load replication. The kinematics measured during load control tests were then used to replicate the activities using kinematic control at the reduced test rate, and in real-time. However, axial compression was maintained in load control across all tests to accurately simulate changes in disc height over time. The rms error (RMSE) between desired and applied loads were used to evaluate the LIKE protocol (Table 1).

Preliminary results demonstrate that the LIKE protocol provides a novel method to replicate and stably control dynamic, complex physiological loads in real-time. Further tests are being completed to include more specimens and additional daily activities to create 24h kinematic activity profiles, which cannot currently be achieved. This provides a valuable method to complete long-term assessments of IVD treatments, investigations into how different activities effect cell viability, and in providing a greater understanding of the mechanisms of disc degeneration.

[1] Chan, et al., 2013. PLoS One,8 (8), e72489.
[2] Bergmann, 2008. "OrthoLoad". Retrieved Apr. 1 2021 from http://www.OrthoLoad.com
[3] Lazaro-Pacheco, et al. In Philadelphia Spine Research Society (PSRS): Skytop, PA, 2022.

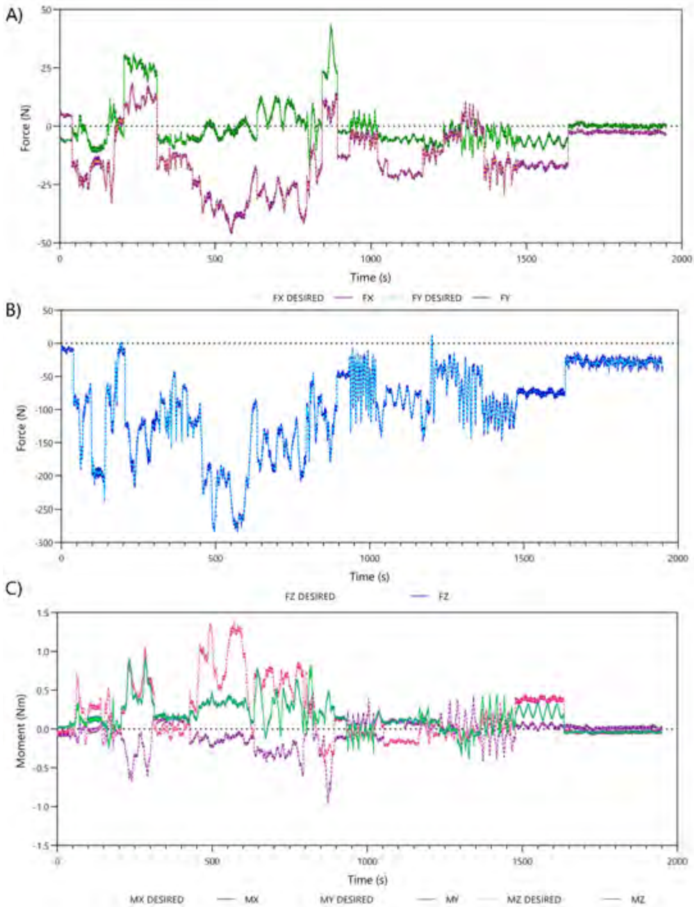

Figure 1: Example of desired and applied six-axis loads for a range of daily activities using load control for shear forces (A),axial compression (B) forces and moment (C).

Axis	Load control (slowed)	Kinematic control (slowed)	Kinematic control (real-time)
Anterioposterior shear (N)	0.47	2.51	4.51
Lateral shear (N)	0.44	4.19	7.22
Axial Compression (N)	2.21	2.45	16.12
Lateral bending (Nm)	0.01	0.22	0.59
Flexion-extension (Nm)	0.01	0.11	0.45
Axial rotation (Nm)	0.01	0.09	0.17

Table 1: RMSE between the desired load (scaled Orthoload data), and the applied load in slowed six-axis load control, slowed kinematic control, and real-time kinematic control shows that the test system is capable of applying complex loads representative of daily activities, and that these loads are also well replicated using the more stable kinematic control method.

Biomechanical responses of adjacent segments post lumbar fusion surgery for osteoporotic patients: the effect of cement-augmentation

Khalaf K[a], Nikkhoo M[b,c], Niu CC[c,d], Cheng CH[b,c]

[a]*Department of Biomedical Engineering, Khalifa University, Abu Dhabi, UAE*
[b]*School of Physical Therapy and Graduate Institute of Rehabilitation Science, College of Medicine, Chang Gung University, Taoyuan, Taiwan.*
[c]*Bone and Joint Research Center, Chang Gung Memorial Hospital, Linkou, Taiwan.*
[d]*Department of Orthopedic Surgery, Chang Gung Memorial Hospital, Linkou, Taiwan.*

While the exact pathogenesis of Adjacent-Segment-Disease (ASD) remains inconclusive, altered bone mass and microstructural degradation in osteoporotic vertebrae are considered among the key risk factors impacting surgical outcomes [1,2].This study aimed to: 1) develop a patient-specific FE-based modeling technique for extracting the mechanical properties of osteoporotic bone, and 2) investigate the effect of cement-augmented lumbar fusion, typically used to improve fusion in osteoporotic bone, on the biomechanics of adjacent levels.

A novel algorithm was developed to extract the mechanical properties based on bone mineral density (BMD) (Fig 1). Using a personalized-poroelastic-osteoligamentous FE model of the spine [3], spinal fusion was simulated at L4-L5, and the biomechanics of the adjacent levels were studied for 30 patients (normal bone (N=15), osteoporotic bone (N=15)). Models of posterior-lumbar-interbody fusion, with-and-without cement-augmentation, were developed and compared after 8h-rest (200N), following 16h-cyclic compressive loading of 500-1000N (40 and 20min, respectively). Movement in different directions (flexion/extension/lateral bending/axial rotation) was simulated using 10Nm moment before and after cyclic loading.

The validity of the extraction algorithm was confirmed by comparing the results of voxel-based and parametric models. No significant differences were observed in adjacent level biomechanics between patients with and without osteoporosis. However, the FE cement-augmented models, subject to daily-activity loading, demonstrated significant differences in disc height loss and fluid loss. The calculated axial stress and fiber strain values were also significantly higher for the cement-augmented models (Fig 2).

Our novel personalized FE-based modeling technique provides a valuable tool for noninvasive, time-and cost-effective analyses of spinal biomechanics with different underlying pathologies. This work demonstrates that osteoporosis does not significantly alter the time-dependent characteristics of adjacent IVDs post-surgery. However, cement-augmentation could increase ASD incidence. Further work is needed to analyze the association between spinal augmentation and fusion outcomes/complications towards improving the stability of the osteoporotic spine.

[1] Helgeson et al., Spine J., 2013 (13)

[2] Chen et al., Clinical Biomechanics, 2009 (24)
[3] Nikkhoo et al., J. Biomechanics, 2020 (102).

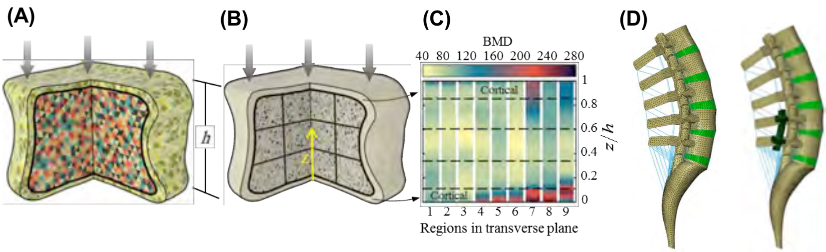

Figure 1: (A) QCT/BMD material-mapped model; (B) Parametric segmented regional model based on (C) the extracted BMD values for 9 regions in transverse plane and 3 layers through the vertebra height. (D) A sample of the pre-op and post-op parametric poroelastic osteoligamentous FE model of the lumbar spine

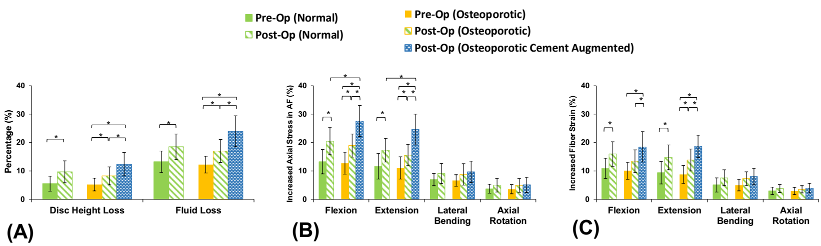

Figure 2: Comparative results of the (A) Disc height loss and fluid loss, (B) Increased axial stress in AF matrix, and (C) Increased collagen fiber strain in AF matrix for different FE model groups.

Numerical investigation of healing process in ovine lumbar spine after nucleotomy

Bashkuev M, Reitmaier S, Checa S, Schmidt H

Julius Wolff Institute, Berlin Institute of Health at Charité – Universitätsmedizin Berlin

Nucleotomy is a common treatment of disc herniations with the aim of decompression of spinal structures. Reitmaier et al. (2014) investigated the effects of surgical interventions on spinal stability in vivo and in vitro using sheep animal model and found significant stiffening of the spine in a long term. The aim of the present study was to investigate the adaptive processes that counter the manually induced instability.

A parametric finite element model of an L4–L5 ovine spinal motion segment developed previously (Bashkuev et al., 2019) was modified to replicate the surgical procedures undergone in the above in vivo study (Fig. 1a). An iterative procedure (Fig. 1b) was implemented to model the healing process. Adaptive changes in the bony structures were governed by an adaptive bone-remodeling algorithm (Huiskes et al., 1987) which regulated the rate of change in bone mineral density (BMD) depending on the strain energy density. Young's modulus of the bony elements was calculated as a cubic function of BMD. New tissue formation was modeled after the mechano-regulation theory by Claes and Heigele (1999) adapted with some modification from our previous works (Bashkuev et al., 2015; Calvo-Echenique et al., 2019). Simulations were performed using following loading conditions to simulate the average daily loads in sheep: 160 N compressive preload was applied in the first step followed by an increase of the compressive load to 220 N and application of a 2.2 Nm flexion moment with and without axial rotation.

The simulations failed to reach equilibrium state in new bone formation for pure nucleotomy, but fusion cage and nucleotomy accompanied by posterior fixation both produced bony structures of comparable stiffness. In all cases, the stiffness was higher in simulations with axial rotation – axial compressive stiffness showed an increase of approximately 20%. Bone density distribution within the vertebrae was also altered in all cases.

The results indicate that sufficient initial stability is crucial for the successful long-term stabilization of the spine which was also found in previous numerical studies. Adaptive processes within the vertebrae as well as new bone formation resulted in bone density patterns optimized for the new mechanical environment to better withstand the altered force flow. These results are in agreement with observations of Reitmaier et al. (2014) and confirm that adaptive processes are responsible for stiffening of the spinal complex.

Acknowledgement
This study is part of the Research Unit FOR 5177 (RE 4292/3-1, CH 1123/9-1)

Bashkuev, M., Checa, S., Postigo, S., Duda, G., Schmidt, H., 2015. Computational analyses of different intervertebral cages for lumbar spinal fusion. J. Biomech. 48, 3274–3282. https://doi.org/10.1016/j.jbiomech.2015.06.024

Bashkuev, M., Reitmaier, S., Schmidt, H., 2019. Is the sheep a suitable model to study the mechanical alterations of disc degeneration in humans? A probabilistic finite element model study. J. Biomech. 84, 172–182. https://doi.org/10.1016/j.jbiomech.2018.12.042

Calvo-Echenique, A., Bashkuev, M., Reitmaier, S., Pérez-del Palomar, A., Schmidt, H., 2019. Numerical simulations of bone remodelling and formation following nucleotomy. J. Biomech. 88, 138–147. https://doi.org/10.1016/j.jbiomech.2019.03.034

Claes, L.E., Heigele, C.A., 1999. Magnitudes of local stress and strain along bony surfaces predict the course and type of fracture healing. J. Biomech. 32, 255–66.

Huiskes, R., Weinans, H., Grootenboer, H.J., Dalstra, M., Fudala, B., Slooff, T.J., 1987. Adaptive bone-remodeling theory applied to prosthetic-design analysis. J. Biomech. 20, 1135–1150. https://doi.org/10.1016/0021-9290(87)90030-3

Reitmaier, S., Volkheimer, D., Berger-Roscher, N., Wilke, H.-J., Ignatius, A., 2014. Increase or decrease in stability after nucleotomy? Conflicting in vitro and in vivo results in the sheep model. J. R. Soc. Interface 11, 20140650–20140650. https://doi.org/10.1098/rsif.2014.0650

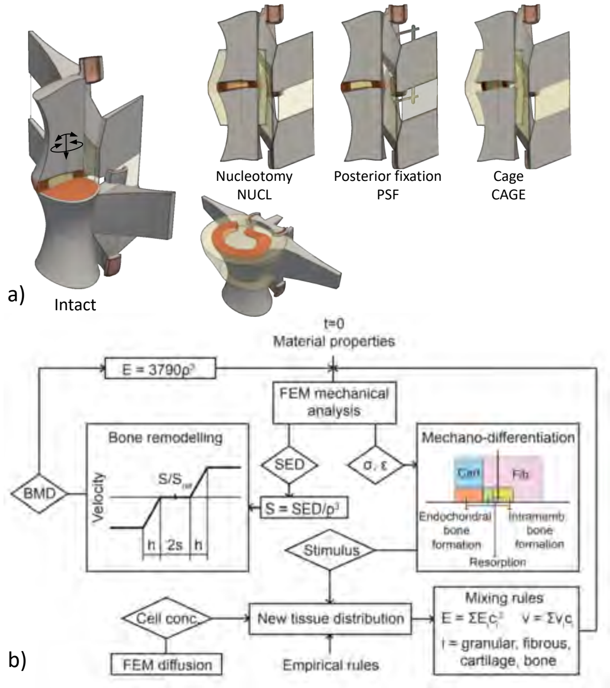

Figure 1: a) Finite element model (FEM) and simulated surgical interventions; b) Tissue healing and bone remodeling algorithm. In the diagram, BMD stands for bone mineral density, SED is strain energy density, S and Sref are actual and reference stimuli, E, v, σ and ε are Young’s modulus, Poisson’s ratio, stress and strain, respectively; ρ – bone density in an element and ci – tissue fractions.

The influence of intervertebral disc geometry on spinal motion segment stiffness: a human 9.4T MRI study

Tavana S[a,b], Shek C[a], Rahman T[a,b], Newell N[a]

[a]*Dept. Bioengineering, Imperial College London*
[b]*Dept. of Mechanical Engineering, Imperial College London*

Geometry plays an important role in the mechanics of the intervertebral disc (IVD). Previous computational studies have found a strong link between IVD geometry and stiffness [1,2]. However, few experimental studies have investigated this link, possibly due to difficulties in non-destructively quantifying internal geometric features. Recent advances in ultra-high resolution MRI provides the opportunity to visualise IVD features in unprecedented detail, giving particular insight to the nucleus-annulus boundary which was previously challenging to assess non-destructively [3]. This study seeks to quantify 3D human IVD geometries using 9.4T MRIs, and to investigate correlations between geometric variations and motion segment stiffnesses.

Thirty human lumbar motion segments (age 40.9±14.3 years) were used for this study, fourteen non-degenerate and sixteen degenerate. 9.4T MRIs were acquired from each specimen (in-plane resolution = 90 µm2, Figure 1). 1kN of compressive axial load was applied to each motion segment so that stiffness could be calculated (0.25 mm/s). Pearson's correlation was used to investigate links between stiffness and the following geometric parameters: IVD height, IVD cross-sectional area, endplate thickness, endplate concavity, nucleus-annulus mid-coronal area ratio, and nucleus-annulus boundary bulge.

IVD stiffness was negatively correlated with the disc height ($R2=0.40$, $p<0.001$) and disc cross-sectional area ($R2=0.38$, $p<0.001$, Figure 2). Positive correlations were found between stiffness and both the nucleus-annulus area ratio ($R2=0.29$, $p<0.001$) and the nucleus-annulus boundary bulge ($R2=0.22$, $p=0.03$). No significant correlation was observed between stiffness and endplate thickness or concavity.

This study advances our understanding of disc structure-function relationships and may lead to novel approaches to non-invasively quantify IVD stiffnesses without the need for mechanical tests (equation in Figure 2). For the first time, the link between the structure of the nucleus-annulus interface and the IVD response to load was investigated. The results presented here could also be used as a valuable source for the validation of computational models.

[1] Meijer, G.J.M et al, Spine 2011;36:929–935.
[2] Niemeyer, F et al, Journal of Biomechanics 2012;45:1414–1423.
[3] Matos, R, et al, Computer Methods and Programs in Biomed 2023; 230: 107337

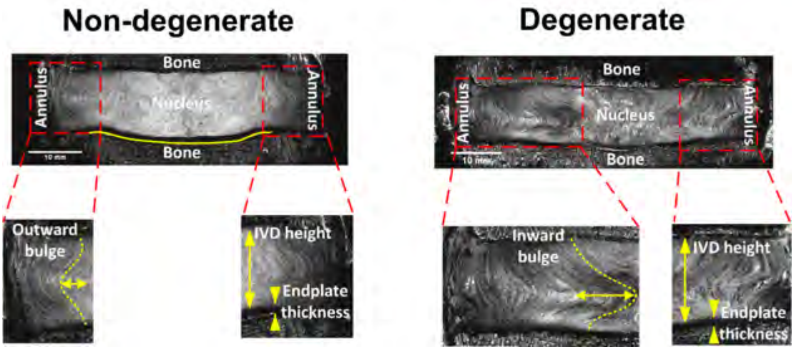

Figure 1: Mid-coronal MRI slices of typical non-degenerate (left) and degenerate (right) discs with expanded views from the annulus regions. The IVD internal structure and the lamella layers were visualised using a T2-weighted RARE sequence. The yellow dashed line identifies the nucleus-annulus boundary and the yellow solid line defines the segmented endplate curvature (concavity). The low signal intensity area between the IVD and bone represents the endplate.

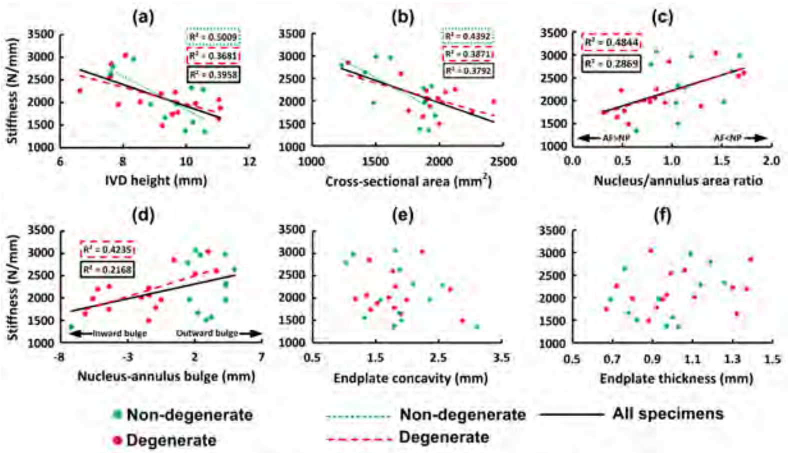

$$Stiffness = (-60)\ IH + (-0.25)\ CA + (168)\ NAAR + (16.5)\ NAB + 2997$$

Figure 2: The motion segment stiffness was linearly correlated in all specimens with the (a) IVD height ($p<0.001$), (b) IVD cross-sectional area ($p<0.001$), (c) nucleus-annulus area ratio ($p<0.001$), and (d) nucleus-annulus boundary bulge ($p=0.03$). No significant correlation ($p>0.05$) was observed between the stiffness and the (e) endplate thickness or (f) endplate concavity. The dotted green regression line indicates non-degenerate specimens, the red dashed regression line defines degenerate samples and the solid black line represents the regression line for all specimens. The negative values of the nucleus-annulus boundary bulge in (d) indicate an inward bulge of the annulus into the nucleus and the positive values define an outward bulge. The trendline (linear) equation between the stiffness and the geometric parameters is reported. In the equation reported IH represents IVD height in mm, CA represents the cross-sectional area in mm2, NAAR represents the nucleus-annulus area ratio, and NAB represents the nucleus-annulus bulge.

Decreasing spinal implant load indicates progression of posterolateral fusion when measured continuously – in vivo proof of concept in sheep

Heumann M[a,b], Benneker LM[c], Constant C[a], Ernst M[a], Richards RG[a], Wilke HJ[b], Windolf M[a]

[a]AO Research Institute Davos, Davos, Switzerland
[b]Institute of Orthopaedic Research and Biomechanics, Trauma Research Center Ulm, Ulm University, Ulm, Germany
[c]Spine Unit, Sonnenhof Spital, Bern, Switzerland

Reliable and timely assessment of bone union between vertebrae is considered one of the key challenges after spinal fusion surgery. In a single-case ovine feasibility study a novel sensor concept demonstrated the ability to objectively assess posterolateral fusion based on continuous implant load monitoring. In this follow-up study, the influence of mono-segmental fusion on the measured implant loads was systematically investigated in a larger sample size using an updated sensor system.

Three Swiss white alpine sheep underwent bilateral facetectomy at level L2-L3 and L4-L5. The segments were stabilized using two pedicle-screw-rod constructs per level. Between each pedicle screw-pair a sensing device was attached to the rod resulting in four implanted sensors per animal. Rod loads were continuously monitored over 16 weeks through wireless data transmission. After euthanasia, the spines were tested for range of motion about the three major axes of loading. A high-resolution CT scan was performed to confirm the fusion success.

After an initial increase in implant load until reaching a maximum at approximately week 4, eleven out of twelve sensors measured a constant decrease in implant load over 16 weeks to on average 52% (SD ±9%) of the maximum (Figure 1). One sensor measurement was compromised by newly forming bone growing against the sensor housing. In agreement, in vitro residual motion of all segments was less than 1°. Bridging bone at each facet as visible on CT confirmed the fusion of all motion segments.

Data obtained by continuous measurement of implant loading of spinal screw-rod constructs may enable objective and radiation-free monitoring of spinal fusion progression. However, the sensitivity along with the design of the current sensor concept needs to be tailored to and validated at the human spine.

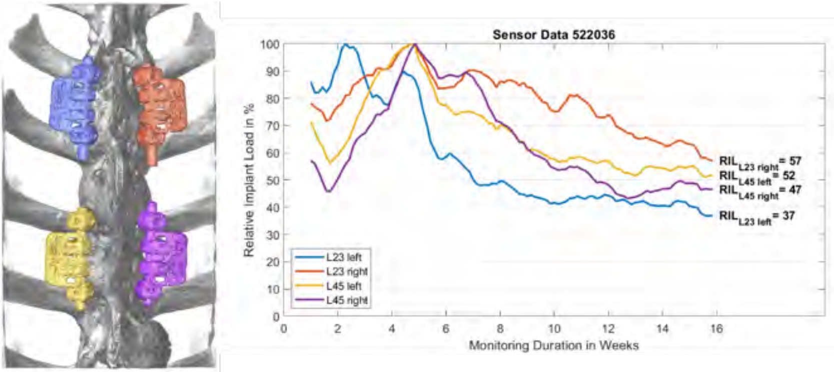

Figure 1: Reconstructed CT image of the lumbar spine of one sheep after euthanasia with related relative implant load (RIL) curves measured by each sensor during the 16-week study

Biomechanical alterations after spinal fusion treatment and their relation to cage subsidence

Ananth Swaminathan S[a], Becker L[b], Taheri N[b], Pumberger M[b], Schmidt H[a], Checa S[a]

[a]Berlin Institute of Health at Charité – Universitätsmedizin Berlin, Julius Wolff Institute, Germany

[b]Center for Musculoskeletal Surgery, Charité - Universitätsmedizin Berlin, Germany

Endplate fractures is a severe complication after spinal fusion that can lead to a risk of cage subsidence [1]. Intraoperatively, surgical damage of the endplate may occur due to different underlying patho-mechanisms [2]. The aim of this study is to investigate the biomechanics after spinal fusion and determine the correlation with the risk for cage subsidence.

A finite element model of an L1-L2 intact lumbar spine was developed from CT scans. Linear elastic properties were used for cortical shell, trabecular bone, cartilaginous endplates, callus and intervertebral cage. Hyper-elastic properties were used instead for annulus fibrosus and annulus pulposus (Fig. 1). A mechano-regulation algorithm simulating the spinal fusion process [3] was implemented to predict the bone tissue distribution after complete fusion.

Compressive strains in the adjacent vertebral bodies were different in the intact model compared to the fusion model post-surgery (Fig. 2). Lower strains in the adjacent vertebral body were predicted in the intact compared to the fusion model. In addition, compressive strains were different between the post-surgery situation and after the bone fusion had occurred. Specifically, lower strains were predicted after complete fusion (Fig. 2), although strains were still higher than in the intact case.

Preliminary results show increased strains after spinal fusion and cage implantation, which may explain the risk of cage subsidence especially in the short term. In the future, we will investigate how these biomechanical alterations relate to tissue degeneration after fusion surgery.

[1] Saville PA, et al, Eur Spine J. 2016 May;25 Suppl 1:230-8.
[2] Parisien. A et al, Int J Spine Surg. 2022 Dec;16(6):1103-1118.
[3] Postigo, S. et al., J Biomech 47, 1514–1519.

Acknowledgements
This study was funded by the German Research Foundation (Deutsche Forschungsgemeinschaft FOR 5177, CH 1123/9-1).

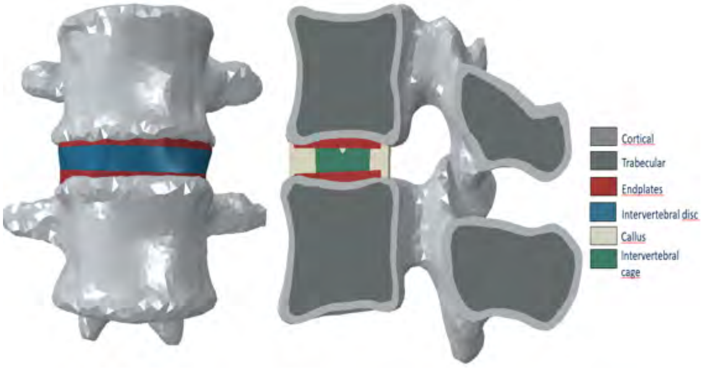

(a) (b)

Figure 1: (a) Finite element model of intact L1-L2 segment (b) Finite element model of the L1-L2 segment after surgery including a callus and an intervertebral cage.

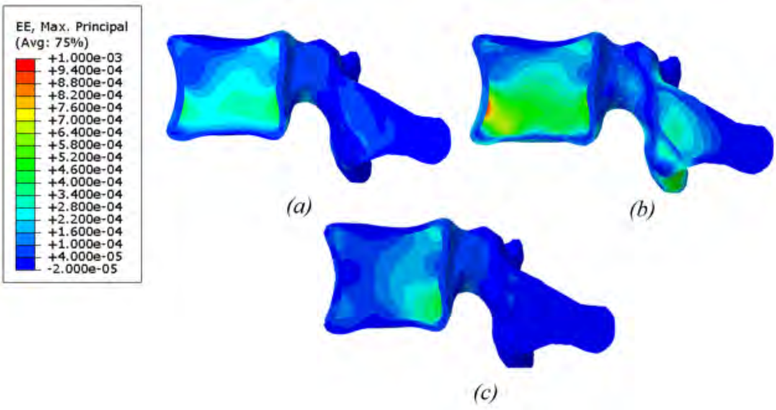

Figure 2: Principal strains (a) Intact L1 segment before surgery (b) Surgical L1 segment post-surgery (c) Surgical L1 segment at the end of the fusion process.

In-silico modelling of the sacroiliac joints is sensitive to ligament pre-tension

Heyland M[a], Maikath D[a], Damm P[a], Hermann KG[b], Ziegeler K[b]

[a]Berlin Institute of Health at Charité – Universitätsmedizin Berlin, Julius-Wolff Institute, Berlin, Germany

[b]Department of Radiology, Charité – Universitätsmedizin Berlin, Germany

Substantial preload in the sacrotuberous ligament (118N±74N; 65N in females; 172N in males [1]) or generally ligament pre-tension changes joint loading. The objective was to investigate the effect of ligament pre-tension on joint surface stress and relative motion using finite element (FE) models of the sacroiliac joints.

FE models were computed from CT scans of eight patients from a larger cohort (N=818, [2]) with known anatomical variants as well as a typical male (TMJ) and a typical female joint (TFJ). Models included information on isotropic, inhomogeneous bone elasticity (material mapping), (Fig. 1), and stiffness of ligaments/muscles (Fig. 2) from literature [3,4]. Different loading conditions and directions (singular, symmetric, and asymmetric) from in-vivo data were implemented (bipedal walking), the sacrum was pinned, and contacts were modelled as pressure-overclosure. A mesh convergence study was performed and yielded relative changes ≤9.0% in translations, ≤6.3% in rotations, ≤12.1% in von Mises stresses, for meshes with element (C3D4) numbers of 75,837, 215,058, and 609,142. Sensitivity analysis of modelling parameters was performed for TFJ with the most sensitive loading scenario (symmetric xyz).

In all load scenarios, stresses were higher in TFJ than TMJ. A loading in anteroposterior direction (y) caused highest stresses and relative mobility. Ligament pre-tension was most sensitive with mean sensitivity factor (change in output / change in input) of 71.04 for translation, 43.09 for rotation, and 2.11 for mean stress. Mean sensitivity factor of load intensity was 1.09 for translation, 0.91 for rotation, and 0.54 for mean stress. In general, relative motion was more sensitive to the parameter variations than resultant stress.

Modelling results were highly sensitive to a variation of ligament pre-tension. That indicates that the individual preloading of ligaments is crucial. However, this must be validated, and the ligament pre-tensions need to be verified in situ.

[1] Steinke, H., Kurz, S., Fischer, B., Schuberth, S., Hobusch, C., & Heyde, C. E. (2022). The sacrotuberous ligament is preloaded in situ. *Journal of the Mechanical Behavior of Biomedical Materials*, 134, 105368.

[2] Ziegeler, K., Kreutzinger, V., Diekhoff, T., Roehle, R., Poddubnyy, D., Pumberger, M., ... & Hermann, K. G. A. (2021). Impact of age, sex, and joint form on degenerative lesions of the sacroiliac joints on CT in the normal population. *Scientific Reports*, 11(1), 5903.

[3] Shi, D., Wang, F., Wang, D., Li, X., & Wang, Q. (2014). 3-D finite element analysis of the influence of synovial condition in sacroiliac joint on the load transmission in human pelvic system. *Medical engineering & physics*, 36(6), 745-753.

[4] Phillips, A. T. M., Pankaj, P., Howie, C. R., Usmani, A. S., & Simpson, A. H. R. W. (2007). Finite element modelling of the pelvis: inclusion of muscular and ligamentous boundary conditions. *Medical engineering & physics*, 29(7), 739-748.

Conflict of interest & Acknowledgements:
KZ reports funding (research grant) from the Assessment of Spondyloarthritis international Society (ASAS) as well as the Rahel Hirsch programme of the Charité Universitätsmedizin Berlin during the conduct of this study. KGH reports lecture fees from MSD, Novartis, and Pfizer as well as consulting fees from AbbVie. He is the co-founder of BerlinFlame GmbH. All other authors have no conflicts of interest to report.

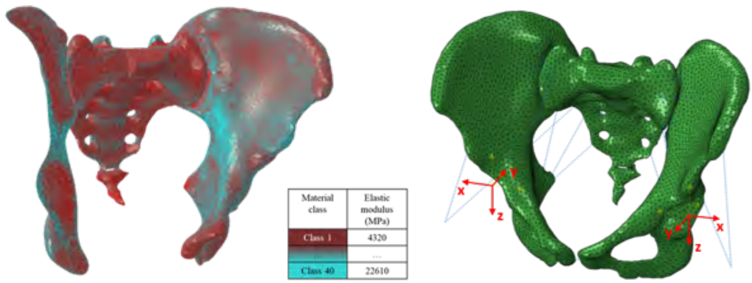

Figure 1: Example of FE-model (TFJ) with density distribution (left) and load application directions (right). Please note that the model on the left shows a cut through the right ileum! Load application directions were medio-lateral (x), antero-posterior (y), and cranial-caudal (z).

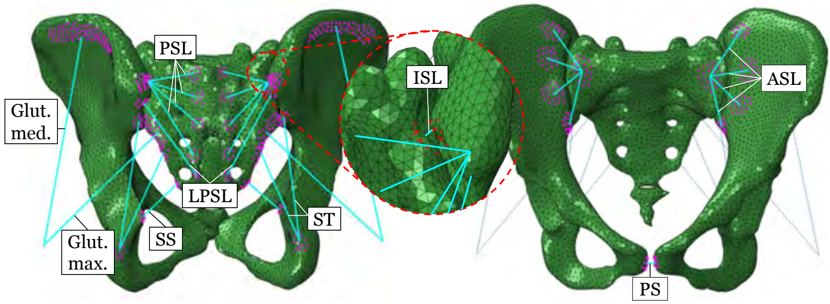

Figure 2: Example of FE-model (TFJ) with ligaments and muscles (frontal plane). left=posterior view; right=anterior view. Glut. Med.=gluteus medius muscle; Glut. Max.=gluteus maximus muscle; SS=sacrospinous ligament; PSL=posterior sacroiliac ligament; LPSL=long posterior sacroiliac ligament; ST=sacrotuberous ligament; ISL=interosseous sacroiliac ligament; ASL=anterior sacroiliac ligament; PS=pubic symphysis.

Multilevel contribution of passive structures in the spine – a cadaveric stepwise reduction study on the torso

Jokeit M[b,c], Cornaz F[a,b,c], Calek AK[a,c], Harshbarger CL[a,b,d], Snedeker JG[a,b], Farshad M[a], Widmer J[b,c]

[a]Department of Orthopedics, Balgrist University Hospital, University of Zurich, Switzerland
[b]Institute for Biomechanics, ETH Zurich, Zurich, Switzerland
[c]Spine Biomechanics, Department of Orthopedics, Balgrist University Hospital, University of Zurich, Switzerland
[d]Institute for Mechanical Systems, ETH Zurich, Zurich, Switzerland

Although many stabilizing structures act in a multi-level fashion, most studies have investigated the passive structures of the spine in isolated, single-level specimens ("functional units"). Little is known about how the upper body is stabilized on a global scale and how forces are distributed between ligaments, muscles, and fasciae.

The aim of this study was to quantify the contribution of multilevel passive structures in the load case of full flexion.

A stepwise reduction study was performed on a cadaveric torso (n=1*) using a custom-built setup with rigid 6-screw fixation of the pelvis. An external fixator at Th11, Th9, and Th7 was used to mount the torso on a mobile frame that allowed only sagittal plane motion. Preloading (dead load of trunk and frame, relaxation time: >30 min) was followed by locking of the mobile frame and gradual resection of the posterior lumbar structures in full flexion. Load cells between base and frame measured the force on the frame for each resection step: skin, latissimus dorsi muscle, serratus posterior inferior muscle, lateral abdominal muscles (obliquus internus/externus and transversus abdominis muscle), thoracolumbar fascia, sacrospinal musculature, interspinal and transversospinal musculature, spinous processes L2-L5 incl. supraspinous and interspinous ligaments, laminae L2-L5 incl. ligamentum flavum, facet joints and pedicles L2-L5, posterior longitudinal ligaments L1/2-L5/S1. The contribution of each structure was derived from the change in force.

Skin, latissimus dorsi muscle, serratus posterior inferior muscle, and lateral abdominal muscles contributed <5% to flexion resistance. Thoracolumbar fascia, sacrospinal musculature, interspinal/transversospinal musculature shared 9%, 15%, and 9% of loading, respectively. The spinal processes with SSL & ISL contributed 41% to passive loading resistance. The laminae incl. LF withstood 7%, and facet joints/pedicles sustained 11% of loading. PLLs showed no contribution.

The posterior ligamentous complex (SSL, ISL) plays an important role in full flexion and may have been underestimated in studies investigating “functional units”.

* Experiments are ongoing, and the number of specimens tested will increase from n=1 to n=3.

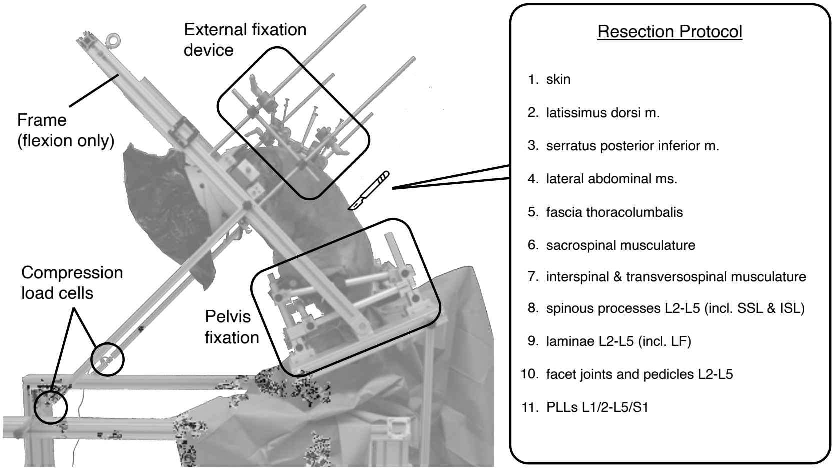

Figure 1: Photo of custom-built setup with external fixation device, pelvis fixation, mobile frame (flexion only), and load cells integrated in rods supporting the frame.

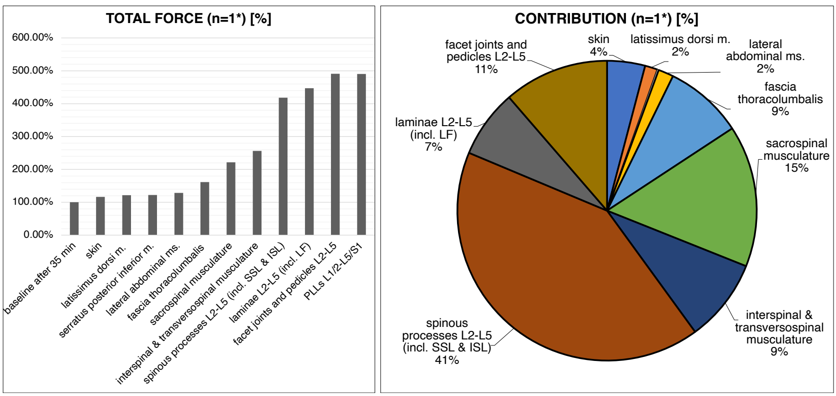

Figure 2: Force measured in compression load cells relative to baseline after 35 min relaxation time (left). Individual contributions of passive structures derived from load increments between resection steps (right).

Trunk postures of surgical staff during surgical procedures measured using inertial measurement units

Brouwer NP[a], Kingma I[a], van Dijk W[b], van Dieën JH[a]

[a]*Department of Human Movement Sciences, Vrije Universiteit Amsterdam, the Netherlands*
[b]*TNO, Leiden, the Netherlands*

Excessive cumulative low-back load, for instance due to prolonged static bending, is considered an important risk factor for low back pain (LBP) [1]. In surgical staff, LBP is prevalent [2] and prolonged static bending is hypothesized to be one of its potential causes [3]. Inertial measurement units (IMUs) allow for motion capture outside the laboratory [4] and may therefore provide insight into postures of surgical staff. The aim of this study was to evaluate the magnitude and duration of trunk postures of surgical staff during surgical procedures.

The trunk segment orientation (i.e., indicating low back load due to upper body weight) of 45 surgical assistants and two surgeons (n=47) was measured during surgical procedures. Per participant, Exposure Variation Analysis [5] was used to evaluate the percentage of the total time of trunk flexion/extension (<-10°; -10-10°; 10-20°; 20-30°; >30°) taking into account posture duration (<10s; 10-60s; 60-300s; >300s). Participants reported their LBP history and perceived low back load during the procedure via a questionnaire.

On average, the procedure duration was 72 minutes (range: 16-392 min) and participants were in an approximately upright posture (i.e., sum of -10-10°; fig. 1) for 77.2% of the total time. Trunk flexion was mostly limited (10-20°) and brief (<10s; fig. 1). Questionnaire response rate was 93.6%. Respondents reported that the measured procedure was representative for an average procedure. A short-lasting (directly after average workday) or long-lasting (frequent or consistent pain) history of LBP was reported by 80% and 47.7%, respectively. History of LBP and perceived low back load during the procedure were not correlated to total trunk flexion (>10°) exposure (percentage or seconds).

Prolonged standing rather than prolonged static bending may explain the high prevalence of LBP among surgical staff [6]. Alternatively, forces exerted during the surgical procedure, or high low back loads during other activities than the procedure itself [7] may contribute. The full study will include up to 100 participants.

[1] Coenen et al. (2013) J Occup. Rehabil.;
[2] Janki et al. (2017) Surg. Endosc.;
[3] Engels et al. (1996) Occup. Env. Med.;
[4] Brouwer et al. (2020) Scand J Sports Sci;
[5] Mathiassen et al. (1991) Ergonomics;
[6] Coenen et al. (2018) Br. J Sports Med.;
[7] Coenen et al. (2014) Occup. Env. Med.

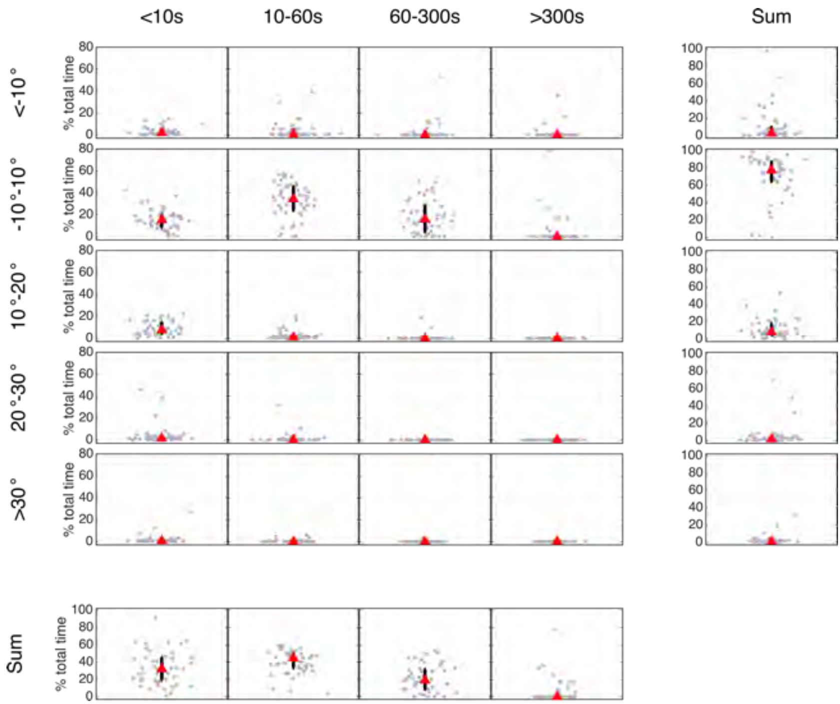

Figure 1: Trunk angle Exposure Variation Analysis during surgery work with trunk flexion/extension angle on the rows and duration of the posture in the columns. The last column and row provide the sum over the corresponding row and column, respectively. Per subplot, the vertical axis depicts the percentage of the total time of the measured procedure. Individual participants are depicted using grey dots at a random position along the horizontal axis. The median and interquartile range are depicted as a red triangle and black line, respectively.

Investigating concurrent validity of inertial sensors to evaluate multiplanar spine movement

Beange KHE[ab], Chan ADC[abc], Graham RB[bc]

[a] *Department of Systems and Computer Engineering, Carleton University, Ottawa, Canada*
[b] *Ottawa-Carleton Institute for Biomedical Engineering, Ottawa, Canada*
[c] *School of Human Kinetics, University of Ottawa, Ottawa, Canada*

There is growing evidence to suggest that objective assessments of spine motion in clinical settings may improve diagnosis and treatment of low back pain; however, gold-standard marker-based optical motion capture systems are expensive, confined to a laboratory space, and require specific expertise to effectively utilize. Inertial measurement units (IMUs) offer a portable and inexpensive alternative, and have potential to support clinical diagnosis and decision-making; however, due to a lack of confidence regarding the validity of IMU-derived metrics, their uptake and acceptance remain a challenge. Previous work confirmed the concurrent validity of IMUs to track uniplanar (i.e., spine flexion) movement; however, evaluation of multiplanar motion tracking was suggested to provide a more comprehensive evaluation of validity.

Ten healthy controls were recruited to perform spine forward flexion, and bilateral lateral bending, axial rotation, and circumduction. Data were simultaneously collected from optical motion capture equipment (Vicon, Oxford, UK) and 3 IMUs (Xsens DOT; Xsens, Enschede, NED) using custom 3D-printed holders placed superficial to C7, T12, and S1 vertebrae. Root mean squared error (RMSE) was calculated for continuous movement, and mean absolute error (MAE) for range of motion (ROM) estimates was compared separately for each movement in sagittal, frontal, and transverse planes.

Overall RMSE=1.33° and MAE=0.74°±0.69 across all movements, sensors, and planes (Figure 1). Results were similar for primary- and off-axis ROM during uniplanar movements (MAEprimary=0.56°±0.49; MAEnon-primary=0.82°±0.82).

IMUs can be considered valid to track multiplanar spine movement and measure spine ROM, and have enabled efficient (i.e., 20 minute) data collections to occur in-clinic. This makes participation in research studies more accessible for patients and families, and provides a foundation for potential large-scale multi-site research studies in the future. Future directions will involve mitigation of error by customizing sensor fusion based on individual sensor specifications, signal quality, and experimental conditions.

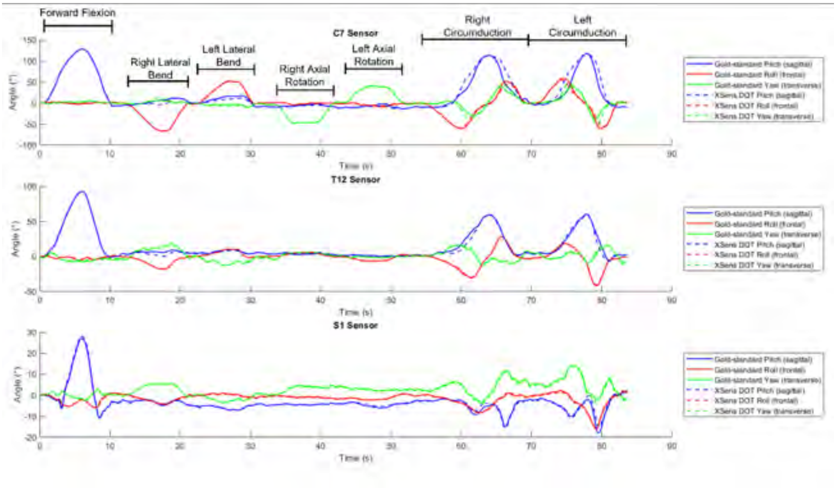

Figure 1: Angular range of motion data from IMUs (dashed) and gold-standard optical motion capture equipment (solid) from one participant during spine forward flexion, and bilateral spine lateral bending, axial rotation, and circumduction.

Dynamic assessment of spine movement patterns using an RGB-D camera and deep learning

Wenghofer J[a], Beange KHE[bc], Ramos WC Jr.[a], Graham RB[ac]

[a]*School of Human Kinetics, University of Ottawa, Ottawa, Canada*

[b]*Department of Systems and Computer Engineering, Carleton University, Ottawa, Canada*

[c]*Ottawa-Carleton Institute for Biomedical Engineering, Ottawa, Canada*

Accurate assessment of spine kinematics is critical for both research and clinical assessment of spine dysfunction. The current gold-standard for assessing spine kinematics is optical motion capture, which involves expensive hardware, placement of retroreflective markers and time-intensive post-processing. Therefore, time- and cost-effective techniques are needed. The purpose of this study was to develop and validate a markerless motion capture system that uses an RGB-D camera and deep learning to calculate kinematics of the lumbar spine.

A two-phase approach was used. In the first phase, fifteen healthy male participants were recruited to develop and train a convolutional neural network (CNN). Participants performed cyclic forward bending and the CNN used the depth data stream from an RGB-D camera to segment the regions of the back's surface into upper and lower spine masks. A first-degree polynomial surface was fit over these masks and the pixel positions were used to define three-dimensional coordinate systems, allowing relative spine movement to be calculated in all planes of movement. The second phase involved validation of the markerless motion capture system against a gold-standard optical motion capture system (Vicon, Oxford, UK). For this phase, 6 healthy male participants were recruited. In a randomized order, participants performed cyclic forward bending both without markers and with retroreflective marker clusters placed in regions congruent with the spine masks. Between system agreement was compared by calculating the root mean square error (RMSE) and the intraclass correlation coefficients (ICCs) of the ensemble averaged curves of five continuous bending cycles.

Low RMSE (0.962- 3.938°) and strong ICCs (0.862-0.983) were found between each method.

These results demonstrate the feasibility of using an RGB-D camera to assess spine kinematics which could have clinical utility in detecting spine dysfunction. Next steps will involve further training and testing of the CNN during multiplanar movements.

Comprehensive assessment of global spinal sagittal alignment and related normal spinal loads in a healthy population

Rieger F[a], Rothenfluh D[b], Ferguson SJ[a], Ignasiak D[a]

[a]*Institute for Biomechanics, ETH Zurich, Zurich, Switzerland*
[b]*Centre de chirurgie spinale, CHUV Lausanne, Lausanne, Switzerland*

Abnormal postoperative global sagittal alignment (GSA) is related to an increased risk of mechanical complications and high revision rates after spinal surgery [1]. Typical clinical assessment of sagittal alignment relies on few selected measures, thus disregarding global complexity and variability of the sagittal curvature. The normative range of physiological spinal loads due to individual GSA has not been yet considered in clinical evaluation. Therefore, the study objectives are to develop a new GSA assessment method that holistically describes the inherent relationships within GSA and to estimate the biomechanical implications on spinal loads.

Vertebral endplates were annotated on full-standing radiographs of 85 non-pathological subjects (age: 45.3 ± 17.4; male:female = 0.57). A Principal Component Analysis (PCA) was performed to derive a Statistical Shape Model (SSM) of GSA variability. Furthermore, associations between identified variability modes and conventional alignment measures were assessed. Simulations of respective Shape Modes (SM) were performed using an established musculoskeletal AnyBody model to estimate normal variation in cervico-thoraco-lumbar compression and shear loads [2].

The first six principal components were found to explain 97.96% of GSA variance. The established SSM provided the normative range of GSA in a healthy population and a visual representation of the main variability modes. The normal variation in identified alignment features was found to influence spinal loads (see Fig. 1), e.g. SM2-2 ± deviation from the population mean shape corresponded to an increase in L4L5-compression by 378.64N (67.86%).

Six unique alignment features were found sufficient to describe GSA almost entirely, demonstrating the value of the proposed method based on PCA and SSM for an objective and comprehensive analysis of GSA. The influence of these features on spinal loads provides a normative reference for the biomechanical assessment of pathological alignment, hence guiding surgical planning of deformity correction in the future.

[1] T. J. Bari et al. Spine Deform, 8(5), 1027–1037, 2020, doi: 10.1007/s43390-020-00112-6
[2] D. Ignasiak et al. J Biomech, 49(6), 959–966, 2016, doi: 10.1016/j.jbiomech.2015.10.010

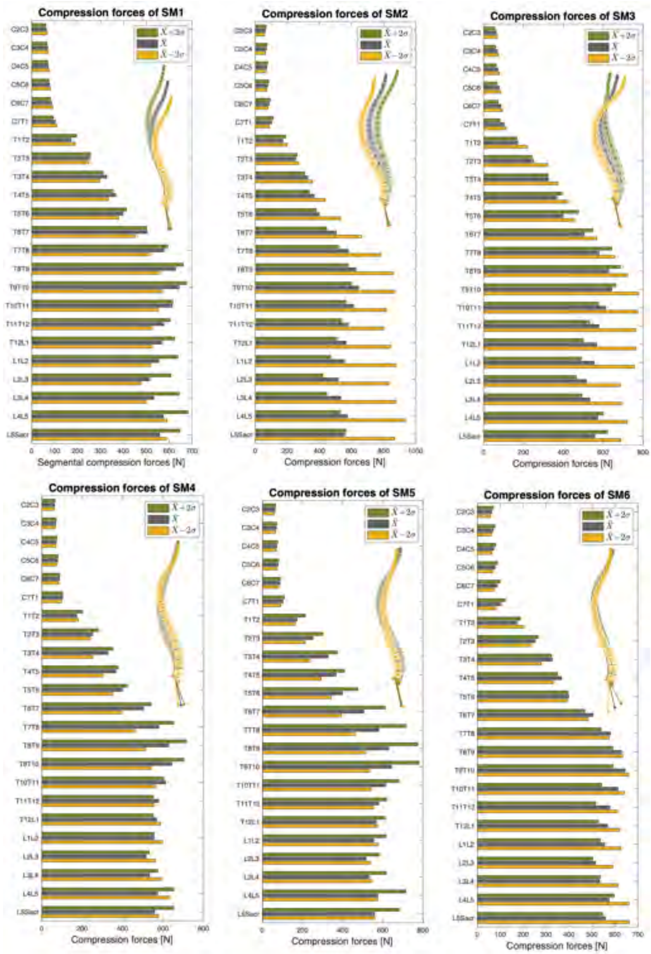

Figure 1: Cervico-thoraco-lumbar compression forces estimated for statistical shape modes SM1-6 assuming a body weight of 75kg. Visual depiction of the normative range of related GSA features is provided in the upper right corner of each graph. SM1: (major share of GSA variance, 48.24%) is related to trunk height and antero-posterior shift of thoracic apex. Higher trunk and more posterior thoracic apex are related to elevated thoraco-lumbar loads. SM2: (30.43% of variance) can be interpreted as an anterior-posterior spinal tilt, thus relates to Sagittal Vertical Axis (SVA). Unexpectedly, more anterior tilt is not related to higher loads, probably because it represents normal bounds of SVA (47.3mm). SM3: (14.49% of variance) depicts changes in global Thoracic Kyphosis (TK) and lower T5-T12 TK, as well as Sacral Slope (SS) and Pelvis Incidence (PI). Long and pronounced kyphosis is related to higher thoracic and lumbar loads. SM4: (1.93% of variance) represents the differences in the length of the lordosis and kyphosis arcs. SM5: (1.6% of variance) encodes a finer scaling of Lumbar Lordosis (LL) and L1-L4 lordosis. Both SM4 and SM5 are mainly related to differences in the loading of middle thoracic segments. SM6: (1.26% of variance) is related to a femoral-sacral alignment variability, hence differences in Global Tilt (GT), PI-LL mismatch and Pelvis Tilt (PT), while affecting loads of the lumbar segments.

Is the healthy range of sagittal spinal curvature optimal for biomechanical loading? A finite element study

Stott B[a,b], Driscoll M[a,b]

[a]*Musculoskeletal Biomechanics Research Lab, Department of Mechanical Engineering, McGill University, Montreal, Quebec, Canada*

[b]*Orthopaedic Research Laboratory, Research Institute MUHC, Montreal General Hospital, Montreal, Quebec, Canada*

Variations in the spine's curvature impact its biomechanical performance. While there is a commonly accepted range for normal spinal curvature, deviations from this range may lead to various spinal conditions and back pain. However, an individual's spinal alignment is unique, resulting in a combination of thoracic and lumbar angles that may provide one's ideal stability and support. This study evaluated the effects that geometric thoracic or lordotic curvature variation have on biomechanical loading.

A thoracolumbar spine finite element model with normal (Healthy) curvature was developed, consisting of the vertebrae, intervertebral discs (IVDs), and spinal muscles from T1-S1. The sagittal profile was varied by 50%, creating four additional models: hypolordotic (HypoL), hyperlordotic (HyperL), hypokyphotic (HypoK), and hyperkyphotic (HyperK) (Table 1, Figure 1). Flexion and extension were simulated for each model. Following validation, IVD and vertebral body (VB) stresses, disc height, and intersegmental rotation were compared across models.

The HyperL and HyperK models exhibited greater disc compression (38%) and VB stresses (12%) compared to the Healthy model. The HypoL and HypoK models demonstrated lower disc compression (-30%) but also showed augmented VB stresses (2%), though notably reduced compared to the hyper-curved models. The Healthy thoracolumbar spine model had the greatest range of motion, measured through intersegmental rotation.

Variation in sagittal alignment resulted in noticeable changes in stress distribution throughout the spine in the present study. Geometrically, the Healthy sagittal profile provided optimal spinal support. The straighter spine models exhibited reduced VB stresses and less compressed discs, indicating a potential mechanism for protecting the spinal column from excessive loads and disc compressions. The hyper-curved spine models displayed inverse trends, demonstrating augmented stresses and disc compressions. The results may provide insight into how variations in sagittal alignment affect biomechanical loading during flexion-extension and consequently influence the development of spinal disorders.

	Kyphosis	Lordosis
Hypo	11.57°	23.46°
Normal	**23.69°**	**44.24°**
Hyper	34.98°	64.29°

Table 1: Cobb angle measurements for the thoracolumbar finite element models

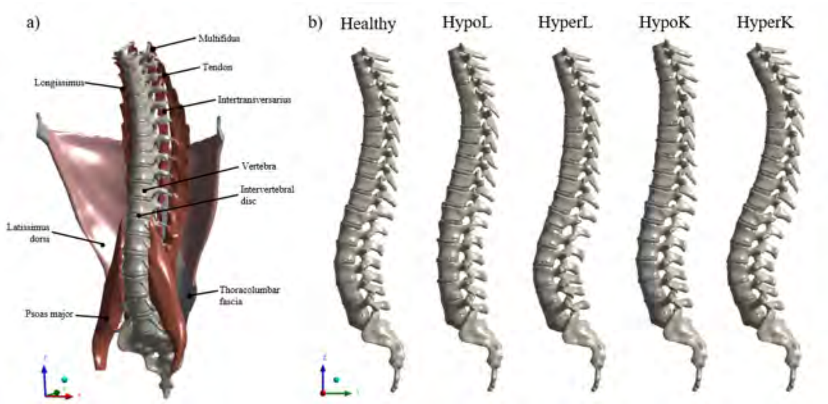

Figure 1: a) Complete thoracolumbar spine model, and b) varying sagittal profiles for each model.

Effect of personalized spinal profile on biomechanical response in an EMG-assisted optimization musculoskeletal model of the trunk

Larivière C[a,b], Eskandari AH[a,b], Mecheri H[a,b], Ghezelbash F[c], Gagnon D[d], Shirazi-Adl A[c]

[a]*Institut de recherche Robert-Sauvé en santé et en sécurité du travail (IRSST), Montreal, Quebec, Canada.*

[b]*Center for Interdisciplinary Research in Rehabilitation of Greater Montreal (CRIR), Montreal, Quebec, Canada*

[c]*Division of Applied Mechanics, Department of Mechanical Engineering, Polytechnique Montréal, Canada*

[d]*Department of Physical Activity Sciences, University of Sherbrooke, Canada*

Recent developments in musculoskeletal (MS) modeling have been geared toward customization. Personalization of the spine profile could markedly affect estimates of spinal loading and stability, particularly in the upright standing posture where large inter-subject variations in the lumbar lordosis have been reported. This study aims to investigate the biomechanical consequences of changes in the spinal profile.

In 31 participants, (1) the spine external profile was first recorded (Figure 1A), followed by (2) submaximal contractions in a dynamometer (calibration of the MS model) and (3) isometric upright standing lifting tasks challenging spine stability while altering load position and magnitude (Figure 1B). EMG signals of 12 trunk muscles and angular kinematics of 17 segments were recorded. For each participant, our MS model [1] was considered using either a generic [2] or a personalized [3] spinal profile (Figure 1C) and 18 biomechanical outcomes were computed and compared.

Regarding the load position, results presented (see Table) list the effect of load height only (P1 vs P2 vs P3) and not load distance (P2 vs P4). According to the 36 ANOVAs and effect sizes, personalizing the spine profile frequently induced similar effects across all lifting tasks. Moderate and strong effect sizes were observed for abdominal (increase) and back (decrease) muscle forces, whereas small effect sizes were seen for spine loading (decrease of compression and shear at L4/L5 and L5/S1) and stability outcomes. According to effect sizes and percent changes (Table), larger changes were estimated in more superficial muscles.

Personalizing the spine profile induced statistically significant ($p < 0.05$) changes that were also of biomechanical relevance according to the corresponding effect sizes.

[1] Eskandari et al., J Electromyogr. Kinesiol., 2023: 68: 102728.
[2] Ghezelbash et al., Biomech Model Mechanobiol, 2016: 15: 1699-1712.
[3] Nerot et al., J Biomech 2018: 70: 96-101.

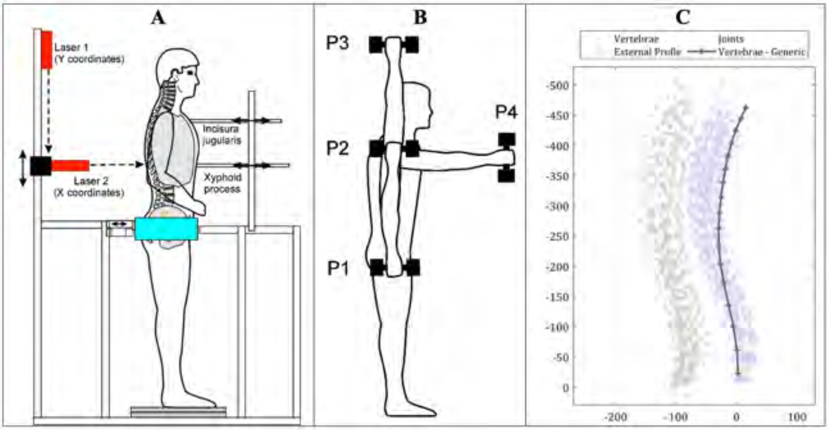

Figure 1: A) Apparatus to measure the spine external profile (S3 to C7 spinous processes) and other trunk landmarks using two laser rulers. B) Illustration of the isometric lifting task with loads in different positions (P1 to P4) and magnitudes (no load: lightweight sticks in the hands; load: 3.5 + 3.5 kg for males and 3.0 + 3.0 kg for females). C) Spinal profiles for personalized [external (grey x) and internal (purple +); for all participants] and generic [black continuous curve; corresponding to a reference subject; the scaling by height to other participants generated small changes] models.

MS model outcome	η_G^2 effect size and statistical significance (*)			Absolute (and %) effect of spine profile factor (personalized minus generic spine) … at each Position			… at each Load	
	S	S×P	S×L	P1	P2	P3	No	With
F-Rectus abdominis (N)	0.462*	0.000	0.000	27 (549)	19 (901)	23 (933)	22 (770)	23 (692)
F-External Oblique (N)	0.131*	0.003	0.003*	60 (70)	44 (58)	59 (64)	59 (75)	49 (54)
F-Internal Oblique (N)	0.006*	0.000	0.000*	9 (14)	10 (13)	14 (19)	7 (11)	15 (19)
F-Iliocostalis (N)	0.275*	0.010*	0.004*	-37 (51)	-42 (53)	-34 (41)	-29 (45)	-46 (50)
F-Longissimus (N)	0.165*	0.002	0.000	-38 (31)	-67 (41)	-53 (31)	-41 (33)	-64 (35)
F-Multifidus (N)	0.036*	0.007*	0.003*	-3 (1)	-72 (21)	-28 (9)	-46 (18)	-23 (7)
F-Compression$_{L4/L5}$ (N)	0.031*	0.003*	0.001*	-87 (9)	-135 (13)	-106 (10)	-85 (10)	-134 (12)
F-Shear $_{L5/S1}$ (N)	0.010	0.001	0.002*	-3 (1)	-26 (6)	-11 (3)	-1 (0)	-26 (6)
Lumbar Stiffness (Nm/rad)	0.000	0.012*	0.004*	85 (19)	5 (1)	61 (15)	59 (15)	41 (9)
Critical q	0.004	0.000	0.024*	0.9 (3)	3.2 (8)	-2.0 (4)	-3.9 (10)	5.3 (14)
Min eigenvalue (J/rad^2)	0.023*	0.054*	0.002	-22 (34)	-8 (15)	15 (41)	0 (0)	-10 (20)

†: Generalized Eta^2 scores of 0.020, 0.130 and 0.260 correspond to small, medium and large effect sizes.
* The 3 ANOVA factors: S = Spine profile (generic vs personalized); P = Position (P1 vs P2 vs P3); L = Load (with vs w/o). ANOVA findings that reached statistical significance ($p < 0.05$) are identified with "*". Results from Position and Load main effects and Position × Load interaction are not provided.

Table: Sensitivity (η_G^2 effect size † and percent changes) of selected MS model outcomes to the Spine-profile main factor and its interaction with Posture and Load, as tested with 3-way repeated ANOVAs: Result corresponding to the effect of load position height (P1 vs P2 vs P3; Figure 1B).

The effect of a soft active exosuit on extensor muscle forces during lifting tasks determined by musculoskeletal models

Yan C[a,b], Banks JJ[a,b], Allaire BT[a], Quirk DA[c], Chung J[c], Walsh CJ[c], Anderson DE[a,b]

[a]*Center for Advanced Orthopaedic Studies, Beth Israel Deaconess Medical Center, Boston, MA, USA*

[b]*Department of Orthopedic Surgery, Harvard Medical School, Boston, MA, USA*

[c]*John A. Paulson School of Engineering and Applied Sciences, Harvard University, Boston, MA, USA*

Back support exosuits offer the potential to reduce musculoskeletal demands. Several studies report lifting with an exosuit reduced back extensor electromyography activity, without estimating muscle forces. This study aims to assess whether a soft active back support exosuit reduces back muscle forces, and determine whether these reductions are associated with applied exosuit forces, user height, or user weight.

Full body musculoskeletal models were created for 14 participants, who performed four lifting tasks (Squat and Stoop, with 6 and 10 kg box) with and without a soft powered exosuit. The exosuit actively provided lifting assistance via a torso mounted actuator cable spanning to two thigh wraps. Measured actuator forces were incorporated into an inverse-kinematic model to estimate peak back extensor muscle forces with and without an exosuit during lifting. Correlation analyses were performed between the change in peak back extensor forces (with minus without exosuit), peak exosuit forces and participant height and weight.

Exosuit use reduced peak back extensor forces during lifting (Figure 1). Reductions in peak muscle forces were similar to applied exosuit forces, but more variable (Table 1). The change in muscle force due to exosuit use was not correlated with height, weight, or peak exosuit force ($p > 0.05$).

The exosuit reduced back extensor muscle forces when lifting, but the amount of reduction was highly variable compared to the relatively tight force control of the exosuit controller. This variability of reduction in back extensor forces was not explained by peak suit force or participants' anthropometrics. This finding suggests additional efforts are needed to understand the complexity of how exosuits reduce back extensor forces. Future work should examine models incorporating anticipatory muscle adjustments, temporal aspects of exosuit force delivery, and human perception of exosuit use to better understand these relationships.

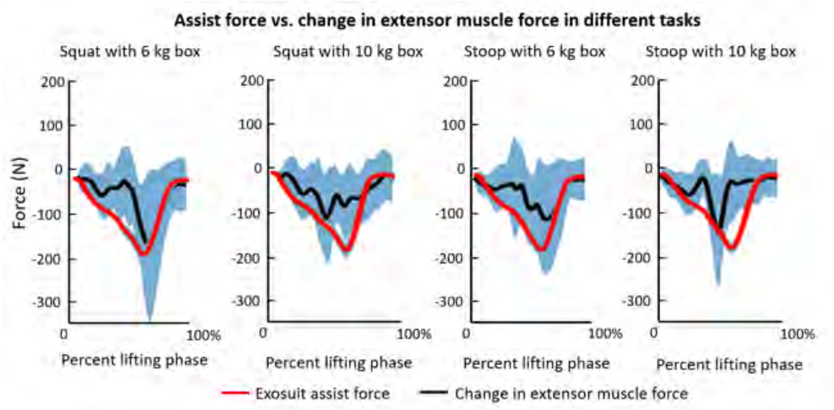

Figure 1: Mean and SD of change in extensor muscle forces due to exosuit use during squat and stoop lifts with 6 and 10 kg box in 14 subjects. The mean of the exosuit assistance forces associated with the lift (red) is plotted on the negative axis for comparison.

Task	**Muscle force change (N)**	**Exosuit force (N)**
Squat 6kg	-248±121 [-138 to -600]	189±20 [150 to 219]
Squat 10kg	-208±69 [-81 to -312]	189±16 [165 to 212]
Stoop 6kg	-202±74 [-113 to -354]	186±11 [167 to 201]
Stoop 10kg	-210±81 [-68 to -384]	186±12 [164 to 209]

Table 1: Mean±SD [range] changes in peak muscle force with exosuit use during lifting of a 6 or 10 kg box using squat or stoop lift posture, and corresponding peak exosuit forces.

Comparison of different back-supporting exoskeletons regarding musculoskeletal loading

Johns J, Schultes I, Heinrich K, Glitsch U

Institute for Occupational Safety and Health, German Social Accident Insurance, Sankt Augustin, Germany

The aim of this study was to determine the supporting effect of one active (A1) and two passive (P1 and P2) back support exoskeletons. Kinematic data and back muscle activity were collected from 12 subjects during simulated lifting and holding of 10 kg. An inverse dynamic top-down modelling approach was used to calculate lumbar loading. During modelling, the exoskeleton support was considered as an orthogonal contact force acting on the thorax segment. For the passive systems, the support was determined experimentally as the flexion angle-dependent torque, and for the active system internal torque sensor data were used. Mean and peak lumbar extension moments, compression forces, and muscle activation were considered in the evaluation. During the lifting task, exoskeletons A1 and P1 showed a reduction of between 12 and 15% for peak and mean L5/S1 lumbar extension moments and compression forces compared to the condition without exoskeleton, while for P2 a decrease of 22-29% was observed. Muscle activity during lifting was lower while using all systems (A1 mean: 25%, peak: 23%; P1 mean: 11%, peak: 17%; P2 mean: 16%, peak: 23%). In the holding task, comparable reductions in mean and peak lumbar loads, ranging from 12 to 23%, were identified for both passive systems, whereas a greater reduction of 39 to 46% was found for A1. Muscle activation data showed a comparable pattern with decreases in mean and peak signals for P1 and P2 of 16-23%, as well as 54% and 53% for A1, respectively. While the performance of the passive exoskeletons was consistent with previous findings, the active system provided greater support during the holding task. These results should be combined with analysis of lower body kinetics in future studies to gain insight into the effects of the greater weight of the active system on whole body loading.

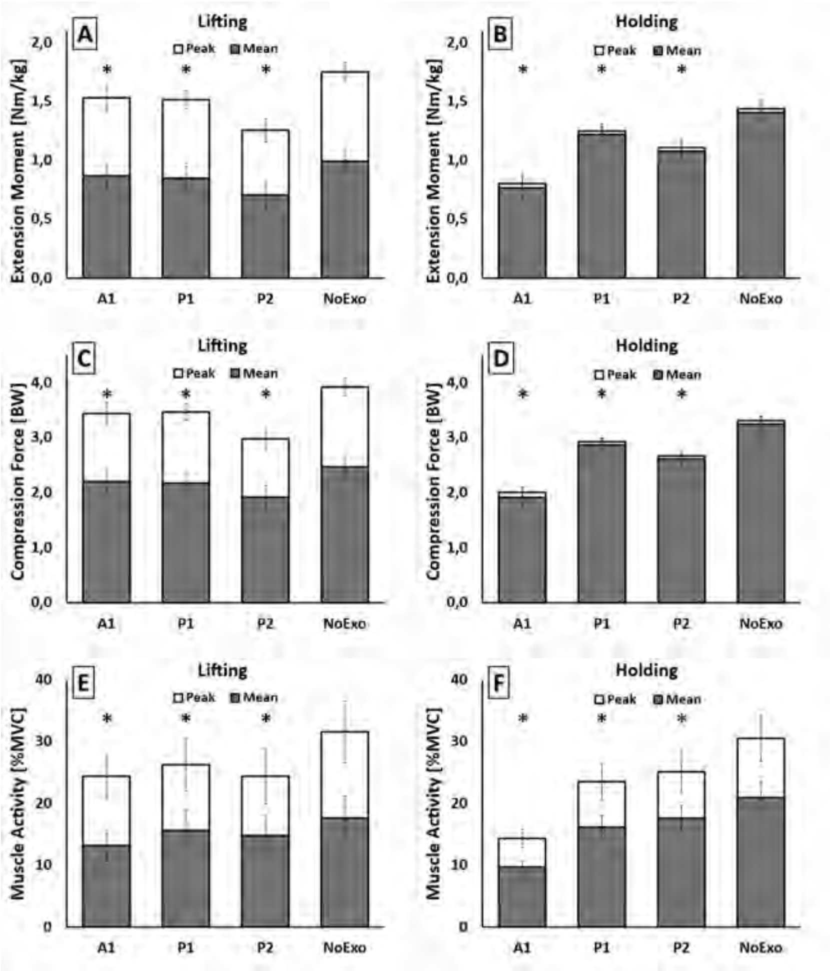

Figure 1: Peak and mean L5/S1 extension moments (normalized to bodyweight), compression forces (normalized to bodyweight) and lumbar muscle activity (in % of the maximum voluntary contraction) during simulated lifting and holding of 10 kg. Error bars indicate ± SD. * - Indicates statistically significant differences of any exoskeleton compared to the NoExo condition.

Numerical investigation of intra-abdominal pressure and spinal load-sharing upon the application of an abdominal belt

Bernier E[a,b], Driscoll M[a,b]

[a]*Musculoskeletal Biomechanics Research Lab McGill University, Department of Mechanical Engineering, Montréal, Canada*

[b]*Orthopaedics Research Lab, Montréal General Hospital, Montréal, Canada*

Chronic low-back pain patients may experience spinal instability. Abdominal belts (AB) have been shown to improve spine stability, increase trunk stiffness, and improve resiliency to spinal perturbations. However, research analyzing the underlying mechanisms contributing to these changes is inconclusive. ABs may increase intra-abdominal pressure (IAP), provide assistance to the trunk extensor moment, and reduce paraspinal muscle contribution to spine stability without increasing spinal compressive loads.

A finite element model of the spine inclusive of the vertebrae and intervertebral discs (IVD) from T1 to S1, ribcage, pelvis, femurs, major thoracolumbar soft tissues, and the abdominal cavity was developed. A second, identical in silico model with a linear elastic AB was developed (E=3MPa, ν=0.49). Both models were subjected to an external spine perturbation, simulating 30° lumbar flexion. Following validation, the models' intersegmental rotation (ISR), IVD pressure, IAP, and longitudinal tensile stresses in the multifidus (MF), erector spinae (ES), and thoracolumbar fascia (TLF) were compared.

The application of an AB resulted in an increase in IAP of 3.8 kPa and a decrease in soft tissue tensile stress of 3.2 kPa. The TLF demonstrated the largest decrease in stress with 22%. The average ISR in the AB model decreased by 7%, with the largest reduction occurring in the lumbar spine. The AB model also showed a 32% average reduction in IVD pressure in the lumbar spine.

Using an AB reduced trunk stiffness, primarily in the lumbar spine. Wearing an AB had minimal effect on reducing tensile stress in the MF and ES. The skewed stress relief towards the TLF suggests its large contribution to spine stabilization and the potential advantage in unloading the structure when wearing an AB.

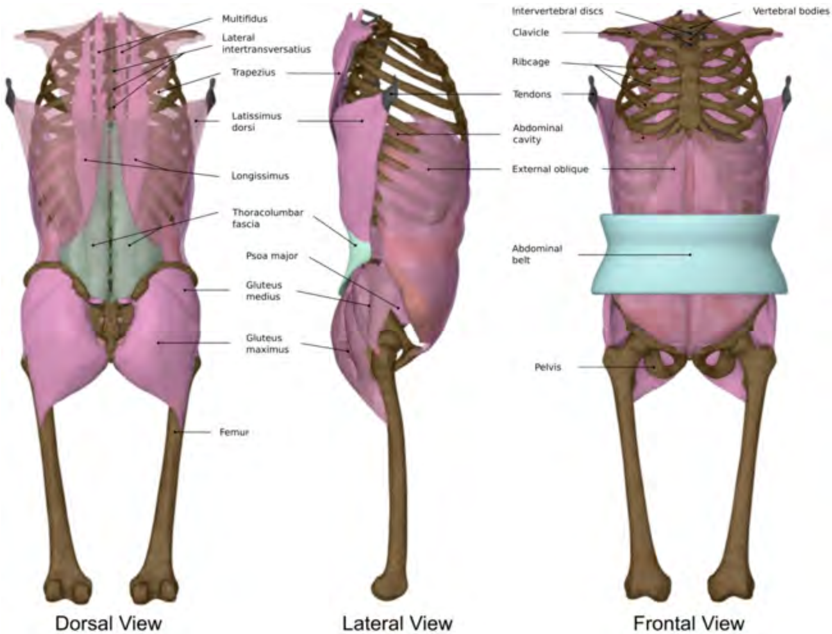

Figure 1: Finite element model of the spine developed using ANSYS (v2022 R1, ANSYS Inc., U.S.A.) including the vertebral bodies, ribcage, pelvis, and femurs modelled as surface bodies, and the intervertebral discs, thoracolumbar fascia, major thoracolumbar soft tissues, and abdominal belt modelled as volumetric deformable bodies.

Effect of obesity on spinal loads during load-handling activities; a subject- and kinematics-specific musculoskeletal modeling approach

Bahramian M, Parnianpour Mo, El-Rich M, Arjmand N

Department of Mechanical Engineering, Sharif University of Technology, Tehran, Iran

Obesity is a growing worldwide health issue playing a role in the etiology of low-back pain and disc degeneration [1-2]. Our previous musculoskeletal modeling investigations indicate that obese, as compared to normal-weight, individuals experience larger spinal loads during load-handling activities [3-4]. In these models, only anthropometric variables (e.g., body weight, muscle moments arms, and body mass distributions) were considered as subject-specific parameters, i.e., kinematics/posture data were considered identical in both normal-weight and obese models. Our recent full-body kinematics measurements on normal-weight and obese individuals during twelve symmetric/asymmetric statics load-reaching activities, however, indicate important kinematics/posture differences between the two groups especially for the tasks performed near the floor, away from body, and at larger load asymmetry angles [5]. The present study, therefore, aims to investigate the effect of obesity on spinal loads using both anthropometric- and kinematics-specific musculoskeletal models. Full-body kinematics data collected via a ten-camera Vicon motion capture system from nine healthy young male normal-weight (BMI=23.9±1.3 kg/m2) and nine obese (BMI=35.3±2.6 kg/m2) individuals while performing twelve unloaded reaching tasks at two heights (0 and 60 cm from the floor), three asymmetric angles (0°, 45°, and 90°), and two horizontal distances (30 and 60 cm from the feet) were used to drive the musculoskeletal models in AnyBody Modeling System (Fig 1a). L5-S1 compression and shear loads were predicted for total of 216 models (18 subjects×12 tasks) (Fig 1b). Results indicated that obese individuals experienced substantially larger L5-S1 loads ($p<0.05$) (Table 1). Mean±standard deviation compression and shear loads (of all tasks) in normal-weight/obese individuals were, respectively, 1674±337/2305±468 N and 508±111/705±150 N. However, variations of the spinal loads with the three hand position variables (height, asymmetry, and horizontal distance) were similar for both groups, i.e., BMI had non-significant interaction effects with the three hand position variables on spinal loads ($p>0.05$) (Table 1).

[1] Heuch et al., 2010, Spine (35), 764-68.

[2] Takatalo et al., 2013, PLoS One (8), e56244.

[3] Hajihosseinali et al., 2015, Journal of Biomechanics (48), 276-82.

[4] Akhavanfar et al., 2018, Journal of Biomechanics (70), 102-12.

[5] Ghasemi and Arjmand, 2021, Journal of Biomechanics (123), 110539.

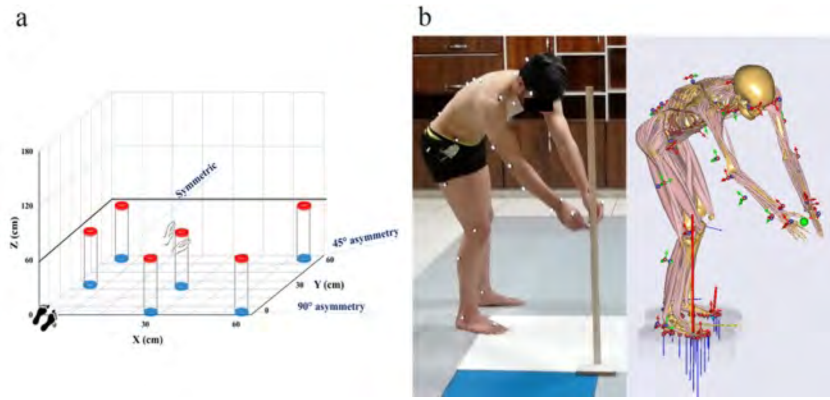

Figure 1: Experimental setup and musculoskeletal modeling: (a) positions of hands during twelve load- handling (reaching) tasks and (b) motion analysis of a subject performing a load-handling (60cm from the floor at 45° asymmetric angle, 60cm from the body) task and the subject-specific full-body musculoskeletal model.

	L5-S1 compression			L5-S1 shear		
	F	p-value	η^2	F	p-value	η^2
BMI	21.2	**<0.001***	0.570	22.3	**<0.001***	0.583
BMI × Load height	1.9	0.186	0.107	2.2	0.159	0.120
BMI × Load asymmetry	1.2	0.317	0.069	1.7	0.197	0.096
BMI × Load distance	1.1	0.318	0.062	1.6	0.226	0.090

Table 1: Results of 4-way mixed-model ANOVA analyses to statistically compare L5-S1 compression/shear loads between normal-weight and obese groups with load height (0 and 60 cm), load distance (30 and 60 cm), and load asymmetry (0, 45°, and 90°) as within-subjects variables. Bold values indicate a significance difference.

In vivo load on knee, hip, and spine during manual materials handling with two lifting techniques

Bender A[a], Brandl C[b,c], Dymke J[a], Schmidt H[a], Damm P[a]

[a]*Julius Wolff Institute, Berlin Institute of Health at Charité, Charité – Universitätsmedizin Berlin, Germany*

[b]*Institute of Industrial Engineering and Ergonomics, RWTH Aachen University, Aachen, Germany*

[c]*Fraunhofer Institute for Communication, Information Processing and Ergonomics FKIE, Aachen, Germany*

The lifting technique is known to have a strong influence on the biomechanical load and, thus, on the risk of musculoskeletal disorders (MSD). However, there is still no consistent evidence of the effectiveness of a particular lifting technique in reducing the risk of MSD compared to other lifting techniques. Hence, the aim of this study was to analyze the loads occurring in vivo for two typical lifting techniques, stoop and squat lifting.

Three groups of patients who received instrumented implants allowing in vivo load measurements at the knee, hip, and lumbar spine (L1/L3) performed two different frontal lifting techniques (i) with straight and (ii) bended knees, lifting a 10 kg weight. The resultant contact force Fres and the orientation of the force vector $\vec{F}_{res}$ in the frontal and sagittal planes were determined intra- and inter-individually and examined for differences using the two-sample t-test of Statistical Parametric Mapping (SPM).

The direct comparison of Fres acting in vivo at the knee, hip and spine during the lifting procedure showed no or very narrow intervals of significant differences between the two lifting techniques (Figures 1 and 2). However, the orientations of the force vector between the two lifting techniques showed significant differences in vivo:

- at the hip joint, orientation of $\vec{F}_{res}$ vary in the frontal and sagittal plane,
- at the knee joint, orientation of $\vec{F}_{res}$ only differ in the sagittal plane,
- at the lower spine, no differences were observed.

The primary difference between the two lifting techniques is not in the load magnitude but in the load direction, which leads to significant ($p<0.001$) differences in torsional and bending moments in the knee and hip. Mechanical loads in the lumbar spine are high with both techniques, but they are not significantly different.

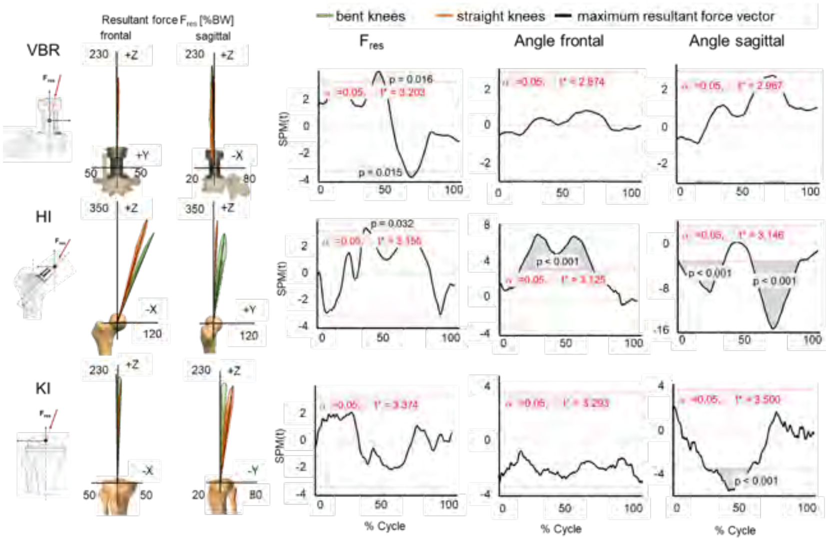

Figure 1: Statistical Parametric Mapping two-sample t-test for comparison of in vivo contact forces Fres[%BW] and orientation of load vectors [deg] in the frontal and sagittal planes when lifting a 10 kg weight with knees bent or straight for vertebral body replacement (VBR), hip implant (HI) and knee implant (KI). Colour coding: green - with knees bent; brown - with knees straight; black - maximum resulting force Fres.

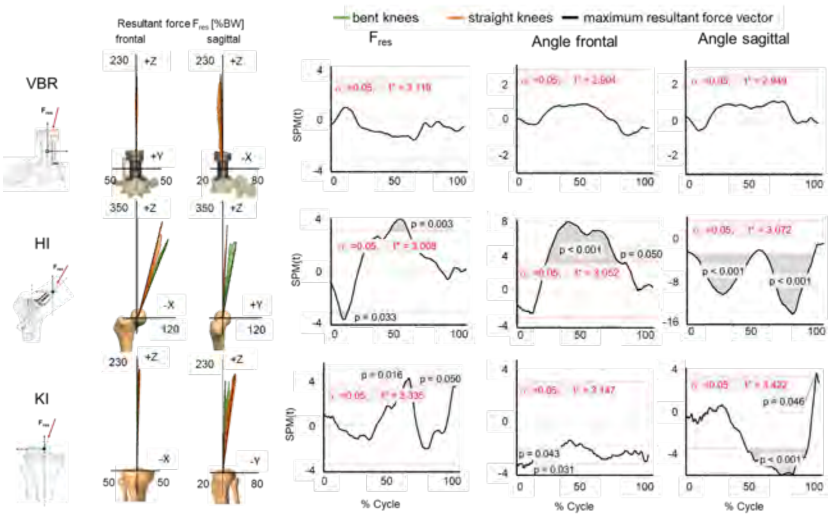

Figure 2: Statistical Parametric Mapping two-sample t-test for comparison of in vivo contact forces Fres[%BW] and orientation of load vectors [deg] in the frontal and sagittal planes, when placing a 10 kg weight with knees bent or straight, for vertebral body replacement (VBR), hip implant (HI) and knee implant (KI). Colour coding: green - with knees bent; brown - with knees straight; black - maximum resulting force Fres.

Lumbar spine loads in repetition-to-failure deadlifts, with and without body armor

Ramirez VJ[a,b], Ghezelbash F[c], Samaan M[b,d], Gao F[b,d], Shirazi-Adl A[c], Bazrgari B[d]

[a]*Military Performance Division, U.S. Army Research Institute of Environmental Medicine, Natick, MA*

[b]*Department of Kinesiology and Health Promotion, University of Kentucky, Lexington, KY*

[c]*Division of Applied Mechanics, Department of Mechanical Engineering, Polytechnique, Montréal, Québec*

[d]*F. Joseph Halcomb III, M.D. Department of Biomedical Engineering, University of Kentucky, Lexington, KY*

The new Army Combat Fitness Test (ACFT) implemented in 2022 includes a 3-repitition, maximum deadlift component, and repetitions-to-failure (RTF) deadlift is widely used to prepare for the ACFT. Additionally, Soldiers often wear body armor during physical fitness training as a training aide. However, little is known on the spine loads during those training exercises and the additional effect of body armor. The primary objective of this study was to determine spinal loads during RTF of 68 kg hex-bar deadlift, with and without body armor (BA).

Nineteen healthy adults (25.6 ± 5.23 years; 1.72 ± 0.07 m height; 79.99 ± 11.55 kg body mass) participated in this study. 3D kinematics of the thorax, pelvis, and hand were recorded. A dynamic, kinematics-driven model of the spine, personalized for each participant [3], was used to estimate temporal variation of spinal loads during the initial and final 10% of repetitions of the RTF deadlift, with and without a 22 kg simulated BA.

The peak compression force at L5/S1 increased from 15,072 ± 2,199 N to 16,989 ± 3,185 N ($p<0.001$) with negligible alterations in the peak shear force, from the initial to the final 10% of RTF. Addition of BA increased the peak compression force to 17,079 ± 2,770 N ($p<0.001$), and the shear force from 4,654 ± 711 N to 5,682 ± 9903 N ($p<0.0001$).

Spinal loads experienced in this study exceeded the current evidence for threshold of injury (compression: 5-10 kN, shear: 1-2 kN). The use of body armor and/or RTF during the deadlift, poses a significant risk of injury. The very large spine forces estimated here and the occurrence of no apparent injury in participants, may suggest mitigating mechanisms, such as much larger muscle lever-arms or wrapping, [3] and intra-abdominal pressure, to protect the spine.

[1] Armed Forces Health Surveillance Branch. 2017. MSMR, 24: 2-8.
[2] Clark, L.L., and S.B. Taubman. 2015. MSMR, 22: 12-16.
[3] Ramirez, et al., 2023. Int J Numer Method Biomed Eng. Jan 6:e3680.

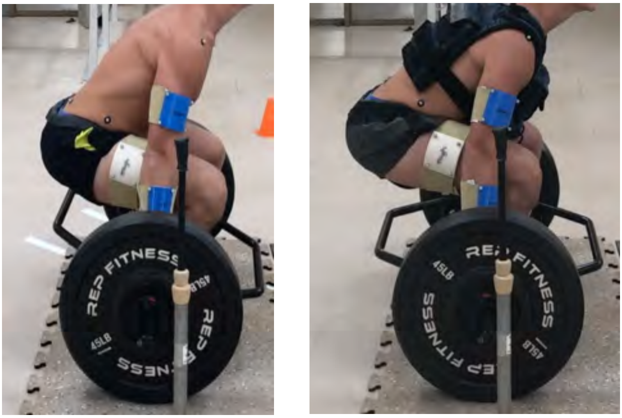

Figure 1: Starting position, or lift-off position, for the 68kg hex-bar deadlift without (left) and with (right) a 22.68 kg weighted vest (simulated body armor).

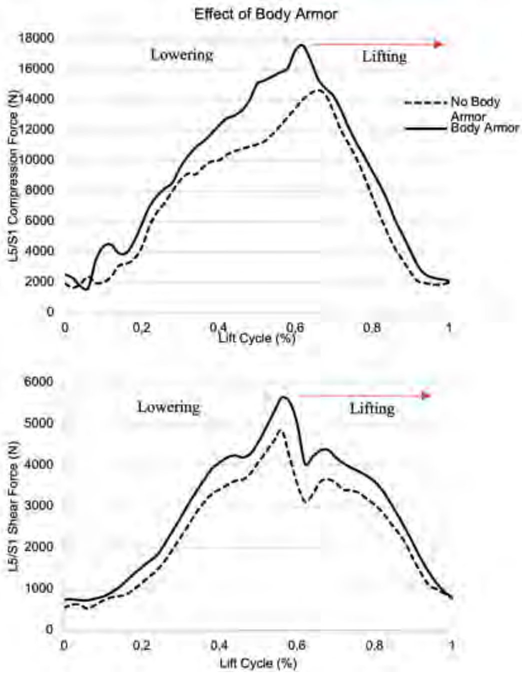

Figure 2: Effect of body armor condition on L5/S1 compression (top) and shear force (bottom) in one participant. The instance of peak compression and shear represents the lift-off position (Figure 1) of the deadlift where the hex-bar is lifted upward to full standing (far right and left).

Integrating novel technologies for spine biomechanics: opportunities and challenges

Ghezelbash F[a], Eskandari AH[b], Bidhendi AJ[a], Shirazi-Adl A[c], Larivière C[b]

[a]*EERS Global, Montréal, Canada*
[b]*Institut de recherche Robert-Sauvé en santé et en sécurité du travail, Montréal, Canada*
[c]*Department of Mechanical Engineering, Polytechnique Montréal, Montréal, Canada*

Advancement of novel technologies such as individualized musculoskeletal (MS) modeling along with 3D human body reconstruction and markerless pose detection through machine learning algorithms have created the opportunity for real-time and on-site biomechanical analyses in various fields such as sports sciences and occupational safety. Here, we integrate foregoing technologies into a comprehensive biomechanical evaluation framework for occupational health and sports science applications.

The proposed framework integrates image-based 3D human body reconstruction through deep neural networks (PIFuHD) to individualize segmental masses (e.g., trunk; estimated from body measures and regression equations based on NHANES database of 24,900 individuals) in a subject specific MS model, which is driven by estimated kinematics from convolutional neural networks (e.g., BlazePose); Figure 1. We evaluated potential and limitations of the proposed workflow in assessing spine biomechanics during various activities such as asymmetric manual materials handling in occupational settings and deadlifting in performance enhancement.

By using a single camera input, a comprehensive analysis of various activities was carried out. Developed regression equations ($R2>0.9$; error< 5%) combined with the image-based 3D human body reconstruction method (i.e., PIFuHD) had, overall, a satisfactory performance (Figure 1); except for a few cases where the reconstructed shapes were distorted. The framework successfully evaluated spine biomechanics when the subject-specific MS model was driven by the estimated pose during asymmetric lift (maximum compression: 4.2 kN; Figure 2) and deadlift of 40 kg weight (caused 13% peak collagen fiber strain; Figure 2).

The integration of new technologies holds a great potential for real-time and on-site evaluation of human performance in occupational and sports activities, particularly to prevent injury and performance improvement. However, as such 3D body reconstruction and markerless pose estimation algorithms are still in their infancies, further improvements in accuracy and robustness are desired.

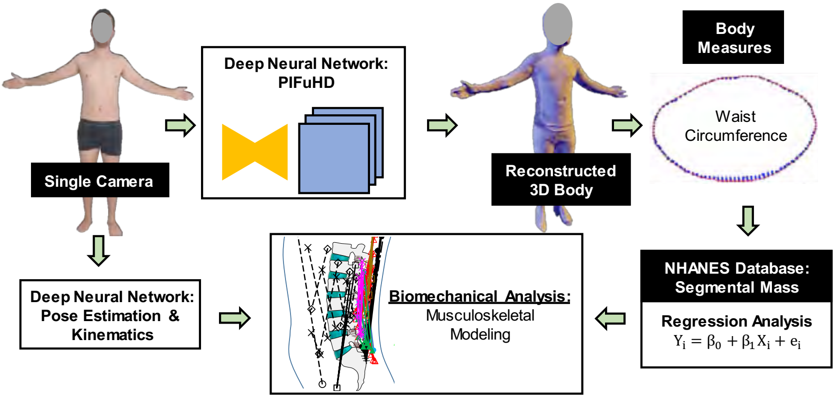

Figure 1: Schematics of the proposed workflow: driven by novel pose estimation algorithms, image-based 3D human body reconstruction to individualize coupled MS models and computed personalized biomechanical parameters.

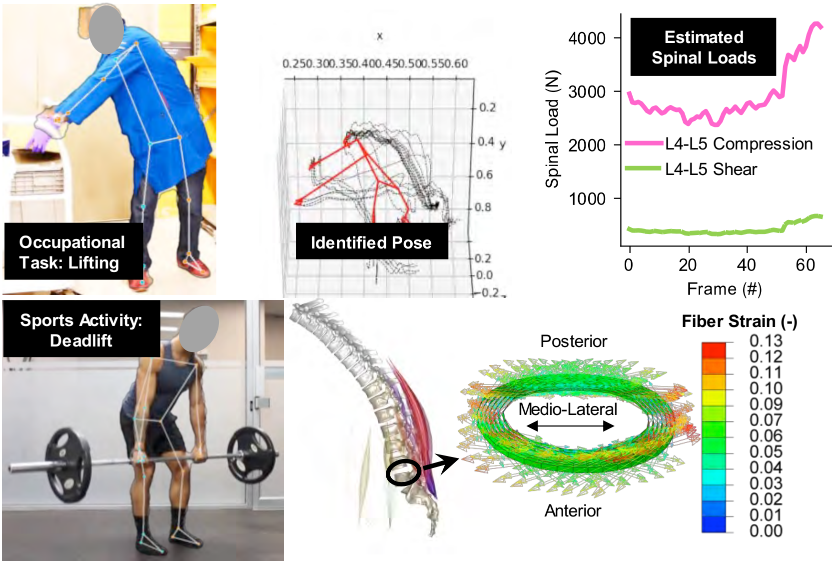

Figure 2: (top) Asymmetric manual materials handling of a 5 kg hand-load in an industrial setting as well as the identified pose (red: identified pose; dashed lines: trajectory of landmarks during the activity) and estimated spinal loads at each video frame. (bottom) Estimated pose, muscle activities, and collagen fiber strains (at the L4-L5 disc) during a deadlift of 40 kg weight.

Estimations of spinal loads using musculoskeletal models driven by measured or neural-network predicted postures during dynamic lifting activities

Hosseini N, Arjmand N

Department of Mechanical Engineering, Sharif University of Technology, Tehran, Iran

Body posture is an essential input of musculoskeletal models that evaluate spinal loads in occupational activities. Posture is either measured in vivo via video-camera motion capture systems or predicted via artificial neural networks (ANNs) [1]. As video-camera measurements are impractical for use in real workstations, we have recently developed an ANN that predicts full-body posture during one- and two-handed static load-handling activities. This ANN, trained based on the posture data of 20 subjects each performing 204 static load-handling activities, uses 3D coordinates of the hand-load, body weight, and body height of the worker to predict 3D coordinates of 41 full-body skin markers. The root-mean-square-error (RMSE) between the ANN predicted and in vivo measured postures during static load-handling activities was ~2.5 cm (averaged for all markers/tasks). The present study aims to: 1) use this ANN to predict full-body posture during twenty-five dynamic lifting tasks (Table 1) performed by seven individuals and 2) predict dynamic spinal loads by the AnyBody Modelling System (AMS) driven by either measured or predicted postures. To predict dynamics postures, hand-load position in dynamic tasks was input into the ANN as function of time. Results indicated that the ANN successfully predicted dynamic postures; the RMSE between the predicted and measured postures for all markers/tasks/subjects (41 markers×25 dynamics tasks×7 subjects) was equal to ~7.4 cm (R2 = 0.98). Moreover, the predicted L5-S1 compression and shear loads by the AMS driven by the predicted or measured postures were in close agreement; normalized RMSEs (averaged for all subjects/tasks) were smaller than 10% (p-value > 0.05) (RMSEs for the L5-S1 compression and shear loads were equal to ~350 and 120 N) (Figure 1). These results indicate the robustness of the ANN to predict statics and dynamics lifting postures as well as their applicability in predicting spinal loads by musculoskeletal models.

[1] Mohseni et al., 2022. Improved artificial neural networks for 3D body posture and lumbosacral moment predictions during manual material handling activities. Journal of Biomechanics 131, 110921.

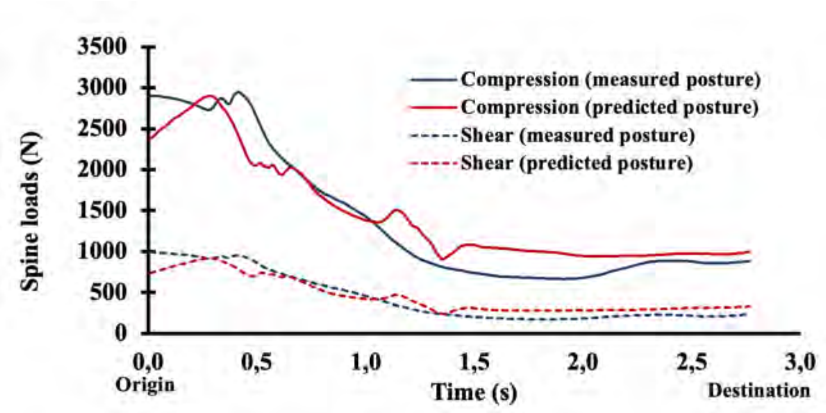

Figure 1: L5-S1 compression and shear loads versus time for two-handed lifting of a 10 kg weight by one of the subjects (body height = 180 cm and body weight = 67 kg) based on the ANN predicted and in vivo measured postures.

	Task 1	Task 2	Task 3	Task 4	Task 5
Origin					
	(0, 55, 170)	(50, 0, 170)	(-55, 0, 0)	(-40, 55, 100)	(40, 55, 0)
Destination					
	(-50, 0, 40)	(-55, 40, 40)	(55, 40, 170)	(55, 0, 0)	(-55, 0, 100)

Table 1: A schematic of the five dynamic lifting tasks each performed in five different ways: one- and two-handed lifting without any hand-load, one-handed lifting of a 5 kg weight, and two-handed lifting of 5 and 10 kg weights. The coordinate system is defined between the feet (x: right lateral, y: anterior, and z: upward). Hand-load position (cm) is given the row below each figure.

Development of an integrated spine biomechanics framework combining in-vivo, in-silico and in-vitro methods

Ebisch I[a], Farris DJ[b], Lazaro Pacheco D[a], Holsgrove TP[a]

[a]*Department of Engineering, Faculty of Environment, Science and Economy, University of Exeter, Exeter, UK.*

[b]*Public Health & Sport Sciences, Faculty of Health and Life Sciences, University of Exeter, Exeter, UK.*

Lifestyle heavily influences intervertebral disc (IVD) loads, but measuring in-vivo loads is not possible without invasive procedures, and the ability to apply these loads in-vitro is limited. While valuable in-vivo load data is available from instrumented vertebral body replacements (IVBR) via the Orthoload-database [2], these data are acquired from participants with a spinal fusion, which may not result in the same loading as a healthy population, or a back pain population that has not had spine surgery. Therefore, this study aimed to develop an integrated framework for the non-invasive estimation of in-vivo IVD loading, and the application of these loads in the in-vitro setting (Figure 1).

A full-body Opensim model was developed by adapting two existing models [3,4]. Kinetic data from five healthy participants performing activities of daily living were acquired and used as inputs for simulations using static optimisation. After validating simulation results using in-vivo data [2,5,6], the estimated six-axis loads were applied to bovine tail specimens.

Estimated spinal loads from the in-silico model followed the same trends as Orthoload-data [2] but resulted in higher magnitude loads. The modelled magnitude in axial compression was comparable to that derived from in-vivo intradiscal pressure measurements of healthy participants [5,6]. This highlights the potential differences between healthy and IVBR populations. Estimated L1/L2 loads were successfully applied to bovine tail specimens, with loads scaled for the smaller size of the IVDs, resulting in similar kinematics in the in-vitro tests as the in-silico models (Figure 2).

A framework has been successfully developed, and key components validated that allows the estimation and application of physiological load profiles to IVDs. This can be used to estimate the complex loads of daily activities in different populations, which will deepen our knowledge of spine biomechanics, mechanobiological processes involved in IVD degeneration, and improve the pre-clinical test methods.

[1] Alzahrani, H., Shirley, D., Cheng, S. W. M., Mackey, M., & Stamatakis, E. (2019). Journal of Sport and Health Science, 8(4), 386–393.
[2] Bergmann, 2008. "OrthoLoad". Retrieved 01/04/2021 from http://www.OrthoLoad.com
[3] Beaucage-Gauvreau, E., Robertson, W. S. P., Brandon, S. C. E., Fraser, R., Freeman, B. J. C., Graham, R. B., Thewlis, D., & Jones, C. F. (2019). Computer Methods in Biomechanics and Biomedical Engineering, 22(5), 451–464.

[4] Senteler, M., Weisse, B., Rothenfluh, D. A., & Snedeker, J. G. (2016). Computer Methods in Biomechanics and Biomedical Engineering, 19(5), 538–548.
[5] Takahashi, I., Kikuchi, S., Sato, K., & Sato, N. (2006). Spine, 31(1), 18–23.
[6] Wilke, H.-J., Neef, P., Hinz, B., Seidel, H., & Claes, L. (2001). Clinical Biomechanics, 16(S1), S111-S126.

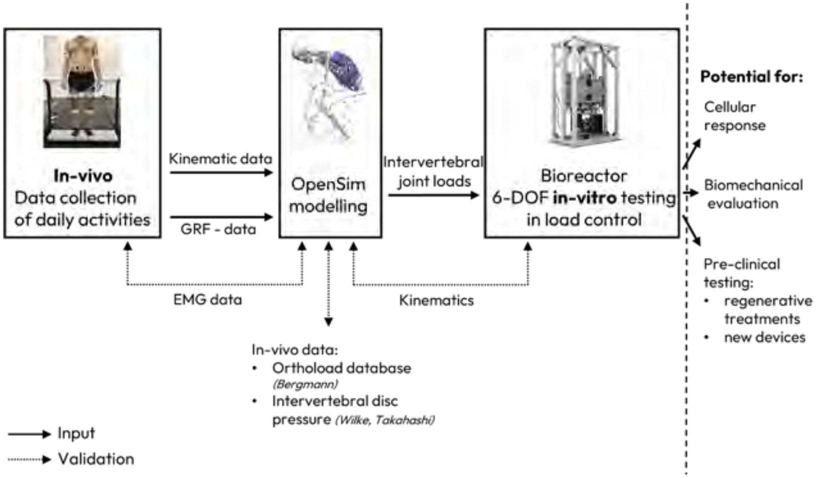

Figure 1: Schematic of framework: From in-vivo data collection of participants performing activities of daily living to six-axis in-vitro testing of spinal specimens.

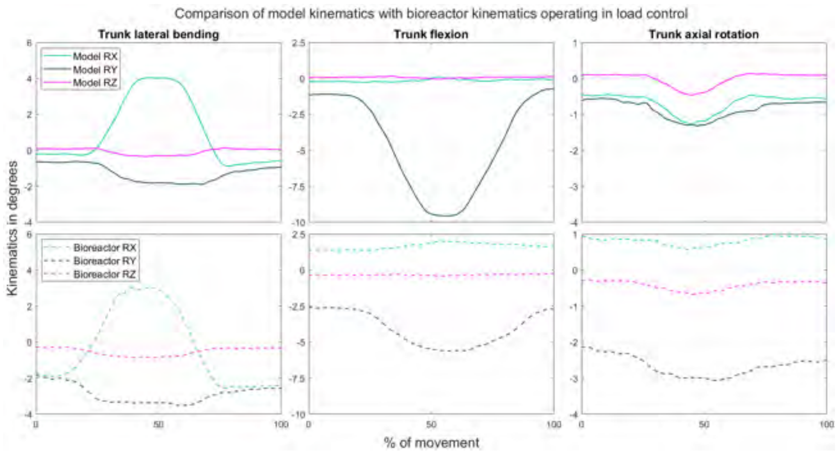

Figure 2: Comparison of model kinematics (rotations around all three axes) at L1/L2 level with bioreactor kinematics for a trunk lateral bending (RX), trunk flexion (RY), and trunk axial rotation (RZ).

A pipeline for automated generation of individualized musculoskeletal spine models reveals substantial differences in spinal loading depending on curvature in large patient cohorts

Lerchl T[a,b], Nispel K[a,b], El Husseini M[a], Sekuboyina A[a], Bodden J[a], Senner V[b], Kirschke JS[a]

[a]*Department of Diagnostic and Interventional Neuroradiology, School of Medicine, Klinikum rechts der Isar, Technical University of Munich, Munich, Germany*
[b]*Associate Professorship of Sport Equipment and Sport Materials, School of Engineering and Design, Technical University of Munich, Munich, Germany*

The influence of biomechanical factors such as spinal alignment, upper body weight distribution, or muscle morphology, are considered to be a central issue to understand, prevent and treat chronic back pain [1]. However, these factors are subject to high interindividual variability. Individualized multibody models (MBS) of the upper body can provide insight into the effects of potential risk factors and thus, help promote a profound understanding of the pathobiomechanics of the spine.

We generated 93 patients-specific MBS models from CT imaging data using our automated validated pipeline for segmentation and individualized modeling of the upper body (Figure 1) [2]. A medical professional clinically assessed the data according to individual anthropometrics and sagittal alignment for later analysis. Using a combination of inverse dynamics and static optimization, we simulated static loading tasks, normalized resulting lumbar loads to individual torso weight and analyzed the results with respect to individual spinal geometry.

On average, normalized compressive loads ranged from 312 % of the torso weight in patients with lordosis in the lower normal range (35° - 45°) to 345 % patients with hyperlordosis (> 55°) (Figure 2), with maximum loading occurring in the L5/S1 level with 364 % and 442 % respectively. Average, normalized anterior-posterior shear forces ranged from 34% in patients with hypolordosis (< 35°) to 65 % in patients with hyperlordosis, with normalized loads up to 41 % and 126 % in L5/S1 respectively.

The results of our study indicate a strong dependence between spinal loads and spinal alignment that goes beyond the purely geometric relationship like the tilting of the lower lumbar vertebral bodies in pronounced lordosis and the associated increase in shear force relative to the absolute force. Our process holds the potential to systematically shed light to individual biomechanical characteristics and their potential effects on spinal loads.

[1] Murtezani A, Ibraimi Z, Sllamniku S, Osmani T, Sherifi S. Prevalence and risk factors for low back pain in industrial workers. Folia medica 2011; 53: 68–74.
[2] Lerchl T, El Husseini M, Bayat A, et al. Validation of a Patient-Specific Musculoskeletal Model for Lumbar Load Estimation Generated by an Automated Pipeline From Whole Body CT. Frontiers in Bioengineering and Biotechnology 2022; 10.

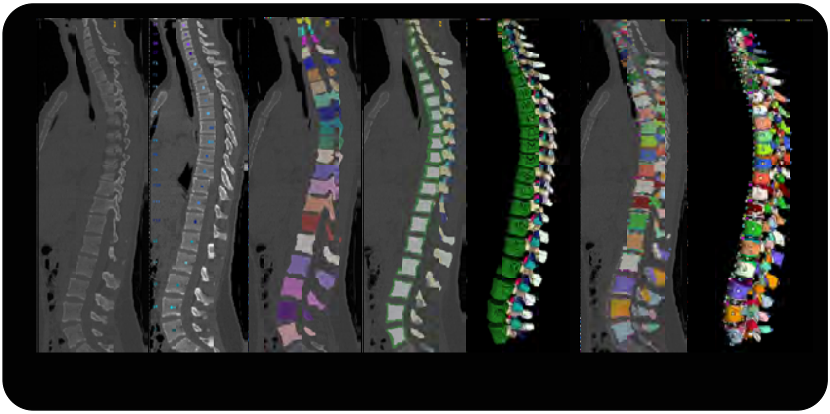

Figure 1: Pipeline Overview from left to right; original data, vertebrae identification; vertebrae segmentation; subregion segmentation (cross-section and 3D rendering); re-alignment in craniocaudal direction and calculation of points of interest; 3D rendering of the final dataset.

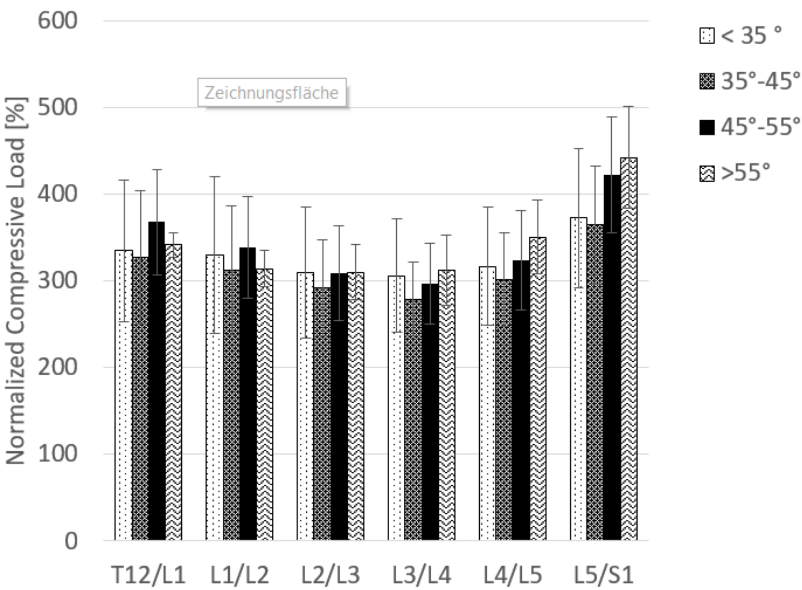

Figure 2: Compressive loads for patients with different lumbar lordosis (< 35°: hypolordosis, 35° - 55°: norm range, > 55° hyperlordosis). Loads were normalized to the individual torso weight of the respective patient.

Assessment of a fully-parametric thoraco-lumbar spine model with articulated ribcage

Bellina E[a], Laurino ME[a], Perego A[a], Pezzinga A[a], La Barbera L[a,b]

[a]*LaBS, Department of Chemistry, Materials and Chemical Engineering "G.Natta", Politecnico di Milano, Milano, Italy.*

[b]*IRCCS Istituto Ortopedico Galeazzi, Milano, Italy*

Spine pathophysiology is often studied using detailed patient-specific finite element (FE) models hardly-generalizable. Parametric spine models promise a more efficient strategy to generate patients' cohorts with predefined features and to test in silico the biomechanical effects of alternative treatment options. The present study aimed at: i) developing a fully-parametric thoracolumbar spine model comprehensive of the ribcage based on few independent parameters to describe both sagittally-balanced/-unbalanced patients; ii) assessing its credibility throughout the comparison with in vitro and in vivo data both in terms of morphology, kinematics and dynamics.

Predictive equations of 38 dependent parameters for each vertebra [Kunkel 2011; Panjabi 1993,1992], plus 17 for the ribcage [Holcombe 2016] were best-fitted assuming the vertebral body posterior height (VBHP) as unique independent parameter. A complete CAD model was built in Solidworks implementing regression equations and adding thoracic kyphosis, lumbar lordosis, and sacral slope (Figure a). The entire FE model of a healthy subject was generated and meshed in Abaqus and a backward stepwise reduction approach ensured the sequential calibration of its material properties.

All dependent parameters describing spinal morphology were predicted within one standard deviation. Ribcage shape and spinal sagittal alignment (Figure) agreed with in vivo measurements on healthy volunteers [Burgos 2021]. Soft tissues calibration ensured an accurate kinematics in every loading direction assuming homogeneous mechanical properties across three thoracic and one lumbar region (Figure c). The predicted IDP values also agreed with the published in vitro data.

A morphologically accurate spine model was generated based on fewer independent parameters than any other available to date: these included one VBHP per vertebra and three sagittal-balance parameters easy to measure on common diagnostic images. The spine model delivered satisfactory predictions to represent an average healthy adult in terms of kinematics and dynamics. The same approach will be systematically used in future studies to generate entire patients' cohorts with a variety of sagittal phenotypes.

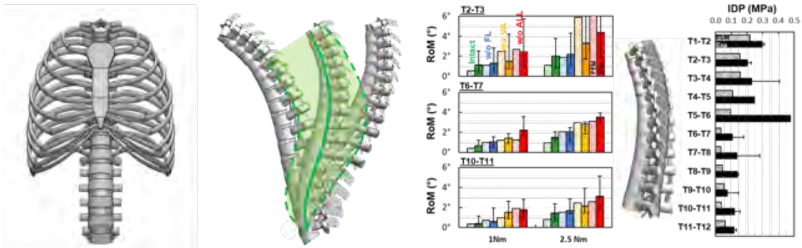

a) Assembled spine model (average morphology)

b) Effect of varying lumbar lordosis vs. *in vivo* sagittal range [*Fasser 2021*; *Bruno 2015*]

c) Thoracic segment (e.g. flexion): predicted RoM and IDP values vs. experiments [Wilke, 2020; Liebsch 2017]

Figure: Assembled thoracolumbar spine model comprehensive of the ribcage representative of a healthy adult (a); Effect of varying the lumbar lordosis in the CAD model compared with typical sagittal profiles for healthy subjects and adult spine deformity patients (b); Range of motions (RoMs) calibrated throughout a backward stepwise reduction approach by comparison with in vitro data and resulting intradiscal pressure (IDP, 2.5Nm) values for representative thoracic functional spinal units (c).

Estimating trunk muscle forces in adolescent idiopathic scoliosis patients during functional activities: a personalized experimentally controlled musculoskeletal modeling approach

Rauber C[a,b], Lüscher D[a,b], Poux L[a], Schori M[c], Deml MC[d], Hasler CC[e], Bassani T[f], Galbusera F[g], Büchler P[b], Schmid S[a,h]

[a]*Spinal Movement Biomechanics Group, School of Health Professions, Bern University of Applied Sciences, Bern, Switzerland*
[b]*Computational Bioengineering Group, ARTORG Center for Biomedical Engineering Research, University of Bern, Bern, Switzerland*
[c]*Physiotherapieschori Bern, Bern, Switzerland*
[d]*Department of Orthopaedic Surgery and Traumatology, Inselspital, University Hospital Bern, University of Bern, Bern, Switzerland*
[e]*Orthopaedic Department and Spine Surgery, University Children's Hospital Base, Basel, Switzerland*
[f]*Laboratory of Biological Structures Mechanics, IRCCS Istituto Ortopedico Galeazzi, Milan, Italy*
[g]*Spine Research Group, Schulthess Klinik, Zürich, Switzerland*
[h]*Faculty of Medicine, University of Basel, Basel, Switzerlan*

Currently performed scoliosis-specific exercises have only limited success in stopping curve progression, most likely related to the lack of biomechanical evidence on dynamic spinal loading. To provide a solid foundation for future finite element simulations of vertebral endplate stresses, this work focused on evaluating personalized experimentally controlled musculoskeletal simulations of trunk muscle forces during functional activities.

We used biplanar radiographs, as well as marker-based motion capture, ground reaction force and electromyography (EMG) data from two patients with thoracolumbar AIS (EXA02: aged 15 years, Cobb angle 45°; EXA03: aged 11 years, Cobb angle 21°) performing various functional activities such as walking, running, and object lifting. Using a fully automated approach [1], 3D spinal shape was extracted, and personalized OpenSim-based musculoskeletal models were created by deforming the spine of pre-scaled children/adolescents full-body models (Figure 1) [2,3]. In contrast to previous work [3], joint centers were determined more accurately, and mass distribution and marker positions were adjusted accordingly. Simulations of functional activities were conducted using an experimentally controlled backward approach and evaluated by calculating cross-correlations (RMP) between predicted muscle forces and EMG activity.

EMG activity and model predictions correlated well for object lifting (RMP>0.95). For walking and running, correlations were slightly lower (0.51<RMP<0.90), with the lowest values found for convex/concave-ratios. Figure 2 shows the results for the examples EXA02-object lifting and EXA03-walking.

The results indicate clear potential of our approach for estimating trunk muscle forces in AIS patients during functional activities, which can be used to control future finite element simulations of vertebral endplate stresses (currently under development). The lower correlations for convex/concave-ratios can be explained by the fact that static optimization does not consider muscle co-contractions. Future work will therefore focus on implementing partial EMG drive from major trunk muscles, along with personalized stiffness properties and muscle geometry.

[1] Galbusera et al., Eur Spine J. 2019;28(5):951-960.
[2] Schmid et al., J Biomech. 2020;102:109305.
[3] Schmid et al., Front Bioeng Biotechnol. 2020;8:159.

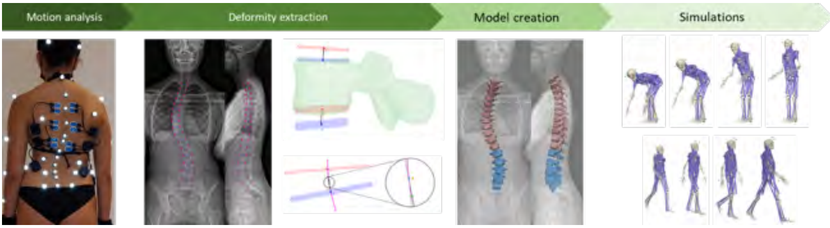

Figure 1: Personalized OpenSim-based musculoskeletal modeling workflow for patients with AIS, including full-body motion analysis, model creation from biplanar radiographs, and simulations of muscle forces during various functional activities using an experimentally controlled backward approach (i.e., inverse kinematics and static optimization).

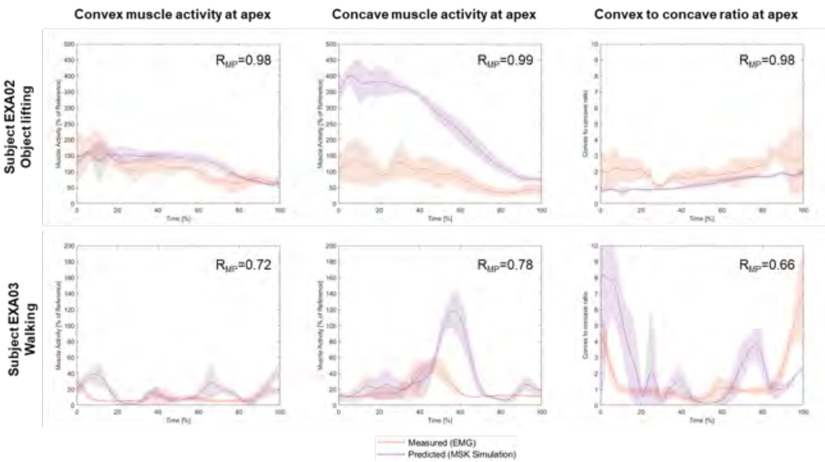

Figure 2: In vivo measured EMG activity and predicted muscle forces at the height of the scoliotic curve apex in the patients EXA02 (top row) and EXA03 (bottom row) during object lifting and walking, respectively. Left and middle column: convex and concave muscle activity in relation to a reference position (upright standing with arms in 90° forward flexion and with holding a 1.5kg-dumbbell in each hand). Right column: ratio between the convex and concave side muscle activity. RMP = cross-correlation coefficient among measured and predicted muscle activity.

Asymmetry of trunk muscle activation in adolescent idiopathic scoliosis during the simulation of forward flexion by musculoskeletal modelling

Bassani T[a], Ignasiak D[b], Cina A[c,d], Galbusera F[c]

[a]IRCCS Istituto Ortopedico Galeazzi, Milan, Italy
[b]Institute for Biomechanics, ETH Zurich, Zurich, Switzerland
[c]Spine Center, Schulthess Clinic, Zurich, Switzerland
[d]Dept. of Health Sciences and Technologies, ETH Zurich, Zurich, Switzerland

Musculoskeletal modelling allows calculating muscle activation in assigned kinematic conditions. A thoracolumbar model with articulated ribcage developed in AnyBody software has been recently adapted to replicate the spine alignment in adolescent idiopathic scoliosis (AIS). The present study exploits that model to replicate the alignment in an available dataset of 66 AIS subjects with Cobb angle ranging from 10° to 45°. Trunk forward flexion from 0° (standing) to 45° is simulated (distributed from T12 to the fixed sacrum, Fig.1e). The asymmetry in erector spinae (ES) and multifidus (MF) muscle activation is calculated between convex and concave side of the scoliotic curve, and distinguished between mild scoliosis (Cobb 10°-25°, 32 subjects) and moderate (Cobb 25°-45°, 34).

The subjects underwent radiological examination in orthostatic position, providing the simultaneous acquisition of frontal and lateral plane images (Fig.1a,b). The 3D spine alignment was replicated in the musculoskeletal model (Fig.1c,d) scaled by subject's weight and height. The asymmetry in muscle activation was evaluated between convex and concave side as (convex - concave)/(convex + concave), providing zero value for balanced activation, and positive and negative values (ranging from 0 to ±1) for larger activation in convex and concave side, respectively.

The asymmetry of ES and MF activation showed a decreasing and increasing trend, respectively, both in case of mild and moderate scoliosis (Fig.2). Compared to relaxed standing, ES activation was found more negative at maximum flexion, with mean±sd value equal to 0.02±0.11 and -0.09±0.21 (mild scoliosis), and -0.01±0.15 and -0.11±0.25 (moderate). Conversely, MF exhibited larger positive values.

The results pointed out the concurrent opposite activation of ES and MF muscle in the lumbar region during forward flexion. This finding suggests the presence of muscle synergy between ES (more involved to straighten the trunk) and MF (stabilizing the motion segments) in presence of scoliosis.

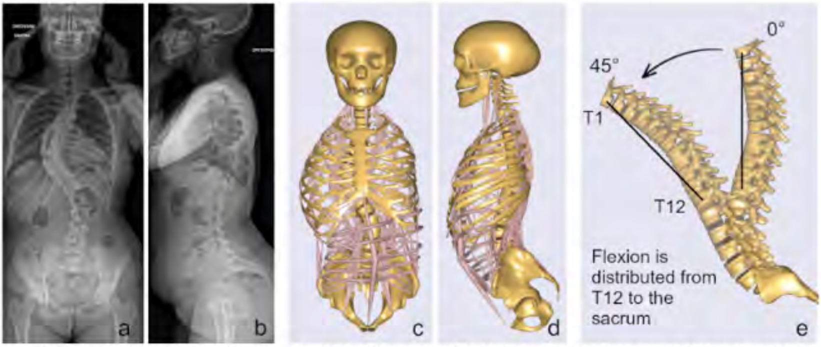

Figure 1. Frontal and lateral radiographic images of one subject (a,b) and corresponding musculoskeletal model in AnyBody software (c,d). Right panel (e): spine in relaxed standing (0°) and at maximum of trunk flexion (45°), with muscles and ribcage not shown to better illustrate the spine alignment.

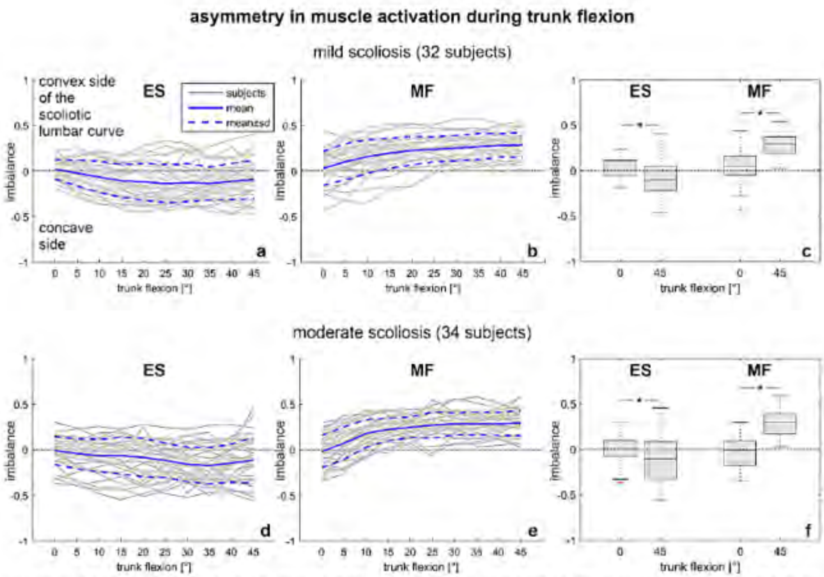

Figure 2. Asymmetry in ES and MF muscle activation in the lumbar section (from T12 to L5) during the trunk flexion movement, in case of mild and moderate scoliosis ((a,b) and (d,e), respectively). Right column: box and whiskers plot of muscle imbalance at minimum (0°) and maximum (45°) level of trunk flexion (c,f), with '' indicating statistical difference with p<.05.*

Does low back pain influence spinal loads during walking in persons with unilateral transtibial amputation?

Butowicz CM[a,b,c], Golyski PR[a,b], Acasio JC[a,b], Hendershot BD[a,b,c]

[a]Extremity Trauma and Amputation Center of Excellence, Bethesda, MD, USA
[b]Walter Reed National Military Medical Center, Bethesda, MD, USA
[c]Uniformed Services University of Health Sciences, Bethesda, MD, USA

Chronic low back pain (cLBP) is highly prevalent after lower limb amputation (LLA) and is associated with reduced quality of life [1]. Our previous work suggested larger trunk motion corresponded to larger spinal loads among persons with vs. without LLA [2], particularly at faster walking speeds [3]. As a next step towards better understanding the relationships between altered kinematics, spinal loads, and cLBP, here we present preliminary data of a larger samplea of persons with LLA, specifically comparing those with and without cLBP (i.e., pain > 3 months and ≥ half the days in the last 6 months). Full-body kinematics during level-ground walking at three speeds (self-selected [SSW], 1.0, and 1.6m/s) were collected for two males with unilateral transtibial LLA, one with cLBP (31yr, 181.0cm, 84.0kg, SSW=1.3m/s) and one without cLBP (34yr, 184.0cm, 97.9kg, SSW=1.4m/s). Peak compressive, mediolateral, and anteroposterior spinal loads (at L5-S1) were estimated from a full-body, transtibial amputation-specific model (Figure 1) developed using validated OpenSim models [4,5], and scaled to each participant. Electromyographic (EMG) activities from lumbar erector spinae (~L3) were used to validate muscle activations estimated using static optimization - normalized EMG activations of erector spinae were relatively consistent with the estimated activations of the model (mean difference=16%). Between individuals, peak compressive forces were 77% larger in the LBP group (Figure 2). Notwithstanding expanded results of the larger sample and inability to support causal mechanisms with the observational design, our findings suggest persons with (transtibial) LLA and cLBP may attempt to freeze degrees of freedom during walking as a protective mechanism to minimize shear force(s). However, repeated exposures to larger compressive forces would likely accelerate disc and vertebral endplate degeneration, further exacerbating the recurrence and chronicity of LBP.

[1] Devan, H et al., (2015). Perceptions of low back pain in people with lower limb amputation: a focus group study. Disability and Rehabilitation, 37(10), 873-883.
[2] Shojaei, I. et al., (2016). Persons with unilateral transfemoral amputation experience larger spinal loads during level-ground walking compared to able-bodied individuals. Clinical Biomech. 32, 157-163.
[3] Hendershot BD et al., (2018). Walking speed differentially alters spinal loads in persons with traumatic lower limb amputation. Journal of biomechanics, 70, 249-254.
[4] Raabe ME, Chaudhari AMW (2016). An investigation of jogging mechanics using the full-body lumbar spine model: Model development and validation. Journal of Biomechanics 49(7): 1238.
[5] Willson AM et al., (2022). Full body musculoskeletal model for simulations of gain in persons with transtibial amputation. Computer Methods in Biomechanics and Biomedical Engineering.

Acknowledgements: This work was supported, in part, by an award (5R03HD086512-02) from the National Center for Medical Rehabilitation Research (NIH-NICHD) and the Office of the Assistant Secretary of Defense for Health Affairs, through the Peer Reviewed Orthopaedic Research Program (award #W81XWH-14-2-0144). The views expressed in this abstract are those of the authors, and do not necessarily reflect the official policy or position of the U.S. Departments of the Army, Navy, Defense, nor the U.S. government.

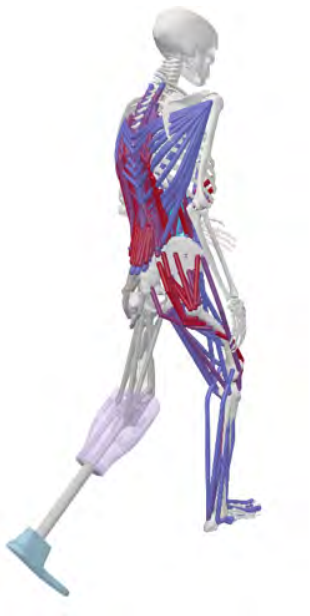

Figure 1: Custom musculoskeletal transtibial amputation-specific model used for estimating L5-S1 joint reaction forces.

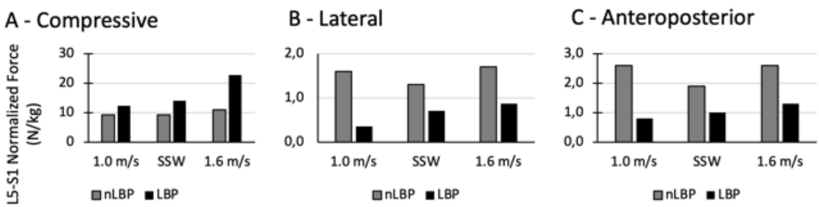

Figure 2: Normalized forces at L5-S1 (A) compression, (B) lateral shear, and (C) anteroposterior shear with increasing walking speed, for a person with transtibial amputation (LLA) and low back pain (LBP) vs. one without LBP (nLBP). For completeness, forces are presented for walking at 1.0 m/s, the individual's self-selected speed (SSW), and 1.6 m/s, and are normalized by body mass.

Effect of low back pain on the biomechanical kinetics/kinematics of the lumbar spine; a combined *in vivo* and *in silico* investigation

Firouzabadi A[a], Arjmand N[b], Zhang T[a], Schmidt H[a]

[a]*Julius Wolff Institute, Berlin Institute of Health at Charité - Universitätsmedizin Berlin, Berlin, Germany*

[b]*Department of Mechanical Engineering, Sharif University of Technology, Tehran, Iran*

Low back pain (LBP), a highly prevalent condition, is the primary cause of disability and work absence worldwide. There is increasing evidence that LBP is multifactorial in nature and caused by a combination of personal, psychosocial, and/or biomechanical factors [1]. Several studies have investigated the biomechanical kinematics and kinetics (e.g., electromyographic (EMG) data) of the lumbar spine toward understanding the etiology of LBP [2]. To improve our knowledge of spinal loads and identify potential musculoskeletal risk factors of LBP, it is necessary to evaluate all the biomechanical kinematics and kinetics of the lumbar spine concurrently. This study, therefore, aims to evaluate spinal loads, kinematics, and trunk muscle EMGs as well as ground reaction forces of both LBP and asymptomatic individuals during a number of activities. Kinematics of 56 skin markers (Vicon, Oxford, UK) and ground reaction forces were collected from 15 LBP and 15 asymptomatic volunteers during standing, peak voluntary flexion, extension, lateral bending, axial rotation, and a symmetric floor-to-hip lifting (10 kg) task (Fig 1). EMG data were also simultaneously recorded from 12 abdominal and back muscles. Kinematics and ground reaction forces were input into a subject-specific inverse dynamic musculoskeletal model (Anybody v.7.3, Aalborg, Denmark) that estimated muscle and spinal forces via an optimization algorithm [3]. Preliminary results (from 3 LPB and 3 asymptomatic individuals) indicated that LBP patients had smaller lumbar, trunk, and pelvis ranges of motions (RoMs) in all anatomical planes (Fig. 2). Moreover, LBP patients experienced slightly larger maximal normalized (to body weight, BW) L4-L5 compressive (14 %BW) and resultant shear (3 %BW) loads during the lifting task (T6). Extensor muscles (erector spinae) had higher maximum normalized EMGs in LBP, as compared to asymptomatic, group during the lifting task (71% of their maximal voluntary contractions for LBP and 63% for asymptomatic individuals). Findings of the current study can provide an evaluation of the spine biomechanical parameters for design of effective injury prevention and appropriate rehabilitation programs.

[1] S. G. Sadler, M. J. Spink, A. Ho, X. J. De Jonge, and V. H. Chuter, “Restriction in lateral bending range of motion, lumbar lordosis, and hamstring flexibility predicts the development of low back pain: A systematic review of prospective cohort studies,” BMC Musculoskelet. Disord., vol. 18, no. 1, pp. 1–15, 2017, doi: 10.1186/s12891-017-1534-0.

[2] C. T. V Swain, F. Pan, P. J. Owen, H. Schmidt, and D. L. Belavy, “No consensus on causality of spine postures or physical exposure and low back pain : A systematic review of systematic reviews,” J. Biomech., vol. 102, p. 109312, 2020, doi: 10.1016/j.jbiomech.2019.08.006.

[3] A. Firouzabadi, N. Arjmand, F. Pan, T. Zander, and H. Schmidt, “Sex-Dependent Estimation of Spinal Loads During Static Manual Material Handling Activities—Combined in vivo and in silico Analyses,” Front. Bioeng. Biotechnol., vol. 9, Nov. 2021, doi: 10.3389/fbioe.2021.750862.

Acknowledgment: This study was financially supported by the German Research Foundation (FOR5177 –SCHM 2572/12-1).

Figure 1: Different tasks performed by each participant

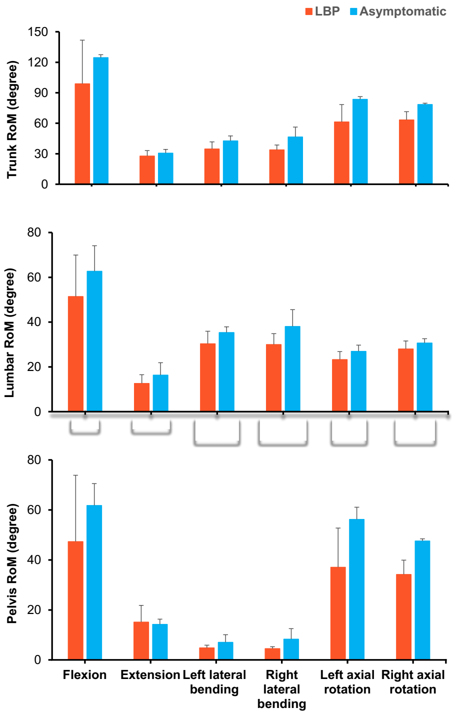

Figure 2: Mean (standard deviations as error bars) of the ranges of motion (RoMs) of LPB and asymptomatic individuals for trunk (A), lumbar (B), and pelvis (C) in different planes.

On lumbar loading during dynamic flexion and return to the standing posture. Effect of lumbo-pelvic rhythm and the range of motion in different age and sex groups.

Arshad R[a,c], Moglo K[a], El-Rich M[b], Schmidt H[c]

[a]*Biomechanics Laboratory, Department of Mechanical and Aerospace Engineering, Royal Military College of Canada, Kingston, ON, Canada*

[b]*Healthcare Engineering Innovation Center, Department of Mechanical Engineering, Khalifa University, Abu Dhabi, United Arab Emirates*

[c]*Julius Wolff Institute, Berlin Institute of Health at Charité – Universitätsmedizin Berlin, Germany*

The lumbo-pelvic rhythm, the lumbar spine and hip range of motion vary in different age and sex groups. A better awareness is required on how these differences might affect lumbar loading during dynamic flexion and return to the standing posture [1,2]. The study aimed to investigate lumbar loads at L4-L5, due to the difference in lumbo-pelvic rhythm, the lumbar and hip range of motion during dynamic full flexion and return to the standing posture.

A musculoskeletal model (AMMR ver. 2.2.3, AnyBody Technology A/S, version 7.2.3) for 50th percentile population was used for inverse dynamic analysis. Based on experimental data of the lumbo-pelvic ratio (0.11 to 3.44), the lumbar (45 to 55°) and the hip (60 to 79°) range of motion; kinematic profiles were re-constructed (Fig. 1) for different age (20-35, 36-50 and 50+ yrs.) and sex groups [3]. Inverse dynamic simulations were performed (a) to estimate the compressive loads at L4-L5 and (b) the inclination angle at peak load.

For males, the peak load decreased (2748, 2468 and 2333 N) with age with overall difference of about 415 N between young and old age group (Fig. 2). In females, peak load for the middle age group was highest (2695 N) as compared to young (2569 N) and old age group (2543 N). The corresponding inclination for males were highest for young age group (89.6°) vs other age groups (71° and 73°) as well as in females (95.7° vs 91.2° and 83°).

The purpose of this study was to investigate age and sex-based differences in the range of motion and L/P rhythm on the spinal loads during dynamic full flexion and return to the upright posture. Notable differences were found in peak lumbar loads and corresponding inclination angles in different age and sex groups. Such knowledge is critical to differentiate between normal vs pathological motion [4] and respective spinal loads.

[1] Vazirian M, Shojaei I, Bazrgari B. Age-related differences in the timing aspect of lumbopelvic rhythm during trunk motion in the sagittal plane. Hum Mov Sci 2017;51:1–8. doi:10.1016/j.humov.2016.10.010.
[2] Shojaei I, Vazirian M, Salt EG, Van Dillen LR, Bazrgari B. Timing and magnitude of lumbar spine contribution to trunk forward bending and backward return in patients with acute low back pain. J Biomech 2017;53:71–7. doi:10.1016/j.jbiomech.2016.12.039.

[3] Pries E, Dreischarf M, Bashkuev M, Putzier M, Schmidt H. The effects of age and gender on the lumbopelvic rhythm in the sagittal plane in 309 subjects. J Biomech 2015;48:3080–7. doi:10.1016/j.jbiomech.2015.07.030.
[4] Esola M a, McClure PW, Fitzgerald GK, Siegler S. Analysis of lumbar spine and hip motion during forward bending in subjects with and without a history of low back pain. Spine (Phila Pa 1976) 1996;21:71–8.

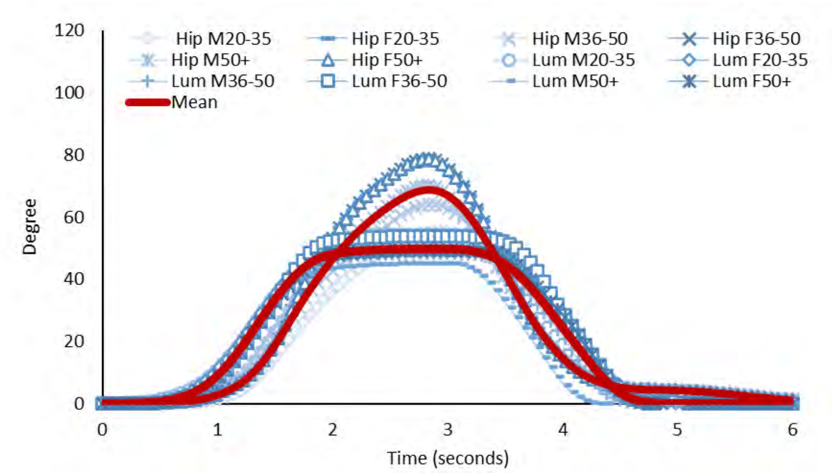

Figure 1: Re-constructed kinematic profiles for different age and sex groups

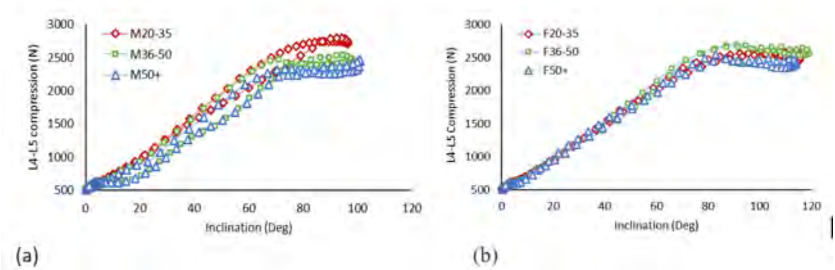

Figure 2: Compressive loads in L4-L5 for full flexion and return cycle in different age and sex groups. (a) Male and (b) Female.

Accuracy of AnyBody Modeling System in predicting ground reaction forces and centers of pressure in lifting activities and effect of the prediction errors on spinal loads

Daroudi S[a], Ismail K[b], Mohseni M[a], El-Rich M[b], Arjmand N[a]

[a]*Department of Mechanical Engineering, Sharif University of Technology, Tehran, Iran*
[b]*Healthcare Engineering Innovation Center, Department of Mechanical Engineering, Khalifa University, Abu Dhabi, United Arab Emirates*

Ground reaction forces (GRFs) and their centers of pressure (CoPs) are essential inputs in musculoskeletal models of the spine that study load-lifting tasks. While GRFs and CoPs are usually measured in vivo via force-plates, they can be predicted based on motion equations, developed in AnyBody Modelling System (AMS) thus eliminating the need for laboratory equipment and in vivo measurements [1,2]. For lifting tasks, this method is only evaluated in a limited number of tasks for normal-weight participants (BMI<25 kg/m2) [3]. We aim to evaluate the accuracy of this algorithm for both normal- and over-weight (BMI>25 kg/m2) individuals during a wide range of lifting tasks. Motion, GRFs and CoPs data were collected from eight normal and four over-weight individuals via a 10-camera Vicon motion capture system and two force-plates. Subjects performed 36 two-handed and 12 one-handed static lifting tasks (Table 1). GRF and CoP values were predicted by AMS (v.7.3) driven by in vivo motion data. Subject-specific bottom-top OpenSim (v.3.2) musculoskeletal models were also driven using both the predicted and measured GRFs/CoPs [4,5] to compare the predicted L5-S1 loads as AMS uses a top-down approach to predict spinal loads. The predicted and measured GRFs/CoPs were compared using t-tests, root-mean-square-errors (RMSEs), and normalized (by in vivo mean values) RMSEs (nRMSE) (Table 2). No significant difference was found between the measured and predicted GRFs/CoPs except for the mediolateral (Fx) and anteroposterior (Fy) GRFs. Such differences were likely due to the small magnitudes of the GRFs in these directions. Moreover, preliminary results of one normal-weight and one over-weight individuals indicated no significant difference between their L5-S1 loads when their musculoskeletal models were driven by either the predicted or measured GRFs/CoPs (Table 2). In conclusion, AMS GRF/CoP prediction algorithm appears to be a robust tool when simulating lifting of both normal- and over-weight individuals.

[1] Fluit R et al., J. Biomech. 2014 (47), 2321–29.
[2] Skals S et al., Multibody Syst. Dyn. 2017 (39), 175-95.
[3] Larsen F et al., Ann. Biomed. Eng. 2020 (48), 805-21.
[4] Favier C et al., Comput. Methods Biomech. Biomed. Engin. 2021 (24), 1310-25.
[5] Delp S et al., IEEE Trans. Biomed. Eng. 2007 (54), 1940-50.

<table>
<tr><th>Group</th><th>Number of subjects</th><th>BMI (kg/m²)</th><th>Body weight (kg)</th><th>Body height (cm)</th><th>Age (years)</th></tr>
<tr><td>Normal-weight</td><td>8</td><td>22.8±2</td><td>71.2±7.3</td><td>175.2±5.8</td><td>24.3±1.7</td></tr>
<tr><td>Over-weight</td><td>4</td><td>27.8±1.1</td><td>92.6±5.6</td><td>182.3±6.2</td><td>24.2±3.2</td></tr>
<tr><th colspan="2">Task parameters</th><th colspan="2">Number of levels</th><th colspan="2">Levels</th></tr>
<tr><td colspan="2">Hand-load horizontal distance</td><td colspan="2">2</td><td colspan="2">~30 and 60 cm from the feet</td></tr>
<tr><td colspan="2">Hand-load vertical distance</td><td colspan="2">2</td><td colspan="2">~0 and 30 cm from the floor</td></tr>
<tr><td colspan="2">Load asymmetry angle</td><td colspan="2">3</td><td colspan="2">0, 45°, and 90° from the sagittal plane</td></tr>
<tr><td colspan="2" rowspan="2">Lifting technique</td><td colspan="2">1 (for one-handed tasks)</td><td colspan="2">stoop </td></tr>
<tr><td colspan="2">3 (for two-handed tasks)</td><td colspan="2">stoop, semi- and full-squat </td></tr>
<tr><td colspan="2" rowspan="2">Total number of tasks</td><td colspan="2">12 one-handed tasks</td><td colspan="2" rowspan="2">48 tasks</td></tr>
<tr><td colspan="2">36 two-handed tasks</td></tr>
</table>

Table 1: Subjects' characteristics (mean±SD) and considered lifting activities for the data collection with an illustration of one- and two-handed lifting activities.

Group	Target		Mean values In-Vivo	Mean values Predicted	RMSE	n-RMSE %	p-value
Normal-weight	GRFs (N)	Fx	21.2	22.6	16.6	78.3	**0.002**
		Fy	15.4	23.2	15.1	98.2	**0.000**
		Fz	440.3	465.8	37.3	8.5	0.294
	CoPs (mm)	CoPx	146	143	17.6	12.0	0.070
		CoPy	149	153	21.1	14.1	0.521
	L5-S1 compression		1363	1388	61.5	4.5	0.804
	L5-S1 shear		525	522	28.2	5.4	0.927
Over-weight	GRFs (N)	Fx	33.6	28.9	19.4	57.7	**0.030**
		Fy	24.5	22.7	14.2	58.0	**0.025**
		Fz	520.2	575.2	36.4	7.0	0.221
	CoPs (mm)	CoPx	143	161.8	15.9	11.1	0.090
		CoPy	152	146.0	26.4	17.4	0.455
	L5-S1 compression		1699	1860	212.2	12.5	0.197
	L5-S1 shear		530	532	87.88	16.6	0.756

Table 2: Mean (in vivo and predicted values), p-values, RMSEs and nRMSEs of GRFs (N), CoPs (mm), L5-S1 compression, and shear loads (N) (based on measured GRFs/CoPs) for normal-weight and overweight groups. Bold values indicate a significant difference (p<0.05).

Comparison of the loads at L4-L5 predicted by the AnyBody and OpenSim full musculoskeletal models

Jiang Z[a], Bassani T[b], Galbusera F[c], Qian Z[a]

[a]*Key Laboratory of Bionic Engineering, Jilin University, Changchun, China*
[b]*IRCCS Istituto Ortopedico Galeazzi, Milan, Italy*
[c]*Spine Center, Schulthess Clinic, Zurich, Switzerland*

AnyBody and OpenSim are two musculoskeletal analysis tools used in biomechanical research. Both systems include musculoskeletal models of the whole human body that, while can be customized by the user, are also frequently used “off-the-shelf”. Regarding the lumbar spine, the stock AnyBody model was validated in a previous study [1] with respect to in vivo pressure measurements in the L4-L5 intervertebral disc [2]. A similar validation is not available for the OpenSim model, as well as a quantitative comparison of the results obtained with the two tools. The objective of this study was then to validate OpenSim regarding the L4-L5 disc pressures for 11 specific motion patterns and to compare the performance of the model with that of the AnyBody model [1].

A male subject (age: 23yrs, height: 172 cm, weight: 72 kg) was instructed to perform 11 motion patterns, 5 of which involving external loads (see Table 1); each pattern was repeated ten times. Three-dimensional motion measurements were conducted with an 8-camera infrared system (Vicon MX) to obtain the kinematic and kinetic data, in order to drive the full body musculoskeletal model. The axial force acting at the L4-L5 level was then predicted with the default lumbar OpenSim model [3], and the pressures were then estimated employing a correction factor (CF) as well as a quadratic equation (QE) [1].

While the predictions of OpenSim and AnyBody models generally agreed between each other and with the in vivo measurements [2], some notable differences could be observed (Figure 1). In particular, the OpenSim model provided more realistic estimations regarding lateral bending and fingers to floor, while Anybody results were generally closer to the in vivo values in tasks involving carrying or lifting a load.

Both OpenSim and AnyBody models are capable of providing realistic estimations of the intradiscal pressure at L4-L5 during various activities. An interesting observation is that in none of the load-bearing motion patterns OpenSim performed better than AnyBody, while in the other tasks the OpenSim predictions tended to be closer to the in vivo measurements with respect to the AnyBody model.

[1] Bassani T, Stucovitz E, Qian Z, Briguglio M, Galbusera F. Validation of the AnyBody full body musculoskeletal model in computing lumbar spine loads at L4L5 level. J Biomech. 2017;58:89-96.
[2] Wilke H, Neef P, Hinz B, Seidel H, Claes L. Intradiscal pressure together with anthropometric data--a data set for the validation of models. Clin Biomech. 2001;16 Suppl 1:S111-26.
[3] Christophy M, Faruk Senan NA, Lotz JC, O'Reilly OM. A musculoskeletal model for the lumbar spine. Biomech Model Mechanobiol. 2012;11(1-2):19-34.

I	II	III	IV	V	VI	VII	VIII	IX	X	XI
standing	flexion-extension	lateral bending	axial rotation	fingers to floor	lifting load knees extended	arms at chest holding load	arms extended holding load	squat lifting load	walking	walking carrying load

Table 1: Motion patterns considered in the study. The red arrows indicate the patterns including load bearing.

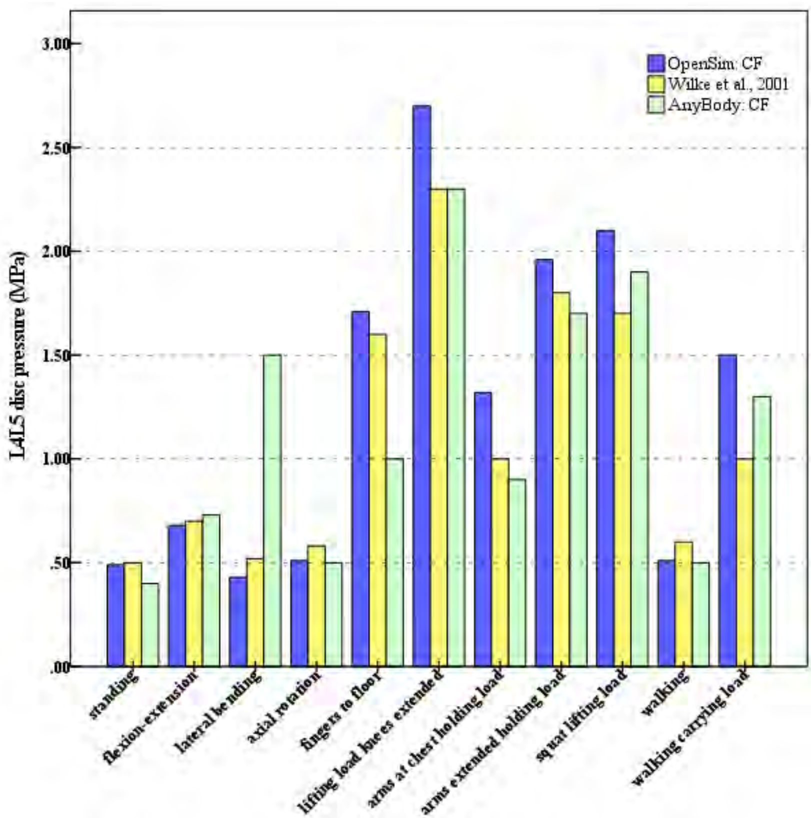

Figure 1: The pressures of L4L5 disc calculated with OpenSim in our study (using a correction factor) and with AnyBody in [1], and the L4L5 disc pressures measured in vivo by [2] in 11 motion patterns.

Validity of evaluating dynamic spine loads without participant-specific measured kinematics

Yan C[a,b], Lynch AC[a], Alemi MM[a,b], Banks JJ[a,b], Bouxsein ML[a,b], Anderson DE[a,b]

[a]*Center for Advanced Orthopaedic Studies, Beth Israel Deaconess Medical Center, Boston, MA, USA*

[b]*Department of Orthopedic Surgery, Harvard Medical School, Boston, MA, USA*

Musculoskeletal models are commonly used to estimate in vivo spinal loads, typically with participant-specific measured kinematics (PSMK) applied to participant-specific models. However, obtaining PSMK data can be costly and infeasible in large studies or clinical practice.

Eleven healthy older men and women, ages 50 to 85 years, performed five dynamic tasks while undergoing motion analysis: 2-hand axial lift, 2-hand sagittal lift, 1-hand sagittal lift, 1-hand lateral lift, and 2-hand window opening simulation. Spinal loads were evaluated using several kinematic inputs (Figure 1) including PSMK trials, ensemble average kinematics (EAK) based on kinematics from all participants, and separately measured individual kinematics (SMIK) from multiple other participants. The dynamic spine loading patterns (Figure 2) and peak loads at T8, T12, and L5 levels were analyzed to assess whether EAK and SMIK differed from PSMK.

Average root mean square errors of EAK and SMIK methods versus PSMK ranged from 18 to 68% body weight for compressive loads and from 5 to 25% body weight for shear loads, with cross-correlations ranging from 0.977 to 0.996. The root mean square errors and cross-correlations between repeated PSMK trials fell within the same ranges. Compressive peak loads evaluated by EAK and SMIK were different than PSMK(I) in only 3 of 15 comparisons (3 levels x 5 activities), and repeated PSMK trials were different in only 2 of 15 comparisons. No differences were found in peak shear loads.

Spine loading magnitudes and temporal profiles using EAK or SMIK produced similar spine loads to PSMK, and notably errors were not larger than between repeated PSMK trials. Thus, appropriate alternate kinematics applied to participant-specific models may produce reasonable estimates of dynamic spinal loading. This could enable increased use of musculoskeletal modeling to estimate spine loading in large population-based studies, clinical research, or clinical practice.

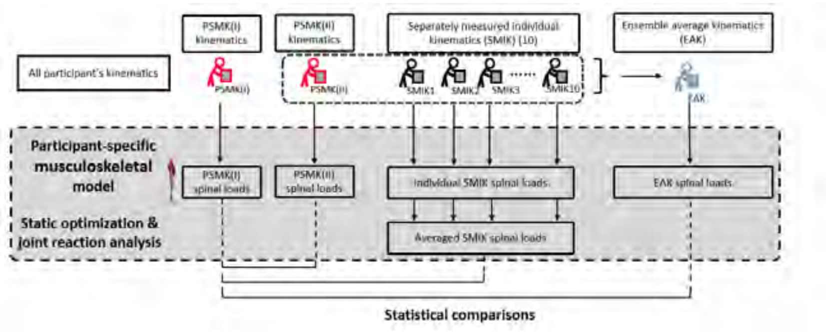

Figure 1: Data processing and analysis flowchart. For a given participant-specific model, there were 13 kinematics inputs used to estimate spine loading via static optimization: PSMK(I), PSMK(II), 10 SMIK and 1 EAK. EAK was an average of kinematics from all subjects. An average SMIK spinal load was generated from the 10 SMIK spinal loads. Statistical analyses were performed comparing PSMK(I) vs. PSMK(II), SMIK, and EAK spinal loads.

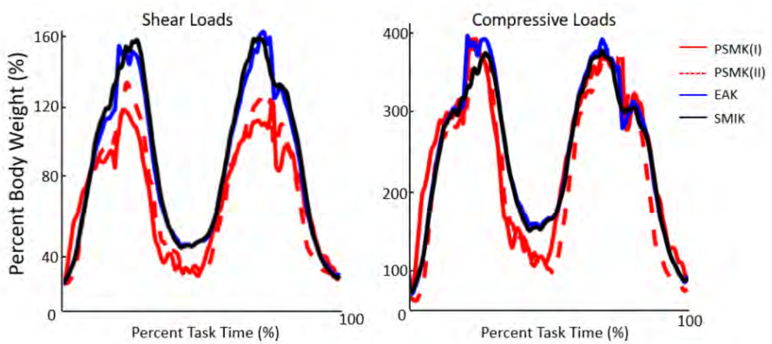

Figure 2: Example of shear and compressive spinal loads at L5 vertebral level during 2-hand sagittal lifting and lowering task, based on participant-specific measured kinematics (PSMK), ensemble average kinematics (EAK), and separately measured individual kinematics (SMIK).

Variation in cervical spine loads during isometric extension in a neutral posture

Arshad R[a], Schmidt H[b], El-Rich M[c], Moglo K[a]

[a]*Biomechanics Laboratory, Department of Mechanical and Aerospace Engineering, Royal Military College of Canada, Kingston, ON, Canada*

[b]*Julius Wolff Institute, Charité – Universitätsmedizin Berlin, Germany*

[c]*Healthcare Engineering Innovation Center, Department of Mechanical Engineering, Khalifa University, Abu Dhabi, United Arab Emirates*

In healthy individuals, the cervical spine response during isometric loading may differ due to inter-individual differences in neck muscle size, muscle strength, or spine segment stiffness [1]. Quantification of differences in cervical loads may facilitate improving non-invasive or invasive interventions. Therefore, the purpose of this study was to estimate the variation in compressive loads during isometric extension in a neutral posture.

A previously developed musculoskeletal model for a 50th percentile male was used to simulate isometric extension in a neutral posture [2]. A horizontal external load of 248 N estimated as an isometric strength (50th percentile male) [3] was applied. The parameters (Table 1): physiological cross sectional area (PCSA) varied from 1 to 2 times, specific muscle strength (MS) from 30 to 120 N/cm2 and intact segment stiffness from 100-300 N/mm (anterior shear) and 1000-2000 N/mm (compression).

Variation of the compressive loads was in the range of 8 to 14%. Estimated compressive loads from the current study were comparable with Moroney et al. (1988) and Van den Abbeele et al. (2018), at C4C5 level [1,4]. While the moment applied at C4C5 level (25.9 to 27 Nm) were almost similar in these studies, the estimation from Fréchède et al. (2020)[4] was significantly lower (353N) as compared to others [1,5] and the current study (948-1148N). ¬

Establishing variability in biomechanical response of healthy population is essential to improve spine care interventions. Here, the differences in cervical loads estimated during isometric extension were notable. Further, to estimate the variations in other loading direction, motion, and possible interaction effects among parameters, we aim to extend the study to isometric flexion, lateral bending, and axial rotation.

[1] Moroney SP, Schultz AB, Miller JAA. Analysis and measurement of neck loads. J Orthop Res 1988;6:713–20. doi:10.1002/jor.1100060514.
[2] Arshad R, Schmidt H, El-rich M, Moglo K. Sensitivity of the Cervical Disc Loads , Translations , Intradiscal Pressure , and Muscle Activity Due to Segmental Mass , Disc Stiffness , and Muscle Strength in an Upright Neutral Posture. Front Bioeng Biotechnol 2022;10:1–11. doi:10.3389/fbioe.2022.751291.
[3] Roos PE, Vasavada A, Zheng L, Zhou X. Neck musculoskeletal model generation through anthropometric scaling. PLoS One 2020;15:1–21. doi:10.1371/journal.pone.0219954.
[4] Fréchède B, Kamalifard R, Dumas R. Distribution of intervertebral compression and shear forces in the cervical spine during isometric tasks. Comput Methods Biomech Biomed Engin 2019;22:S180–2. doi:10.1080/10255842.2020.1714232.

[5] Van den Abbeele M, Li F, Pomero V, Bonneau D, Sandoz B, Laporte S, et al. A subject-specific biomechanical control model for the prediction of cervical spine muscle forces. Clin Biomech 2018;51:58–66. doi:10.1016/j.clinbiomech.2017.12.001.

Variable	PCSA	MS	CS	SS
Variation levels	*4*	*10*	*3*	*3*

Table 1: Design table for 324 simulation tests. CS (segment compressive stiffness), SS (shear stiffness).

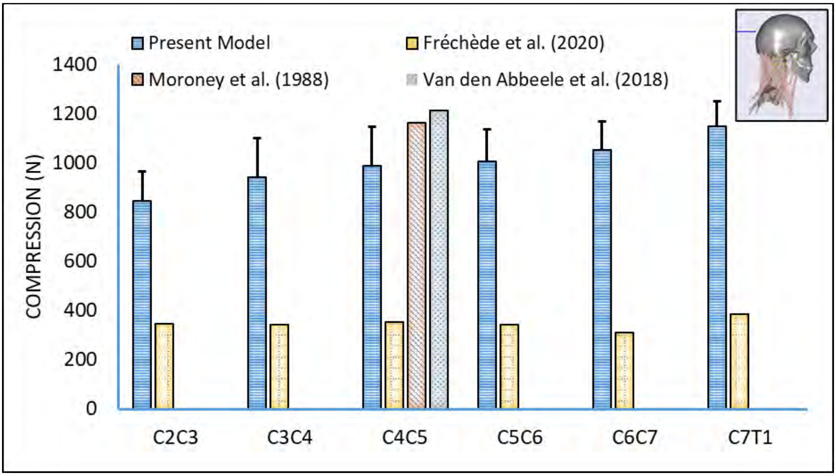

Figure 1: Range of compressive force at C2C3 to C7T1 level during isometric extension.

Integrated subject-specific Finite Element Musculoskeletal Model of trunk with ergonomic and clinical applications

Ghezelbash F[a], Eskandari AH[b], Shirazi-Adl A[c], Larivière C[b]

[a]*EERS Global, Montréal, Canada*

[b]*Institut de recherche Robert-Sauvé en santé et en sécurité du travail, Montréal, Canada*

[c]*Department of Mechanical Engineering, Polytechnique Montréal, Montréal, Canada*

Biomechanical models of the trunk incorporate either passive finite element (FE) spine models, or active components using multi-body musculoskeletal (MS) models. Passive FE models accurately represent the spine while overlooking muscles. Conversely MS models, often simplify the spine and overlook model individualization. Here, we developed a novel subject-specific coupled detailed FE-MS model of the trunk and explored its applications in ergonomics and surgical interventions.

A parametric detailed FE model was constructed (Figure 1a) and integrated with a muscle architecture. The active-passive model was individualized based on imaging datasets and statistical shape models. To validate the model, we compared the responses of the annulus fibrosus and ligamentous spine against experiments, along with estimated muscle activities and intradiscal pressures with in vivo measurements. Also, we evaluated the performance of the model in ergonomics (i.e., passive exoskeleton; Figure 2a) and selected interventions (nucleotomy and spinal fusion).

The model had a satisfactory performance in predicting the responses at tissue-level, disc-level, entire passive lumbar spine (Figure 1b), intradiscal pressure (Figure 1c) along with muscle activity. Wearing an exoskeleton reduced intradiscal pressure (1.9 versus 2.2 MPa; Figure 2b) and maximum tensile stress in the annulus fibrosus (2.6 versus 3.9 MPa at L5-S1 disc) during forward flexion. Spinal fusion (L4-L5 segment) increased the intradiscal pressure in the upper adjacent disc, but nucleotomy had a minimal effect on the estimated intradiscal pressures. Nucleotomy substantially affected the load transfer by increasing facet contact stresses at the same level (Figure 2c).

Unlike conventional MS models with simplified spine, and in contrast to passive models (overlooking active components); here, we developed a detailed coupled FE-MS model which was individualized by novel scaling algorithms. This framework provides new outputs such as strain/stress fields in discs/facets (essential for a comprehensive risk analysis) and realistically simulates various surgical procedures in identifying their effects on active-passive responses.

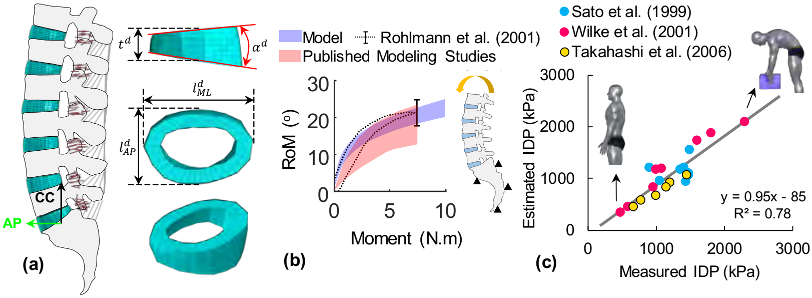

Figure 1: (a) Parametric finite element model of the lumbar spine. Predicted (b) range of motion (RoM) and (c) intradiscal pressures (IDP) versus experiments.

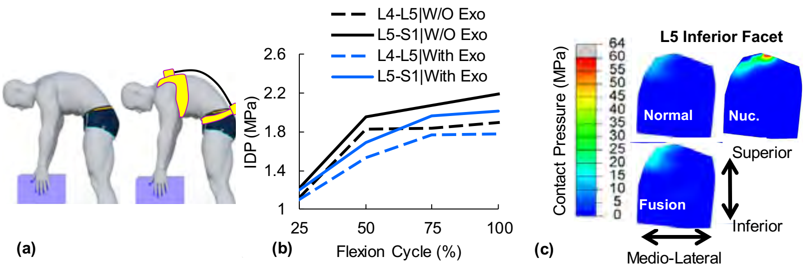

Figure 2: The effects of using an (a) exoskeleton on (b) intradiscal pressures during forward flexion. (c) The effects of different surgical interventions on facet contact stresses of the L5 inferior facet in forward flexion with 10 kg hand-load.

On the use of normatisation for group-level analysis of spine loads

Howarth SJ[a], Zehr J[b], Beach TAC[b], Graham RB[c]

[a]Division of Research and Innovation, Canadian Memorial Chiropractic College, Toronto, Canada
[b]Faculty of Health, University of Waterloo, Waterloo, Canada
[c]Faculty of Health Sciences, University of Ottawa, Ottawa, Canada

A biomechanics-related example of normalisation is the division of joint loading estimates (dependent variable) by body mass (confounder) to control for potential differences in the confounder between groups (sexes); however, the ratio is only useful, statistically, if the relationship between the numerator and denominator is a straight line passing through zero. This proof-of-principle used a subset of previously published data to demonstrate a more valid approach for statistically analysing lumbosacral joint loads if normalisation is being considered. Eight male and eight female participants completed 10 contiguous lifts using a self-selected pace and style. Lumbosacral reaction kinetics were calculated using a bottom-up inverse dynamical linked-segment model. Joint compressive and shear forces were quantified by combining the reaction forces with a decomposition of the net muscle force using a single-equivalent muscle model. Peak joint shear force and the peak reaction moment for each participant were normalised by body mass. Two normalised representations of peak joint compressive force were determined, one with respect to body mass and the other to predicted joint compressive strength. Normalised lumbosacral loads were compared between sexes by t-tests. Analyses of covariance with body mass as a covariate compared absolute lumbosacral loads between sexes. Decisions of statistical significance between sexes were the same for absolute and normalised representations of the lumbosacral joint shear, reaction moment and joint compression (compressive strength normalised) (Table 1). Body mass normalised joint compression was not statistically different between males and females ($p=0.051$); however, the analysis of covariance revealed a difference between sexes for absolute joint compression ($p=0.019$). This proof-of-principle demonstrated that statistical interpretation of lumbosacral joint loads can be affected by normalisation. Relevance of this proof-of-principle will be further elucidated by using larger datasets. Investigators should carefully consider their research question and examine their data to determine whether normalisation is necessary.

	Height (m)	Mass (kg)	Age (y)	COMPRESSION Strength (N)	COMPRESSION Abs (N)	COMPRESSION Norm (N/kg)	COMPRESSION Norm (N/N)	SHEAR Abs (N)	SHEAR Norm (N/kg)	MOMENT Abs (N)	MOMENT Norm (Nm/kg)
MALE	1.89	99.6	19	11598	3989	40.1	0.34	1124	11.3	183	1.84
	1.73	76.1	24	9354	3015	39.6	0.32	847	11.1	135	1.77
	1.87	83.6	24	9953	3959	47.4	0.40	672	8.0	168	2.01
	1.81	75.4	23	9372	3726	49.4	0.40	620	8.2	153	2.03
	1.75	68.6	19	9124	3079	44.9	0.34	685	10.0	136	1.98
	1.78	70.1	24	8875	3334	47.6	0.38	737	10.5	144	2.05
	1.80	84.3	22	10156	3682	43.7	0.36	539	6.4	153	1.81
	1.78	78.3	22	9677	3428	43.8	0.35	720	9.2	151	1.93
FEMALE	1.64	53.8	25	6538	2357	43.8	0.36	491	9.1	96	1.78
	1.77	72.8	23	8202	2602	35.7	0.32	596	8.2	102	1.40
	1.60	61.5	21	7448	2146	34.9	0.29	458	7.4	82	1.33
	1.62	72.2	22	8228	2592	35.9	0.32	790	10.9	105	1.45
	1.65	70.1	29	7544	3085	44.0	0.41	546	7.8	114	1.63
	1.55	50.3	22	6480	2293	45.6	0.35	410	8.2	84	1.67
	1.56	76.5	22	8571	2381	31.1	0.28	496	6.5	95	1.24
	1.64	83.4	19	9343	3734	44.8	0.40	456	5.5	116	1.39
$\bar{X}_M$	1.80	79.5	22.1	9764	3527	44.6	0.36	743	9.3	153	1.93
s_M	0.06	9.9	2.1	852	373	3.5	0.03	178	1.7	16	0.11
$\bar{X}_F$	1.63	67.6	22.9	7794	2649	39	0.34	530	8.0	99	1.49
s_F	0.07	11.4	3.0	989	522	6	0.05	119	1.6	13	0.19
p					**0.019** 0.401*	**0.051**	0.333	0.119	0.122	<0.001	<0.001

Table 1: Participant demographics, estimated compressive strength, joint compression, joint shear and reaction moment. P-values for “Abs” are from analyses of covariance comparing male (M) and female (F) data with either mass or compressive strength (*) as the covariate. P-values for “Norm” are 2-sample t-tests comparing male and female data. Boldfaced p-values denote where differences of statistical interpretation occur between the “Abs” and “Norm” dependent measures.

Abstracts Poster

P1 **Degenerative changes in biomechanics, gene expression, and composition of intervertebral disc: 8 week animal study**
Yalda Alibeigian

P2 **Spine loading in male and female during dynamic flexion and return to the standing posture**
Rizwan Arshad

P3 **Segmentation of vertebrae in MRI data of the German National Cohort**
Cagdas Aslan

P4 **Effects of non-extensible lumbar belts on static and dynamic postural stability**
Jingyuan Bai

P5 **Analysis of the degree of mechanical wear in the transpedicular stabilization of the spine**
Małgorzata Żak

P6 **The impact of velocity and motion planes on lumbar time-varying muscle synergies during trunk flexion**
Mehrdad Davoudi

P7 **Pure bending stiffness in a fully 3D printed L1-S1 lumbar spine model**
Siril Teja Dukkipati

P8 **Pullout strength of thoracic spine pedicle screws inserted by freehand or patient-specific drill guides; a finite element analysis**
Fahimeh Hosseini

P9 **Effect of upper body mass distribution and thorax flexibility on spinal loads prediction in upright and flexed posture using personalized musculoskeletal models**
Abdul Aziz Vaqar Hulleck

P10 **Body mass distribution along the spine affects biomechanics of spinal sagittal alignment**
Dominika Ignasiak

P11 **Mechanical testing of lumbar cadaveric muscle and thoracolumbar fascia suggests evidence towards physiological stress shielding of musculoskeletal soft tissues**
Emily Newell

P12 **Coupled MBS and FEM models of the lumbar spine – unidirectional vs. bidirectional co-simulation**
Kati Nispel

P13 **Approximate facet area and volume of convex polytope satisfying equilibrium conditions during spinal muscular exertions as new additional candidates for neuromuscular strength of spine,** Mahdi Parnianpour

P14 **Methods of evaluating mechanical parameters and the stability of the cervical interbody fusion cage**
Celina Pezowicz

P15 **Biomechanical simulation of the upper body in different sitting positions**
Maximilian Praster

P16 **How can we capture back health? Association between self-reported and objectively measured back health among sedentary office workers**
Antje Reschke

P17 **Effect of DLC coating of growth-guidance system implants on changes in mechanical and kinematic properties of the spine**
Sylwia Szotek

P18 **Comparison of load-sharing and axis of rotation in generic and individualised neuromusculoskeletal models of the spine**
Robert Rockenfeller

Degenerative changes in biomechanics, gene expression, and composition of intervertebral disc: 8 week animal study

Alibeigian Y[a], Hosseini S[a,b], Ghezelbash F[c]

[a]*Department of Stem Cells and Developmental Biology, Cell Science Research Center, Royan Institute for Stem Cell Biology and Technology, ACECR, Tehran, Iran*
[b]*Department of Cell Engineering, Cell Science Research Center, Royan Institute for Stem Cell Biology and Technology, ACECR, Tehran, Iran.*
[c]*EERS Global, Montréal, Canada*

Mechanical damage to an intervertebral disc can initiate a chain of events, leading to disc degeneration and pain. Disc damage (such as puncture) and degeneration can alter tissue structure, composition and therefore its material properties. Therefore, the aim of this study is to investigate the effects of disc degradation on mechanical properties of the annulus fibrosus and bony endplates and their likely relationship with biochemical composition.

A rabbit model of disc degeneration was created by puncturing an intervertebral disc in an ultrasound-guided surgery (Figure 1a). After 8 weeks, disc degeneration was evaluated by using magnetic resonance (MR) imaging. In order to investigate the effects of degeneration on material properties, we carried out various mechanical tests on the annulus fibrosus (peeling and uniaxial tension) as well as endplates (three-point bending). In addition, the gene expression of bone and cartilage genes as well as calcium content and insoluble collagen were measured to assess the effects of degeneration of tissue calcification and collagen cross linking.

MR images confirmed the degeneration state in rabbit discs after 8 weeks. Mechanical tests showed a slight decrease in mechanical peeling strength (0.52 versus 0.48 N/mm; Figure 2). Failure flexural stress of healthy bony endplates was measured at ~43 MPa. The expression of alkaline phosphatase, osteocalcin and collagen II genes increased significantly in degenerated discs compared to healthy ones. Due to degeneration, calcium content increased (indicating the start of endplate calcification) and the amount of insoluble collagen was decreased, and this could indicate reduction in cross-link density in the degenerated discs.

The rabbit model of disc degeneration demonstrated alterations in the biochemical composition of the annulus fibrosus and end plate, potentially affecting mechanical properties, as indicated by changes in calcium content and collagen cross-linking.

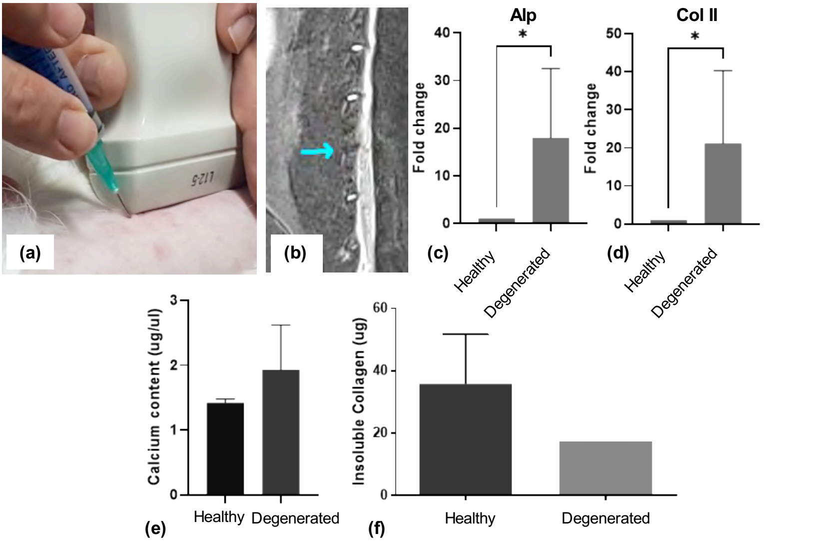

Figure 1: (a) Ultrasound-guided surgery to puncture the disc. (b) MR imaging confirmed disc degeneration (darkened degenerated disc was marked by an arrow). Changes in the gene expression of (c) alkaline phosphatase (Alp), and Collagen II (Col II). (e) Calcium and (f) insoluble collagen content measured at annulus/endplate junction. Asterisk (*) indicates statistical significance (p<0.05).

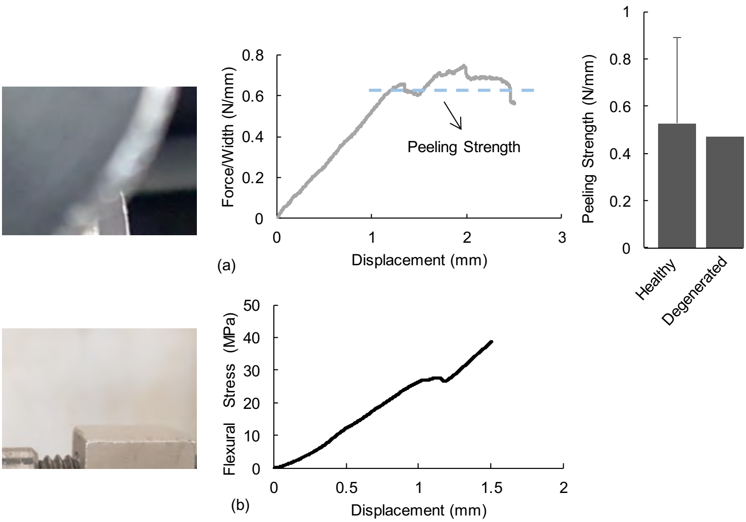

Figure 2: (a) Peeling and (b) three-point bending tests on annulus fibrosus and bony endplates, respectively.

Spine loading in male and female during dynamic flexion and return to the standing posture

Arshad R[a,c], Moglo K[a], El-Rich M[b], Schmidt H[c]

[a]*Biomechanics Laboratory, Department of Mechanical and Aerospace Engineering, Royal Military College of Canada, Kingston, ON, Canada*

[b]*Healthcare Engineering Innovation Center, Department of Mechanical Engineering, Khalifa University, Abu Dhabi, United Arab Emirates*

[c]*Julius Wolff Institute, Berlin Institute of Health at Charité – Universitätsmedizin Berlin, Germany*

Full flexion expose lumbar spine to extensive loading. In dynamic full flexion and return to the standing posture, spine loading varies with spatially and temporally nonlinear kinematics. The study aimed to estimate the lumbar loads in a 50th percentile male and female, by applying nonlinear kinematics for dynamic full flexion and return cycle.

An inverse dynamic musculoskeletal model of a 50th percentile male and female (AMMR ver. 2.2.3, AnyBody Technology A/S, version 7.2.3), was considered. The model anthropometrics and segmental dimensions were adjusted by using linear regression equations [1], whereas distribution of the body mass to individual segments were according to ratios in literature [2]. For dynamic flexion, a single kinematic profile was reconstructed from Epionics SPINE measurement data and used for both sexes [3] (Fig. 1). Compressive loads at T12-L1 and L4-L5 were estimated. Average T12-L1 compressive load was compared with publicly available data (www.orthoload.com) from telemetrized vertebral body replacement [4,5].

For T12-L1, the dynamic loading and unloading pattern was comparable with in vivo measurements (Fig 2). The peak values were higher (≅ 50 %) and the occurrence of peak load was later than in vivo measurements (38% vs 34% of flexion and return cycle). At maximum forward flexion the estimated as well as in vivo loads were less than peak loads. The difference between in silico and in vivo measure was about 65%. The peak loads were higher in male (T12-L1: 1637 N and L4-L5: 2435 N) than female (T12-L1: 1350 N and L4-L5: 2046 N), during return phase of the cycle.

Initial results showed loading and unloading of the lumbar spine comparable to in-vivo measurements. The estimated peak loads in healthy population were higher from in vivo measurements in patients with vertebral body replacement. In addition, sex differences in compressive loads were estimated with male having compressive loads higher than female.

[1] Peebles L, Industry GBD of T and, Norris B. Adultdata: The Handbook of Adult Anthropometric and Strength Measurements : Data for Design Safety. Department of Trade and Industry; 1998.

[2] Winter DA. Biomechanics and Motor Control of Human Movement. John Wiley & Sons, Inc.; 2009.

[3] Pries E, Dreischarf M, Bashkuev M, Putzier M, Schmidt H. The effects of age and gender on the lumbopelvic rhythm in the sagittal plane in 309 subjects. J Biomech 2015;48:3080–7. doi:10.1016/j.jbiomech.2015.07.030.

[4] Graichen F, Arnold R, Rohlmann A, Bergmann G. Implantable 9-channel telemetry system for in vivo load measurements with orthopedic implants. IEEE Trans Biomed Eng 2007;54:253–61. doi:10.1109/TBME.2006.886857.

[5] Rohlmann A, Gabel U, Graichen F, Bender A, Bergmann G. An instrumented implant for vertebral body replacement that measures loads in the anterior spinal column. Med Eng Phys 2007;29:580–5. doi:10.1016/j.medengphy.2006.06.012

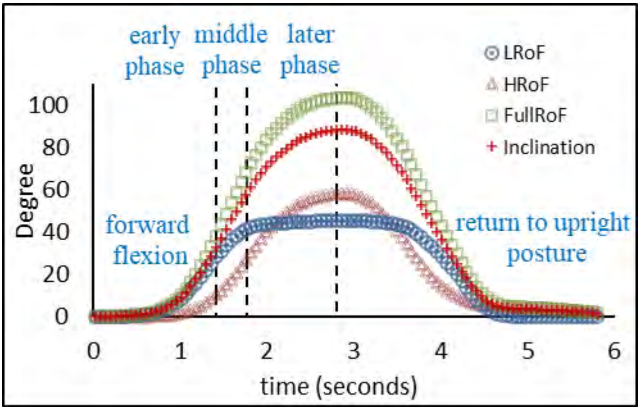

Figure 1: Dynamic flexion and return cycle. LRoF: Lumbar range of flexion, HRoF: Hip range of flexion, FullRoF: full range of flexion.

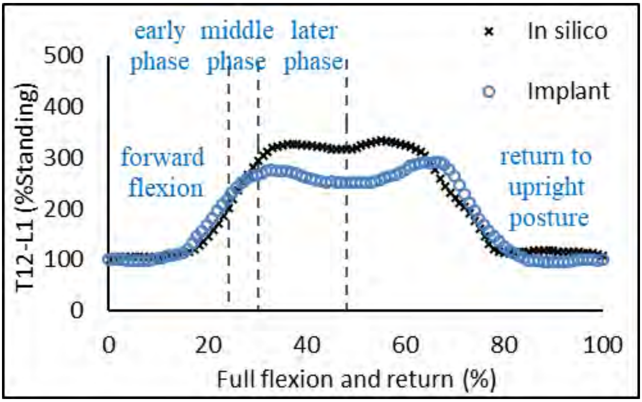

Figure 2: Average T12-L1 compressive load for dynamic full flexion and return cycle..

Segmentation of vertebrae in MRI data of the German National Cohort

Aslan C[a], Arias-Lorza AM[a], Becker L[b], Taheri N[b], Zachow S[a]

[a]*Visual and Data-Centric Computing, Zuse Institute Berlin (ZIB), Berlin, Germany*
[b]*Julius Wolff Institute, Charité – Universitätsmedizin Berlin, Germany*

A large population analysis of the spinal morphology is a prerequisite to identify and establish biomarkers for spinal diseases, which is one of the reasons the German National Cohort (GNC) has been established [1]. In order to conduct an in-depth analysis of the spinal morphology, a large database of segmented spines is needed. In this work, we evaluated the feasibility of an AI-based algorithm to segment spinal structures in the complete GNC-MRI spine database.

The GNC spinal sub-database is comprised of sagittal T2w-MRI of at least 30 000 subjects covering the full spine with an in-plane resolution of 0.86 mm and a slice distance of 3.3 mm. In order to automatically segment the spine, we utilize the nnU-Net algorithm [2], which is a self-configuring deep learning-based biomedical image segmentation method leading the board of several biomedical segmentation challenges. Based on five manually labeled binary classifications, we trained a first nnU-Net to create 16 additional pseudo-labels, which is a method to increase the amount of data artificially. We then trained a second nnU-Net on the resulting 21 segmentations and evaluated the algorithmic segmentation results for all 21 subjects applying a five-fold cross-validation.

We show that the nnU-Net achieves a median dice score of 0.966 (Min: 0.905, Max: 0.998), which measures the overlap between the segmentations of the predicted set and the training set, see Figure 1. Both sets are comprised of single-label annotations.

Our quantitative evaluation of the results indicate that the nnU-Net is capable of segmenting the MRIs from the GNC database. However, due to the highly anisotropic resolution, the image intensity bias, and the noise in the MRI, it is challenging and time consuming to create a training set that contains all smaller spinal structures, such as cervical vertebrae, and/or vertebral processes. Therefore, we aim to create a highly accurate training set for each single vertebra validated by medical experts for the training of an algorithm to then annotate the complete GNC spine database, which will be included in our final submission.

[1] Bamberg F et al. (2015): Whole - Body MR Imaging in the German National Cohort: Rationale, Design, and Technical Background. Radiology 277(1): 206 – 20
[2] Isensee, F et al. (2020). nnU-Net: a self-configuring method for deep learning-based biomedical image segmentation. Nature Methods, 1-9

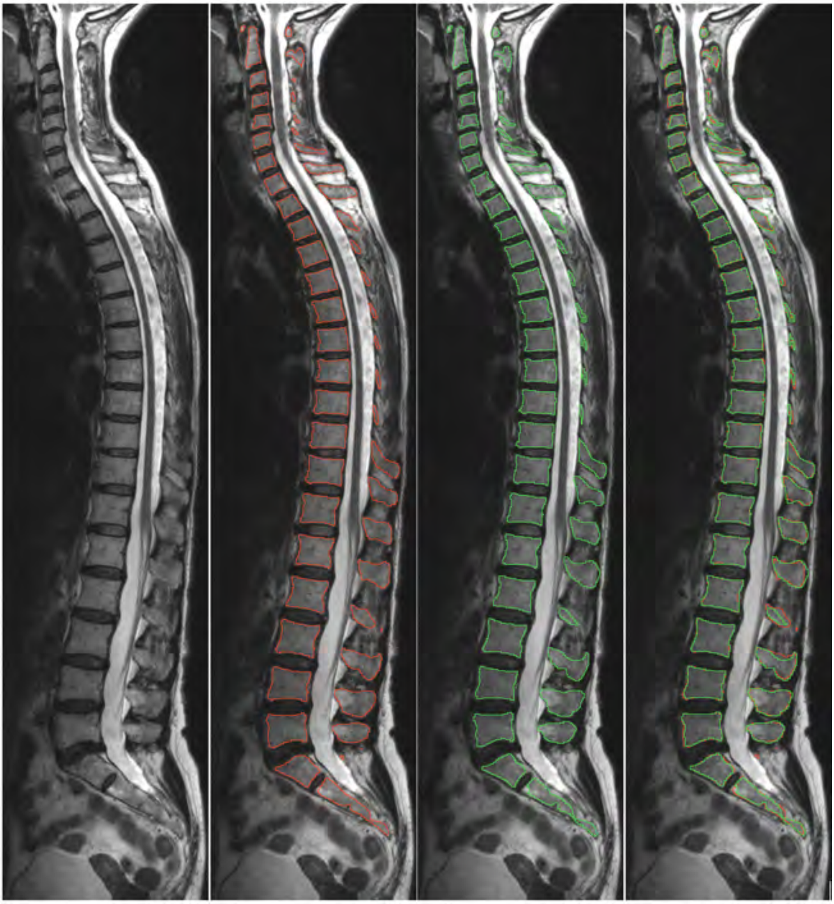

Figure 1: Segmentation result of the nnU-Net for one subject from the cross-validation set. From left to right: Input MRI, MRI and spine prediction overlay (red contours), MRI and manually segmented spine overlay (green contours), MRI and overlay of both (red and green contours).

Effects of non-extensible lumbar belts on static and dynamic postural stability

Jingyuan Bai[a], Jian Wang[a,b]

[a]*Department of Sports Science, College of Education, Zhejiang University, Hangzhou, China*
[b]*Center for Psychological Sciences, Zhejiang University, Hangzhou, China*

Previous studies have shown that increased intra-abdominal pressure can help reduce spinal loading and improve spine stability. The use of a non-extensible lumbar belt (NEB) has been suggested as a way to elevate intra-abdominal pressure and enhance spinal stability. The NEB has been utilized in the healthcare field to help alleviate low back pain and improve spine function. However, the impact of the NEB on both static and dynamic postural stability remains unclear. This study aimed to examine the effect of the NEB on static and dynamic postural stability in healthy individuals.

A total of 28 healthy male participants were recruited to complete four static postural stability tasks and a dynamic postural stability test. Center of pressure (COP) values during 30 seconds of quiet standing and dynamic postural stability index (DPSI) with and without the NEB were analyzed.

The NEB had no significant effect in all COP variables in the static postural tasks. The results of a repeated measure two-way ANOVA indicated the NEB significantly improved the dynamic postural stability in YBT score and DPSI ($F_{(1,27)}$ = 5.506, p =.027, ${\eta_p}^2$=.169 and $F_{(1,27)}$ = 83.94, p =.000, ${\eta_p}^2$=.757 respectively).

Our findings suggest that the use of the NEB leads to improved dynamic postural stability in healthy individuals, while having no significant effect on static postural stability.

Parameter	EO		EC		EOMAT		ECMAT	
	Without NEB	NEB	Without NEB	NEB	Without NEB	NEB	Without NEB	NEB
EA	303.8±319.6	314.6±296.3	405.3±351.3	443.7±209.5	970.5±351.4	758.7±599.7	2216.7±1711.4	2106.2±1631.8
	(107.9-420.4)	(112.5-435.9)	(206-554.3)	(272.6-559)	(711.9-1106.4)	(362.3-1095.6)	(1075.7-2786.9)	(1274.2-2665.6)
PL	302.7±78.2	305.6±55.5	417.2±92.1	411.0±90.4	543.3±108.7	517.3±126.8	1123.6±343.9	1136.6±407.4
	(250.2-344.3)	(264.9-344.7)	(350-470)	(363.8-469.8)	(459.7-603.8)	(403.8-586.2)	(897.3-1341.1)	(916.1-1326.5)
ML	1.22±0.35	1.23±0.29	1.65±0.44	1.61±0.44	2.12±0.43	2.13±0.61	4.56±1.30	4.65±1.49
velocity	(0.95-1.49)	(1.00-1.35)	(1.43-1.86)	(1.29-1.91)	(1.81-2.35)	(1.70-2.51)	(3.66-5.19)	(3.69-5.05)
AP	1.32±0.35	1.31±0.24	1.82±0.43	1.81±0.45	2.46±0.54	2.26±0.53	4.89±1.81	4.86±2.08
velocity	(1.08-1.57)	(1.12-1.40)	(1.54-2.03)	(1.57-2.21)	(2.01-2.94)	(1.81-2.68)	(3.89-5.52)	(3.63-5.74)

The values of all parameters are presented as man ± standard deviation followed by 1st quartile and 3rd quartile in brackets. EO: Eyes open on firm ground; EC: Eyes closed on firm ground; EOMAT: Eyes open with a foam mat; ECMAT: Eyes closed with a foam mat; EA: Elliptical area; PL: Path length of COP trajectory; ML: Mediolateral; AP: Anteroposterior.

Table 1: The results of 28 subjects in four static postural stability tasks.

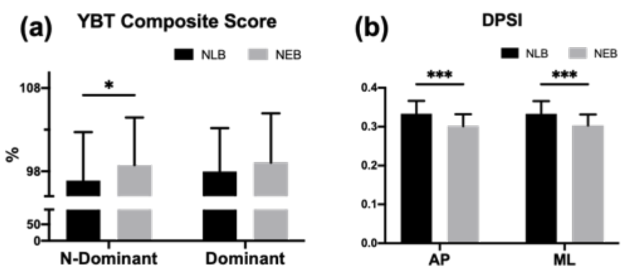

NEB: non-extensible lumbar belt; NLB: no lumbar belt; (a) N-Dominant: non-dominant leg; Dominant: dominant leg; * represents $p < 0.05$. (b) AP: anterior-posterior jump; ML: medial-lateral jump; *** represents $p < 0.001$.

Figure 1: The results of 28 subjects in two dynamic postural stability tasks.

Analysis of the degree of mechanical wear in the transpedicular stabilization of the spine

Szkoda-Poliszuk K[a], Żak M[a], Brończyk A[b], Pezowicz C[a]

[a]*Department of Mechanics, Materials and Biomedical Engineering, Wroclaw University of Science and Technology, Wroclaw, Poland*

[b]*Department of Fundamentals of Machine Design and Mechatronic Systems, Wroclaw University of Science and Technology, Wroclaw, Poland*

One of the innovative solutions for treating scoliosis in children is stabilization systems that allow spinal modeling without the need for revision surgery while allowing uninhibited growth. Designs of such stabilizers use kinematic pairs, allowing the screw to slide along the rod. Unfortunately, friction between the sliding elements of the stabilizer causes wear and tear, resulting in the deposition of titanium alloy particles in the surrounding tissues. Currently, solutions are being sought to eliminate friction products through coatings. The study aimed to assess the mechanical properties and evaluate the frictional wear of a sliding screw-rod connection used in spinal stabilizers.

The tests were carried out for two groups of single sliding kinematic screw-rod pairs made of Ti6Al4V titanium alloy and with diamond-like carbon (DLC) coating, in which the head of the polyaxial bolt was aligned with the axis of the bolt. The established research goal was realized by achieved conducting mechanical tests (100,000 load cycles), microscopic tests and topographic studies of the mating surfaces of the elements of the stabilizer kinematic pair.

Mechanical tests made it possible to determine the average value of the friction force over successive cycles. Analysis of the surface topography made it possible to decide on an isometric map of the surface of the nuts. The amount of tribological wear was determined by measuring the depth of the cavity conducted along profiles at different rubbing heights.

The friction force was shown to increase (from 0N to 14N) with successive cycles for standard implants. For implants with DLC coating, the friction force was smaller and practically constant (from 0N to 4N). As a result of the titanium rod's friction against the nuts' surface, there was surface wear in the contact areas of these elements.

The impact of velocity and motion planes on lumbar time-varying muscle synergies during trunk flexion

Rouchi MB[a], Davoudi M[a,b], Meftahi N[c,d], Shokouhyan SM[a], Parnianpour M[a], Khalaf K[e], Rashedi E[f]

[a]Department of Mechanical Engineering, Sharif University of Technology, Tehran, Iran.
[b]Clinic for Orthopaedics and Trauma Surgery, Heidelberg University Hospital, Heidelberg, Germany.
[c]Physical Therapy Department, School of Rehabilitation Sciences, Shiraz University of Medical Sciences, Shiraz, Iran.
[d]Rehabilitation Sciences Research Center, Shiraz University of Medical Sciences, Shiraz, Iran.
[e]Department of Biomedical Engineering and Health Engineering Innovation Center, Khalifa University, Abu Dhabi, UAE.
[f]Department of Industrial and Systems Engineering, Rochester Institute of Technology, Rochester, NY, USA.

Although the extent of which the central nervous system uses muscle synergies as a movement control strategy remains an open area of research, it is widely agreed that synergies facilitate the robustness of the neuromuscular system, allowing for effective postural control and flexible movement. This work aimed to investigate the muscle activation patterns of the trunk and time-varying muscle synergies using a novel 18-muscle 3-DOF, 3-D musculoskeletal model of the lumbar spine developed by the authors.

24 different biaxial trunk movements were simulated via the optimization of kinetic and kinematic measures towards obtaining the corresponding muscle activation patterns at 3 different velocities. These patterns were subsequently used to extract the principal (phasic and tonic) spatio-temporal synergies associated with the observed muscle activation patterns in the range of simulated movements.

Four dominant synergies were able to explain a considerable percentage (about 75%) of the variance of the simulated muscle activities. The extracted synergies were spatially tuned in the direction of the main simulated movements (flexion/extension and right/left lateral bending). The temporal patterns demonstrated gradual monotonic shifts in tonic synergies and biphasic modulatory components in phasic synergies with spatially tuned time delays. The increase in velocity resulted in an elevated amplitude coefficient and accelerated activation of phasic synergies.

Our results suggest the plausibility of a time-varying synergies strategy in the dynamic control of trunk movement. Further work is needed to explore leveraging these concepts in various applications, such as rehabilitation and musculoskeletal biomechanics, towards providing more insight into the mechanisms underlying trunk stability and flexibility.

Pure bending stiffness in a fully 3D printed L1-S1 lumbar spine model

Dukkipati ST[a,b], Driscoll M[a,b]

[a]*Musculoskeletal Biomechanics Research Lab, Department of Mechanical Engineering, McGill University, 817 Sherbrooke St. W, Montréal, QC H3A 0C3, Canada*

[b]*Orthopaedic Research Laboratory, Research Institute MUHC, Montreal General Hospital, 1650 Cedar Ave, LS1.409, Montréal, QC H3G 1A4, Canada*

Traditional spine biomechanical studies employ either cadavers or finite element (FE) modelling techniques, both of which have their respective limitation in cost and time. Cadaveric studies introduce high variability in measurements across patients. FE models are computationally demanding depending on model level of detail. Validated analogue spine models complement these conventional methods with low cost and high fidelity.

An L1-S1 analogue model of the spine was developed consisting of vertebral bodies, intervertebral discs with intertransverse and interspinous ligaments. Stereolithography 3D printing was solely employed to manufacture these models. The soft tissues and the vertebrae were printed using Flexible 80A and Durable resins (Formlabs, USA). The model was subjected to a load-controlled pure bending moment up to 7.5Nm in flexion-extension (F-E), lateral bending (LB), and axial rotation (AR) with a custom bending jig (Instron Electroplus E10000, USA). Rotation of motion (ROM) was recorded to plot model rotational stiffness. Results were compared to historic in vivo L1-S1 data.

The viscoelastic nature of the underlying materials in the model construction resulted in a hysteretic response under loading and unloading much like a human spine. At +7.5Nm flexion, the model ROM was 12.92±0.11° (in vivo: 16.58°[1]). In LB and AR, the model exhibited left-right symmetry. Model ROM in LB was found to be 13.55±0.11° at +7.5Nm (in vivo: 13.32°[1]) and -13.79±0.19° at -7.5Nm (in vivo: -17.1°[1]). In AR, model ROM was recorded as 19.82±0.19° at +7.5Nm (in vivo: 14.44°[1]) and -15.57±0.12° at -7.5Nm (in vivo: -13.81°[1]). In extension, the model exhibited approximately twice the stiffness compared to its human counterpart.

This custom 3D printed analogue model of the lumbar spine has rotational stiffness within 20% of the in vivo flexion, lateral bending, and axial rotation responses and offers high degree of reproducibility. More material choices and testing are necessary to better control model stiffness and statistically quantify it. With further development, these models could pave way for fast and inexpensive in vivo comparable and reproducible spinal biomechanical testing.

[1] M. Rao, “Explicit Finite Element Modeling of the Human Lumbar Spine,” University of Denver, Denver, CO, 2012.

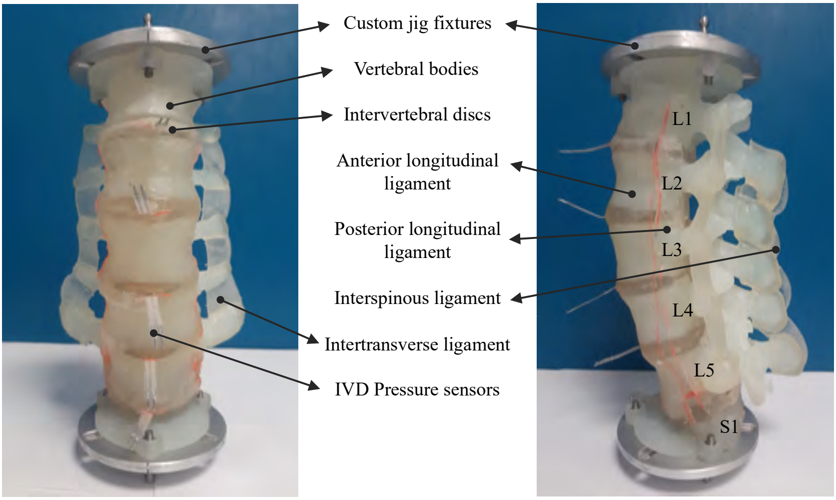

Figure 1: Developed novel 3D printable analogue lumbar spine segment.

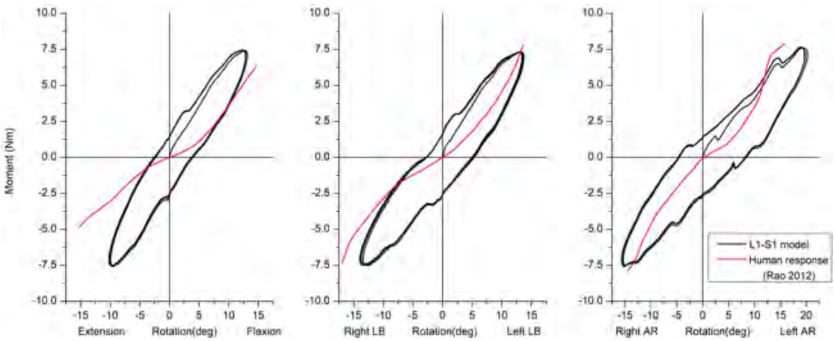

Figure 2: Model ROM in F-E, LB, and AR.

Pullout strength of thoracic spine pedicle screws inserted by freehand or patient-specific drill guides; a finite element analysis

Hosseini SF[a], Khalaf K[b], Azimi P[c], Arjmand N[a]

[a]*Department of Mechanical Engineering, Sharif University of Technology, Tehran, Iran*
[b]*Department of Biomedical Engineering, Khalifa University and HEIC, Abu Dhabi, UAE*
[c]*Neuroscience Research Center, Shahid Beheshti University of Medical Sciences, Tehran, Iran*

Although pedicle screw (PS) placement plays a critical role in the success of spinal instrumentations, there remains little consensus on quantitative placement methods. We have designed/fabricated bilateral vertebra/patient-specific drill-guides for thoracic PS placements (Figure 1a) [1]. A significant reduction in PS placement deviation from the preplanned positions occurred when drill guides were used; improving the success rate from ~72% (freehand placements with some PS breaches (Figure 1b)) to 94% (guided). This work aimed to use finite element (FE) analyses to evaluate the pull-out strengths of the PSs inserted either by freehand or guided techniques. Two identical 3D-printed T1-T12 models of a severe scoliosis (47°) patient were analyzed; one model bilaterally screwed at all vertebrae by the freehand approach, and one by the guides (24 PSs in each model). The FE models were consequently constructed using CT images of the screwed vertebrae (Figure 1b) with the cancellous bone and titanium screws as isotropic-elastic materials and surface-to-surface contacts between the screws and vertebrae (friction-coefficient of 0.6 in the tangential and hard-contact in the normal directions). Fracture modeling with the element deactivation feature available in ABAQUS was used to simulate bone failure using a fracture strain threshold [2]. A 0.5 mm outward axial displacement was applied to the head of the screw, and the reaction forces at the bone-screw contacts were calculated (elements with the ultimate deformation were deleted). The pull-out strengths were then determined from the strain-force curves. The mean±sd pullout strength was 809.4±249.9 (N) and 704.2±309.8 (N) for the guided and freehand techniques, respectively ($p=0.186$) (Figure 2). As the cancellous bone was modeled by a homogenous material, the improvement in the 3D orientation of the screws inserted by the guides could be downplayed. Nevertheless, the current modeling approach provides an effective tool for predicting the screw pullout forces towards informed preoperative planning in spinal instrumentations.

[1] Ashouri-Sanjani et al. (2021). Design, fabrication, and accuracy of a novel noncovering lock-mechanism bilateral patient-specific drill guide template for nondeformed and deformed thoracic spines. HSS Journal 17 (2), 213-222.
[2] Miles et al. (2015). Subject-specific finite element modeling of periprosthetic femoral fracture using element deactivation to simulate bone failure. Med. Eng. Phys. 37 (6), 567–573.

Figure 1: (a) Oue novel bilateral vertebra- and patient-specific drill guides for pedicle screw (PS) placement and (b) the meshed T8 and pedicle screws FE model in the case that screws were inserted using the free-hand technique with the right screw having a medial breach/malposition.

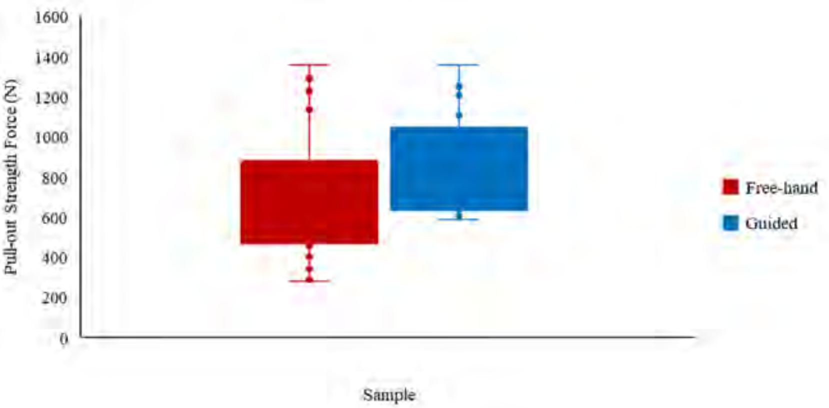

Figure 2: A box-plot comparing the pull-out strength PDS inserted by the template guides and freehand technique.

Effect of upper body mass distribution and thorax flexibility on spinal loads prediction in upright and flexed posture using personalized musculoskeletal models

Hulleck AA[a], Ignasiak D[b], Liu T[c], Khalaf K[a], El-Rich M[a]

[a]Khalifa University, Abu Dhabi, United Arab Emirates
[b]Institute for Biomechanics, ETH Zurich, Zurich, Switzerland
[c]Human Performance Lab, Faculty of Kinesiology, University of Calgary, Calgary, Alberta, Canada

Realistic prediction of spinal loads in various postures using subject-specific musculoskeletal (MSK) models requires accurate determination of body segment parameters such as upper body mass distribution, centers of mass (CoM) and segmental moments of inertia [1] as well as a realistic representation of thoracic region [2]. The current study quantified influence of subject-specific mass distribution and thorax flexibility, both separately and in combination, on spinal loads in neutral standing and at 60⍰ forward flexion using personalized upper body MSK models.

Fifteen anthropometric measurements [1], in addition to subject’s weight and height, were recorded for two normal weight (NW) (BMI 22.13±2kg/m2), two overweight (OW) (BMI 27±0.4kg/m2), and two obese (OB) (BMI 31.15±0.18kg/m2) healthy male subjects. The upper body base model with rigid thorax (RT), available in AnyBody repository, and the model with flexible thorax (FT) developed by Ignasiak 2016 [2] were used. Flexion was simulated using lumbo-pelvic rhythm for normal weight and obese subjects [3]. L1-S1 spinal loads predictions using uniform scaling algorithm (Uni-Scal), the default algorithm in AnyBody, and our new approach based on the subject’s body shape and internal tissues distribution (BS-Scal) [1]Formatting... were compared and analyzed using One-Way ANOVA. Effects of the mass distribution and thorax flexibility on disc compressive forces, analyzed individually and combined, were significant ($p<0.05$) in upright posture for all subjects. In flexion, the mass distribution had no significant effect on spinal loads with rigid thorax. Thorax flexibility only affected disc compression for overweight and obese subjects when Uni-Scal was used, but also affected the disc compression for normal weight subjects when BS-Scal algorithm was used. Shear force had no significant effects in any of the cases. Uni-Scal algorithm overestimated compression in NW but predicted smaller values in OW and OB subjects. The discrepancy increased when flexible thorax was used with BS-Scal was used.

[1] Liu T, Khalaf K, Hebela N, Westover L, Galbusera F, El-Rich M. Prediction of human male trunk mass distribution using anthropometric measurements: A feasibility study. J Biomech 2021;122:110437.
[2] Ignasiak D, Ferguson SJ, Arjmand N. A rigid thorax assumption affects model loading predictions at the upper but not lower lumbar levels. J Biomech 2016;4913:3074-8.

[3] Ghasemi M, Arjmand N. Spinal segment ranges of motion, movement coordination, and three-dimensional kinematics during occupational activities in normal-weight and obese individuals. J Biomech 2021;123:110539.

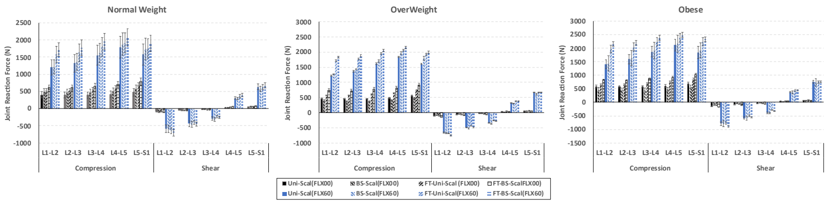

Figure 1: Predicted Spinal loads using different MSK model personalization approaches.

			FLX (00)			FLX (60)		
			Mass effects (RT) Uni-Scal * BS-Scal	T. Flexibility effects (Uni-Scal) RT * FT	Mass and T. Flexibility effects Uni-Scal (RT)*BS-Scal (FT)	Mass effects (RT) Uni-Scal * BS-Scal	Thorax Flexibility (Unif-Scal) RT * FT	Mass and T. Flexibility effects Unif-Scal (RT) *BS-Scal (FT)
p-values	COMPRESSION	NW	0.0121	0.0012	0.0001	0.6591	0.0710	0.0114
		OW	0.0193	0.0043	0.0000	0.5522	0.0219	0.0061
		OB	0.0042	0.0358	0.0002	0.7749	0.0212	0.0040
	SHEAR	NW	0.9494	0.9165	0.9640	0.9416	0.9594	0.9792
		OW	0.8950	0.8698	0.6822	0.9402	0.9336	0.9953
		OB	0.8511	0.7957	0.7899	0.9843	0.9056	0.9717
L1L2	COMPRESSION	NW	19.76	31.52	54.98	1.28	31.78	42.94
		OW	-15.25	23.31	57.96	3.91	41.06	50.77
		OB	-20.89	11.77	41.87	2.59	40.94	53.85
	SHEAR	NW	13.05	6.49	31.18	2.51	9.51	20.93
		OW	-24.67	-9.07	40.12	2.95	4.39	15.32
		OB	-32.25	-23.24	20.12	0.30	-1.68	11.42
L2L3	COMPRESSION	NW	2.71	32.27	55.60	2.71	23.43	34.31
		OW	-17.75	24.24	58.26	4.72	29.28	37.34
		OB	-22.26	12.96	42.69	2.41	28.17	38.20
	SHEAR	NW	9.67	4.07	27.93	4.86	-6.64	1.85
		OW	-26.17	-10.20	61.38	5.47	-10.22	-2.08
		OB	-32.24	-24.95	34.93	0.73	-14.95	-5.81
L3L4	COMPRESSION	NW	4.15	41.83	67.59	4.15	16.02	25.78
		OW	-19.07	32.84	69.51	5.69	20.80	26.98
		OB	-22.98	21.18	53.92	2.38	19.59	27.21
	SHEAR	NW	-12.21	59.97	100.83	10.27	-19.02	-12.12
		OW	-21.97	21.13	110.71	10.29	-23.20	-13.98
		OB	-27.58	0.57	71.82	2.17	-26.91	-17.44
L4L5	COMPRESSION	NW	5.46	42.79	68.62	5.46	7.13	15.76
		OW	-16.65	34.74	69.25	6.67	12.45	16.99
		OB	-21.30	23.64	53.60	2.51	12.61	18.04
	SHEAR	NW	50.60	107.37	171.97	-1.02	19.16	31.08
		OW	-85.59	55.75	24.38	-1.70	18.58	18.38
		OB	-86.03	34.91	18.25	-1.19	15.10	18.26
L5S1	COMPRESSION	NW	9.64	40.49	64.77	9.64	10.71	20.23
		OW	-14.07	32.20	63.24	11.69	19.68	24.02
		OB	-19.45	21.43	47.88	4.85	21.25	26.43
	SHEAR	NW	28.41	31.15	61.34	-8.58	0.00	7.56
		OW	-16.32	15.47	-8.39	-7.87	-0.45	-0.54
		OB	-22.23	6.72	-13.13	-3.00	-1.22	-0.25

Table 1: Predictions using MSK model with right thorax (RT) and uniform scaling (Uni-Scal) compared to their counterparts using flexible thorax (FT) and/or body shape scaling (BS-Scal), values with significant difference (p< 0.05) in one-way ANOVA are highlighted in gray color. Negative values indicate underprediction and positive indicates overprediction of the personalization technique compared to base RT and Uni-Scal model.

Body mass distribution along the spine affects biomechanics of spinal sagittal alignment

Ignasiak D[a], Hulleck AA[b], Liu T[c], Galbusera F[d], Ferguson SJ[a], El-Rich M[b]

[a] Institute for Biomechanics, ETH Zurich, Zurich, Switzerland
[b]Khalifa University, Abu Dhabi, United Arab Emirates
[c]Human Performance Lab, Faculty of Kinesiology, University of Calgary, Calgary, Alberta, Canada
[d]Schulthess Clinic, Zurich, Switzerland

Spinal sagittal alignment is a biomechanical factor influencing patient outcomes. Body mass is considered clinically relevant, but the effects of individual body shape are rarely considered when analysing sagittal alignment biomechanics. Computational spine models, which may advise preoperative planning, typically are scaled uniformly to patient body mass and height. The aim of this study was to evaluate the errors in model-predicted spinal loads associated with sagittal alignment, that are introduced by neglecting the subject-specific body mass distribution along the spinal column.

An established AnyBody model of the thoracolumbar spine was used [1]. Representative sagittal alignment profiles (aligned, moderately and severely malaligned) were obtained from a previous study [2]. Body mass distribution (segmental masses and locations of center of mass) was assessed in 6 healthy male volunteers, using a previously established method [3]. For each combination of a sagittal alignment profile and body parameters, two models were constructed: one scaled uniformly to BM and BH, and one with individualized body mass distribution (Figure 1). Inverse static simulations were performed to estimate segmental compression and shear loads.

Across considered sagittal alignment cases, errors in segmental loads due to neglected body mass distribution ranged from -0.06 to 0.25 BW or -18% to 34%, for compression (Figure 2), and -0.1 to 0.03 BW for shear. The largest compression errors were found for aligned and moderate sagittal profiles, and shear errors – for severe malalignment and L5/Sacrum joint.

The mean magnitude and range of error due to disregarding personal body mass distribution is markedly influenced by spinal sagittal alignment and spinal level. This highlights the impact individual body shape has on the biomechanics of spinal sagittal alignment, which – upon further studies – has a potential to improve clinical understanding and practise in the future.

[1] Ignasiak et al., J Biomech 2016, https://doi.org/10.1016/j.jbiomech.2017.11.033
[2] Ignasiak et al., Eur Spine J 2022, https://doi.org/10.1007/s00586-022-07477-4
[3] Liu et al., J Biomech 2021, https://doi.org/10.1016/j.jbiomech.2021.110437

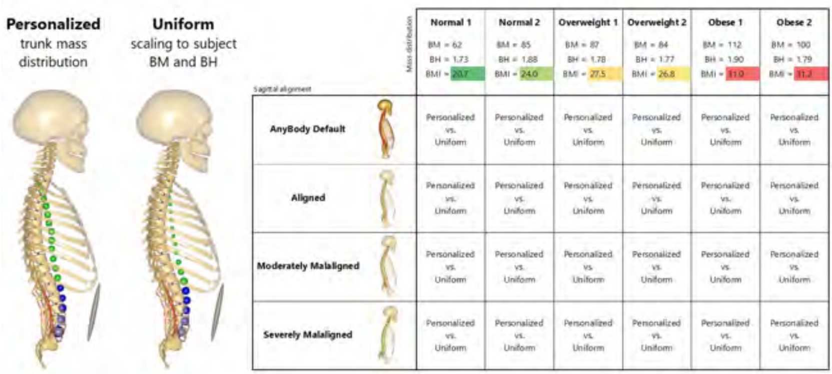

Figure 1: Overview of the study design. Predictions of thoracolumbar spine models representing fully personalized trunk mass distribution (individualized segmental masses and locations of centers of mass) were compared against predictions made with models uniformly scaled to body mass and height. Simulations were performed for representative sagittal alignment profiles in combination with body parameters of 6 healthy volunteers, representing a range of body mass and body shape types.

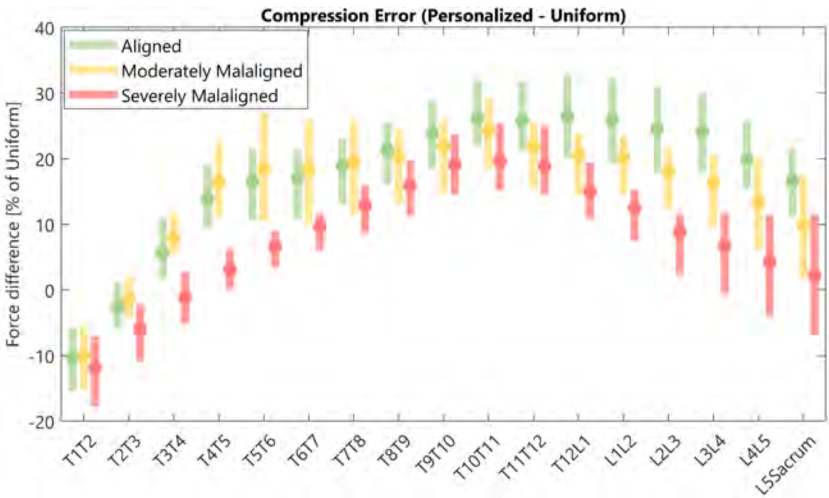

Figure 2: Relative errors in model-predicted segmental compressive forces (calculated as a difference between forces predicted with personalized and uniform model, relative to predictions of the uniform model). Errors averaged over the body mass distribution cases are depicted with a round symbol and the bars indicate the error range (minimum to maximum).

Mechanical testing of lumbar cadaveric muscle and thoracolumbar fascia suggests evidence towards physiological stress shielding of musculoskeletal soft tissues

Newell E[a,b], Ouellet J[c,d], Driscoll M[a,b]

[a]*Musculoskeletal Biomechanics Research Lab, Department of Mechanical Engineering, McGill University, Montreal, Quebec, Canada*
[b]*Orthopaedic Research Laboratory, Montreal General Hospital, Montreal, Quebec, Canada*
[c]*Department of Paediatric Surgery, McGill University, Montreal, Quebec, Canada*
[d]*Department of Pediatric Surgery, McGill University Health Centre, Montreal, Quebec, Canada*

Studies investigating mechanical property changes in soft tissues affected by low back pain (LBP) have indicated a load allocation bias skewed towards the thoracolumbar fascia (TLF), potentially resulting in physiological stress shielding. Thus, this study investigates the potential for physiological stress shielding through the analysis of stress distributions during mechanical testing of cadaveric lumbar soft tissues.

Ethical approval was obtained prior to testing (IRB no. A04-M13-18A). Using a male cadaver, 48 TLF samples and 15 erector spinae (ES) samples were excised.

Samples underwent individual tensile tests to determine the elastic modulus and hysteresis using a custom-built apparatus (Figure 1). Next, 20 pairs of TLF samples and seven TLF-ES pairs underwent dual tensile testing, allowing for stress distributions analysis between samples. All tests involved cyclic loading/unloading (0 to 2% strain) followed by loading to 6% strain at a strain rate of 0.25%/s.

Nonparametric statistical tests were conducted. $P<0.05$ was considered significant.

Table 1 outlines the mechanical properties obtained from the TLF and ES. Dual tension testing demonstrated elevated stress on the (stronger) TLF relative to a weaker TLF sample ($p<0.001$) and to an ES sample ($p<0.005$) at 6% strain.

Individual tensile test results suggest the TLF is stronger (i.e. higher moduli) and more vulnerable to hysteresis than the ES. Parallel tension tests indicate the (stronger) TLF undergoes elevated stress relative to the (weaker) TLF and the ES. Such results suggest a stress allocation bias towards (stronger) TLF samples. For LBP patients, skewed stress distributions may result in the TLF withstanding the majority of stress, preventing muscles from receiving regular loading. As muscles may undergo atrophy and reduced muscle strength, this may promote this skewed stress distribution, leading to cyclical stress shielding. Thus, this study suggests a load allocation bias towards the TLF, indicating possible stress shielding within lumbar musculoskeletal soft tissues.

Figure 1: Custom-built apparatus used for individual and dual tension testing of cadaveric samples (a) without samples undergoing testing and (b) with thoracolumbar fascia and erector spinae samples inserted.

	Thoracolumbar Fascia	Erector Spinae
No. of Samples	48	15
Elastic Modulus (MPa)	150.85 (58.41)	0.63 (0.29)
Hysteresis (Nmm)		
Cycle 1	0.39 (0.06)	0.16 (0.03)
Cycle 2	0.28 (0.03)	0.15 (0.03)
Cycle 3	0.27 (0.03)	0.15 (0.03)

Table 1: Average (standard deviation) of the cadaveric samples' mechanical properties obtained from individual tension tests.

Coupled MBS and FEM models of the lumbar spine – unidirectional vs. bidirectional co-simulation

Nispel K[a,b], Lerchl T[a,b], Kirschke JS[a], Senner V[b]

[a]*Dept. of Diagnostic and Interventional Neuroradiology, School of Medicine, Klinikum rechts der Isar, Technical University of Munich, Munich, Germany*

[b]*Associate Professorship of Sport Equipment and Sport Materials, School of Engineering and Design, Technical University of Munich, Munich, Germany*

Bidirectionally coupled MBS and FEM simulations are promising to investigate the relation between back pain and pathological changes in the spine [1]. To quantify their advantages over the unidirectional coupling approach, we compared them regarding their accuracy and efficiency.

We implemented both, a unidirectional and a bidirectional co-simulation of the lumbar spine (L2-L5) using equal geometries. For the unidirectional co-simulation, we implemented an MBS model (M) containing joints with 3 in the sagittal plane and an FEM model (F) of a functional spinal unit with a hyperelastic IVD. We synchronized the respective intervertebral disc (IVD) representations by adapting the stiffness properties of the MBS joint (M) in an iterative process until deformations matched those in an isolated FEM IVD model (IF). We then executed the MBS simulation (M) and used resulting joint loading as boundary conditions in the respective FEM model (F). The bidirectional co-simulation model equaled the MBS model (M), but included an FEM IVD at L4-L5 instead of a joint (Figure 1). Two reference points (RP) were chosen for data exchange at the center of the L4-L5 endplates, respectively. The two respective modeling approaches were compared regarding modeling time, computation time, IVD deformation, stress distribution and adjacent joint kinematics.

Comparing modeling time and computation time, the bidirectional co-simulation showed advantages over the unidirectional approach. Deformations, stress distributions and adjacent joint kinematics varied for both approaches (Table 1).

The differences in IVD deformation and stress distribution demonstrate the vulnerability of spine models to the representation of IVDs. Joint representations of the IVD fail to represent detailed IVD deformations and therefore, using the MBS input in FEM simulations may be less accurate in unidirectional co-simulations. In further studies, the interface between the vertebrae and the IVD can be improved by using multiple RPs instead of two [2].

[1] Nispel, K et al., Recent Advances in Coupled MBS and FEM Models of the Spine – A Review, Bioengineering 2023 [Manuscript submitted for publication]

[2] Monteiro, N et al., Structural analysis of the intervertebral discs adjacent to an interbody fusion using multibody dynamics and finite element cosimulation, Multibody Syst Dyn 2011; 25:245-270

	Unidirectional co-simulation	Bidirectional co-simulation
Modeling time	+	-
Computation time	+	-
IVD deformation		
Anterior	+	-
Center of endplate	+	-
IVD stress distribution	Higher max. stress	Lower max. stress
Adjacent joint ROM	-	+

Table 1: Comparison of the unidirectional and bidirectional simulation of the spine. "+" indicating a higher value, "-" a lower result in comparison.

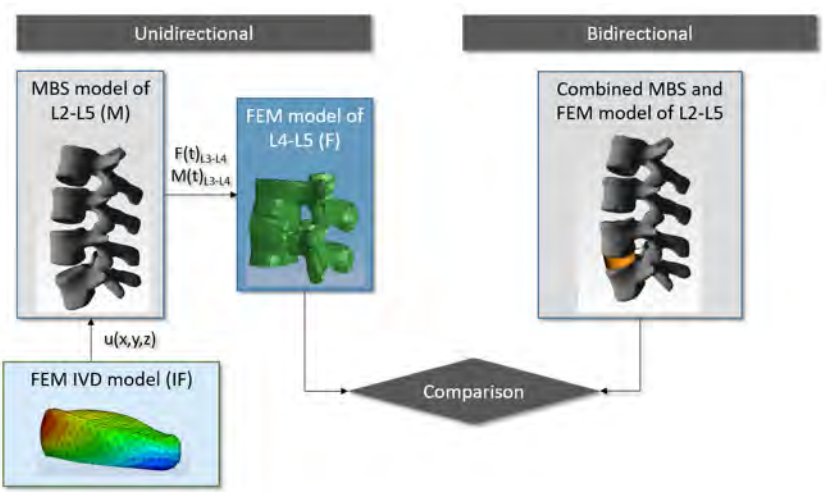

Figure 1: Data flow between the models in this study. Left: Unidirectional co-simulation including the MBS model (M) and FEM model (F) of the lumbar spine. Joint definitions for the MBS model were derived in an iterative process such that they matched the deformation of an isolated FEM model (IF). Right: Bidirectional co-simulation model.

Approximate facet area and volume of convex polytope satisfying equilibrium conditions during spinal muscular exertions as new additional candidates for neuromuscular strength of spine

Posner M[a], Parnianpour Mahdi[b], Parnianpour Mo[c]

[a]*Dept. Industrial and Systems Engineering, Ohio State University, Columbus USA*
[b]*Dept. of Mechanical Engineering, Amir Kabir University of Technology, Tehran Iran*
[c]*Dept. of Mechanical Engineering, Sharif University of Technology, Tehran Iran*

Traditional uniaxial spine dynamometers measure spinal exertions (torque generation) in any of the six cardinal directions. If we consider a typical static exertion during a maximal exertion, the equilibrium condition at any level of the spine can be shown as $Ax=b$; $0 \leq x \leq xm$. In this study, we have assumed a 10 muscle model representation at L3 level, A is a 3x10 matrix and x represents a column vector of the 10 muscle forces: bilateral rectus abdominus, erector spinae, internal and external obliques and latissimus dorsi. The muscle forces are constrained to be positive and bounded by the maximum muscle stress of 50 N/m2. A(i,j) represents the torque generation of jth muscle for unit muscle force in ith plane (i.e. the three cardinal planes of sagittal, coronal and transverse planes).

These equations correspond to a convex polytope that defines the strength surface in the space of b. Any point interior to the surface corresponds to feasible torques that the neuromuscular system can generate. Any point outside this surface will exceed the strength and if exposed can lead to overexertion or injury. Posner (1999) has used qhull to compute the Volume of convex hull and Area of facets of the strength surface— as the surface consists of patched planes in b (i.e. imagine a soccer ball). These two metrics along the traditional uniaxial maximum exertions may prove to be more comprehensive means to quantify the neuromuscular strength. In sensitivity analysis, the effect of 10% increase in single or bilateral combined muscle force (simulating the effects of physical exercise) showed that erector spinae muscle had the greatest effects on Volume and Area estimated in this study. Estimated Area increased by 3.7 and 7.8%, respectively by single and bilateral erector spinae force increase, whilst Volume increased by 5.5. and11%.

Methods of evaluating mechanical parameters and the stability of the cervical interbody fusion cage

Żak M, Nikodem A, Pezowicz C

Department of Mechanics, Materials and Biomedical Engineering, Wroclaw University of Science and Technology, Wroclaw, Poland

In the case of interbody fusion cages, it is required to achieve optimal conditions between the geometry and the mechanical parameters to achieve a stable connection at the border with the bone tissue. In our work, we present the research results of the cervical interbody fusion cage based on assessing mechanical properties and the conditions related to osseointegration resulting from the adopted geometry. The cage was designed as a titanium alloy Ti6Al4V implant strengthened with mesh lattice structures to obtain larger osseointegration between the implant and bone tissue. Based on the indentation test, the stiffness and the maximum force values of the modification of the geometrical dimensions of the mesh lattice structures were determined. Also, was performed adhesion test for Balb/3T3 fibroblasts and NHOst osteoblasts. The research showed that an essential geometric parameter influencing the mesh strength is the height of the connection point between the arms of the mesh cells. There was no significant influence of the mesh geometry on the number and survival of Balb/3T3 and NHOst cells. Fibroblast cells more readily formed colonies in the area where cells of the mesh meet, unlike osteoblasts, which were more numerous at their tips.

The mechanical parameters and quality of the construction cervical interbody fusion cage were determined in: a uniaxial compression test to the failure of the implant (with ASTM F2077 standard), CT scan and microscopic analysis. With a non-destructive load in the force range up to 500N, the implant stiffness was from 14 to 17KN/mm. On the other hand, the value of the ultimate forces does not exceed 40kN and the stiffness 22kN/mm. The CT scan showed that the structure of the implant is continuous and that there are no closed pores in the implants printed. The average porosity calculated from CT scans of control volume was 0.15÷0.3%.

Biomechanical simulation of the upper body in different sitting positions

Praster M[a], Ditsche J[a], Hildebrand F[a], Ignasiak D[b]

[a]*Clinic for orthopedics, trauma and reconstructive surgery, RWTH Aachen, Germany*
[b]*Institute for Biomechanics, ETH Zurich, Switzerland*

This study aims to determine the lumbar strain caused by sitting in different positions. The study is based on a musculoskeletal model in Anybody. This model represents the torso. In order to implement angular parameters of the spine and to represent realistic sitting positions, this model will be modified during the work. The aim is to define an optimal sitting position based on joint reaction forces and moments as well as muscle activity of the lumbar spine. For this purpose, different sitting positions are measured using a raster stereographic measurement system. The orientation of the individual vertebrae in relation to the horizontal is defined by the flexion-extension angle in the sagittal plane and implemented in a corresponding musculoskeletal model. This musculoskeletal model is based on the thoracic and lumbar vertebrae. These vertebrae can be treated individually. The alignment of the vertebrae is defined by the implemented flexion-extension angles to accurately reproduce a previously recorded sitting position. After applying the musculoskeletal model and running the inverse dynamics, the output parameters compression force, shear force along the sagittal axis, muscle activity and flexion-extension moment are compared across the different sitting positions. The subjects represent, among other things, their daily and consciously upright sitting position. Increased versions of thoracic kyphosis and lumbar lordosis are also compared. As a result of the comparison, the daily sitting position is defined as optimal, because low compression forces act on the lumbar spine and the back muscles are only slightly stressed. An upright sitting position, on the other hand, puts a lot of strain on the back muscles, causing them to tire quickly. In addition, it becomes clear that the optimal sitting position depends on balancing thoracic kyphosis and lumbar lordosis.

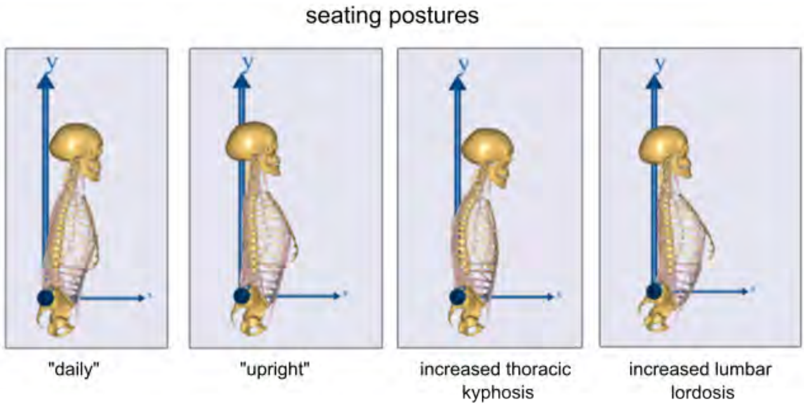

Figure 1: Four different sitting positions are shown as examples based on the comments of a test person. The sitting positions 'daily' and 'upright' are shown, which are chosen by the test person himself/herself, and the sitting positions according to instructions with increased thoracic kyphosis and increased lumbar lordosis

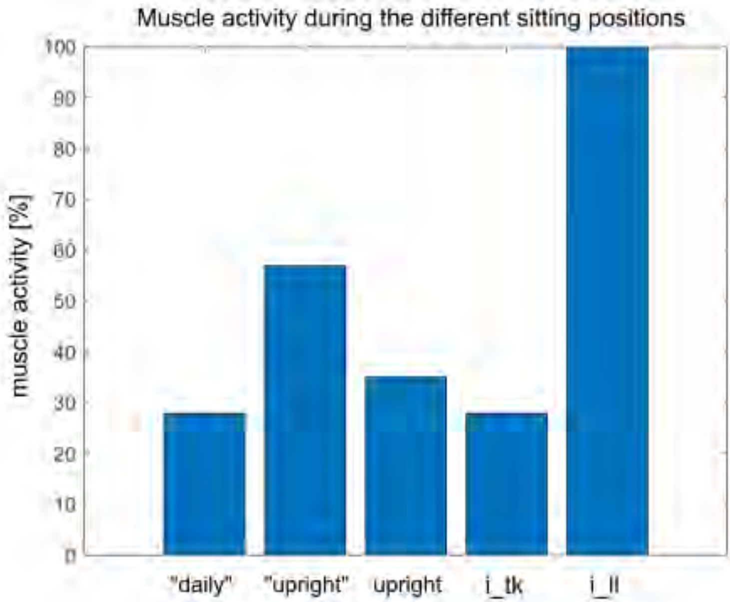

Figure 2: Muscle activity during the five sitting positions. "Daily" and "Upright" are the self-selected positions. Upright, increased thoracic kyphosis (i_tk) and increased lumbar lordosis (i_ll) are the predefined positions.

How can we capture back health? Association between self-reported and objectively measured back health among sedentary office workers

Reschke A[a], Wilhelm LO[a], Lederle N[a], Heinzel M[b], Hahn S[b], Schmidt H[b], Fleig L[a]

[a]MSB Medical School Berlin, Department of Health psychology, Berlin, Germany
[b]Julius-Wolff-Institute, Berlin Institute of Health at Charité – Universitätsmedizin Berlin, Germany

The prevention and treatment of lower back pain needs to consider both self-reported and objective parameters of back health (BH). The aims of the present study were to describe self-reported and objective spinal posture (POS) and mobility (MOB) as indicators of BH in sedentary office workers, and to correlate self-reported with objective parameters.

82 healthy employees (62% women, 32±12 yrs., 1.74±0.10 m, 70±13 kg) answered a questionnaire on self-reported POS and MOB. Objective POS and MOB were statically measured using MediMouse M360 during sitting and standing: upright, maximum flexion and extension, left and right lateral bending (Tables 1 and 2). Lumbar-, thoracic-, sacral- and inclination angles (°) and degrees of deviation from mean of cohort were analyzed descriptively (mean[±SD]). Indicators of deviation for POS and MOB were calculated (>2 SD from mean of cohort) per measurement condition, and summed up for subsequent correlation analysis.

Self-reported POS was 3.2±0.9 pts. and MOB 4.1±1.1 pts. Angles for POS and MOB with differences from mean are shown in Tables 1 and 2. Deviations were highest at sacrum for SSiF and SStF (POS), SSiF-SSiU and SStF-SStU (MOB); and at sacrum and thoracic spine for SSiE and SStE (POS), SSiE-SSiE and SStE-SStU (MOB). Objective sum score for POS was 2.5±2.4 and for MOB 1.5±1.9. Self-reported POS did not correlate significantly with scores for objective POS. Self-reported MOB did correlate positively with thoracic angle of MOB for FStLL-FStU ($r=.23$, $p=.04$) and SStF-SStU ($r=.29$, $p=.01$).

Participants estimated their POS and MOB from moderate to good. Objective BH was characterized by small variances for POS and MOB, with higher deviations below lumbar spine for flexion, and below or above lumbar spine for extension. For specific spinal segments and positions, subjective and objective back health parameters revealed small-to-moderate associations, comparable with, for example, self-reported and accelerometer-based measured physical activity.

Acknowledgements: All authors are supported by institutional funds. We thank Deutsche Forschungsgemeinschaft (DFG; FOR 5177) and Bundesministerium für Bildung und Forschung (01EC1905F) for funding this project. L.F. and H.S. are supported by Deutsche Forschungsgemeinschaft (DFG; FOR 5177) and by Bundesministerium für Bildung und Forschung (01EC1905F). L.O.W., S.H. and N.L. are supported by Bundesministerium für Bildung und Forschung (01EC1905F).

Back Posture	Measurement condition	Angles in spinal sections	M	±SD	Difference to M (°, ABS)
Posture	Sagittal Standing Upright (SStU)	Thoracic angle	38.4	9.6	7.4
		Lumbar angle	-27.3	8.6	6.6
		Sacral angle	15.9	7.7	6.0
		Inclination angle[3]	0.7	2.7	2.2
Posture	Sagittal Standing Flexion (SStF)	Thoracic angle	65.3	10.9	8.7
		Lumbar angle	21.3	9.2	7.2
		Sacral angle	72.2	14.3	11.1
		Inclination angle	107.9	13.1	10.5
Posture	Sagittal Standing Extension (SStE)	Thoracic angle	27.0	17.0	14.2
		Lumbar angle	-37.4	11.9	8.7
		Sacral angle	8.3	15.6	11.7
		Inclination angle	-21.8	17.4	9.1
Posture	Sagittal Sitting Upright (SSiU)	Thoracic angle	32.4	9.8	7.6
		Lumbar angle	-6.1	11.9	9.5
		Sacral angle	3.4	9.7	7.9
		Inclination angle	4.6	4.0	3.0
Posture	Sagittal Sitting Flexion (SSiF)	Thoracic angle	72.6	10.8	8.0
		Lumbar angle	20.3	8.7	7.1
		Sacral angle	48.9	15.7	12.6
		Inclination angle	84.8	13.0	11.0
Posture	Sagittal Sitting Extension (SSiE)	Thoracic angle	18.7	16.6	13.5
		Lumbar angle	-29.0	12.5	9.6
		Sacral angle	9.0	14.6	12.1
		Inclination angle	-16.1	10.2	8.1
Posture	Frontal Standing Upright (FStU)	Thoracic angle	-0.9	5.5	4.2
		Lumbar angle	-0.8	5.4	4.3
		Sacral angle	1.6	5.1	4.3
		Inclination angle	0.6	2.5	2.0
Posture	Frontal Standing Left Lateral Bending (FStLL)	Thoracic angle	35.2	13.8	10.4
		Lumbar angle	19.2	7.4	5.7
		Sacral angle	6.0	5.0	4.0
		Inclination angle	31.0	8.0	6.2
Posture	Frontal Standing Right Lateral Bending (FStRL)	Thoracic angle	-37.7	13.3	9.7
		Lumbar angle	-19.1	8.5	6.9
		Sacral angle	-4.5	6.2	4.9
		Inclination angle	-30.4	8.3	6.3
Posture	Frontal Sitting Upright (FSiU)	Thoracic angle	-1.1	4.9	3.7
		Lumbar angle	-0.3	4.2	2.7
		Sacral angle	0.8	4.3	3.5
		Inclination angle	0.3	2.6	2.2
Posture	Frontal Sitting Left Lateral Bending (FSiLL)	Thoracic angle	39.1	12.9	9.9
		Lumbar angle	14.6	7.2	5.6
		Sacral angle	3.9	4.8	3.9
		Inclination angle	26.5	8.7	7.1
Posture	Frontal Sitting Right Lateral Bending (FSiRL)	Thoracic angle	-41.0	13.9	10.8
		Lumbar angle	-13.9	6.7	5.2
		Sacral angle	-4.2	6.6	5.2
		Inclination angle	-26.9	9.5	7.3

[1]Mean value (M) of angle was defined by the sum of angles in all segments for lumbar spine or thoracic spine (a segment is built by two neighbored vertebral bodies, e.g., for lumbar spine: "lumbar angle" describes the sum of angles of all lumbar segments L1/L2, L2/L3, L3/L4, L4/L5, L5/S1) or the angle between L5/S1 for sacrum; [2]Posture angles were determined from end-of-range position (e.g., upright standing position or maximum flexion); [3]Inclination angles describe the angles of inclination of the sacrum and body axis, relative to the perpendicular

Table 1: Mean1±SD of angles for posture2 (lumbar-, thoracic-, sacral-, inclination angle) (°) during the different measurement conditions; Degree of deviation/Difference from the mean (M) of the sample cohort (absolute values [°])

Back Mobility	Measurement condition	Angles in spinal sections	M	±SD	Difference to M (°, ABS)
Mobility	Sagittal Standing Flexion (SStF)	Thoracic angle	26.8	11.4	8.9
	- Sagittal Standing Upright (SStU)	Lumbar angle	48.6	9.2	7.1
		Sacral angle	56.3	13.6	11.0
		Inclination angle[3]	107.2	13.5	11.0
Mobility	Sagittal Standing Extension (SStE)	Thoracic angle	-11.4	15.2	12.2
	- Sagittal Standing Upright (SStU)	Lumbar angle	-10.1	11.1	7.4
		Sacral angle	-7.6	12.2	8.4
		Inclination angle	-22.5	17.3	9.3
Mobility	Sagittal Sitting Flexion (SSiF)	Thoracic angle	40.2	11.2	8.7
	- Sagittal Sitting Upright (SSiU)	Lumbar angle	26.4	11.4	9.0
		Sacral angle	45.5	14.3	11.2
		Inclination angle	80.2	13.4	11.0
Mobility	Sagittal Sitting Extension (SSiE)	Thoracic angle	-13.7	14.3	11.3
	- Sagittal Sitting Upright (SSiU)	Lumbar angle	-22.9	13.7	10.8
		Sacral angle	5.6	14.3	11.3
		Inclination angle	-20.7	10.0	7.8
Mobility	Frontal Standing Left Lateral Bending (FStLL)	Thoracic angle	36.1	13.5	10.1
	- Frontal Standing Upright (FStU)	Lumbar angle	20.0	8.5	6.7
		Sacral angle	4.3	4.4	3.5
		Inclination angle	30.1	8.5	6.0
Mobility	Frontal Standing Right Lateral Bending (FStRL)	Thoracic angle	-36.8	14.0	10.6
	- Frontal Standing Upright (FStU)	Lumbar angle	-18.3	7.3	5.6
		Sacral angle	-6.1	5.5	4.3
		Inclination angle	-31.0	8.1	6.0
Mobility	Frontal Sitting Left Lateral Bending (FSiLL)	Thoracic angle	40.2	13.4	10.8
	- Frontal Sitting Upright (FSiU)	Lumbar angle	14.9	7.7	6.1
		Sacral angle	3.1	5.1	3.9
		Inclination angle	26.2	8.5	6.8
Mobility	Frontal Sitting Right Lateral Bending (FSiRL)	Thoracic angle	-39.9	13.7	10.4
	- Frontal Sitting Upright (FSiU)	Lumbar angle	-13.7	6.6	5.3
		Sacral angle	-5.0	5.2	4.1
		Inclination angle	-27.2	9.3	7.1

[11]Mean value (M) of angle was defined by the sum of angles in all segments for lumbar spine or thoracic spine (a segment is built by two neighbored vertebral bodies, e.g., for lumbar spine: "lumbar angle" describes the sum of angles of all lumbar segments L1/L2, L2/L3, L3/L4, L4/L5, L5/S1) or the angle between L5/S1 for sacrum [2] Mobility angles were derived from the difference between end-of-range (flexion/extension/left and right lateral bending) and starting testing position/s (upright) (e.g., "standing-upright to flexion": standing flexion minus standing upright); [3]Inclination angles describe the angles of inclination of the sacrum and body axis, relative to the

Table 2: Mean1±SD of angles for mobility2 (lumbar-, thoracic-, sacral-, inclination angle) (°) during the different measurement conditions; Degree of deviation/Difference from the mean (M) of the sample cohort (absolute values [°])

Effect of DLC coating of growth-guidance system implants on changes in mechanical and kinematic properties of the spine

Żak M[a], Szotek S[a], Szkoda-Poliszuk K[a], Filipiak J[a], Wrzosek M[b], Kołtowski K[c], Menartowicz P[d], Pezowicz C[a]

[a]Department of Mechanics, Materials and Biomedical Engineering, Faculty of Mechanical Engineering, Wrocław University of Science and Technology, Poland
[b]Department of Internal Diseases With Clinic for Horses, Dogs and Cats, Faculty of Veterinary Medicine, Wrocław University of Environmental and Life Sciences, Poland
[c]Department of Pediatric Surgery and Urology, Wroclaw Medical University, Poland
[d]St. Hedwig of Silesia Hospital, Poland

Early onset scoliosis (EOS) is a three-dimensional curvature of the spine and trunk that occurs in children nine years of age or younger. The EOS tend to develop progressively, requiring early surgical intervention with spine stabilization. Currently stepwise treatment method involving the displacement of the stabilizer by operating methods is being used. It is necessary to develop a solution that would allow scoliosis to be corrected as soon as possible while reducing the number of operations and the risk of complications.

The research aimed to develop a modification of the internal spine stabilizer for the treating scoliosis in children by increasing its abrasion resistance and thus reducing the risk of tissue degradation and disorders in the kinematics of the spine column. The study used the scoliosis stabilisation system offered by NovaSpine, which has kinetic pairs in its design to allow relative displacement of stabiliser components without external intervention.

In order to increase the abrasion resistance of the mating surfaces and increase the mobility of the stabiliser spine system, a DLC (Diamond Like Carbon) coating was applied to the implant components. Then, tests were carried out to assess the mechanical and kinematic properties of the spine-stabilizer (SI) system for selected modifications. At this study stage, a more than 8% decrease in SI stiffness was demonstrated for DLC-coated implants compared to implants without DLC. Then, in vivo study was carried out on domestic pigs, assessing the effect of the applied modification on the reduction of the mass of titanium alloy particles infiltrating into the tissues surrounding the implant and determining the effect of modified stabilizing systems on changes in the vertebra bone structure. As a consequence, the increased mobility of the stabilizer follower node led to excessive movement between the transpedicular screw and the bone tissue, leading to their loosening and inflammation.

Comparison of load-sharing and axis of rotation in generic and individualised neuro-musculoskeletal models of the spine

Hammer M[a,b], Rockenfeller R[c,d,e], Riede JM[a], Meszaros-Beller L[a,f], Little P[f], Pivonka P[f], Schmitt S[a,b,f]

[a]*Institute for Modelling and Simulation of Biomechanical Systems, University of Stuttgart, Germany*

[b]*Stuttgart Center for Simulation Science (SC SimTech), University of Stuttgart, Germany*

[c]*Mathematical Institute, University of Koblenz, Germany*

[d]*School of Science, Technology and Engineering, University of the Sunshine Coast, Queensland, Australia*

[e]*School of Biomedical Sciences, University of Queensland, Brisbane, Australia*

[f]*School of Mechanical, Medical and Process Engineering, Queensland University of Technology, Brisbane, Australia*

Individualisation of spine models will benefit the subject-specific treatment of spinal injuries and diseases but poses a major challenge to state-of-the-art biomechanics simulation studies. Here, we compare the kinematics and internal forces of generic population-based and subject-specific individualised spine models. More precisely, we present the differences in load sharing between ligaments, muscles and intervertebral discs (IVDs) as well as finite helical axis (FHA) trajectories.

We investigated the differences in the lumbar kinematics and load sharing between a generic and a subject-specific neuro-musculoskeletal spine model during purely muscle-driven flexion-extension movements. Both models are fully articulated with six degree of freedom joints in the entire thoracolumbar spine. The generic model is based on a validated passive lumbar spine model [1], whereas the subject-specific model was derived from it by geometric individualisation [2]. We applied the FHA analysis from [3] to predict the trajectory of the axis of rotation in both models.

All forward-dynamic simulations were performed in the biophysics simulator for muscle-driven systems demoa (http://get-demoa.com).

In upright stance, compressive as well as rotational loading was higher in the individualised model. During flexion, the contribution of passive structures to the net joint torque was markedly lower in the individualised model than in the generic model with a predominant muscle contribution (Fig. 1). Mean FHA visualises differences between flexion and extension and both models (Fig. 2).

While generic models remain valuable for general population-oriented research questions, subject-specific modelling seems key to individualised treatment of spine injuries and diseases. We show how to individualise the geometry and the resulting differences in the dynamics, i.e., load sharing and FHA. Nevertheless, both simulation results lie within an acceptable corridor of reported literature data.

[1] Mörl et al., Biomech Model Mechanobiol (2020). https://doi.org/10.1007/s10237-020-01322-7
[2] Meszaros-Beller et al., Biomech Model Mechanobiol (2023).
https://doi.org/10.1007/s10237-022-01673-3
[3] Rockenfeller et al. Comput Biol Med (2021). https://doi.org/10.1016/j.compbiomed.2021.104528

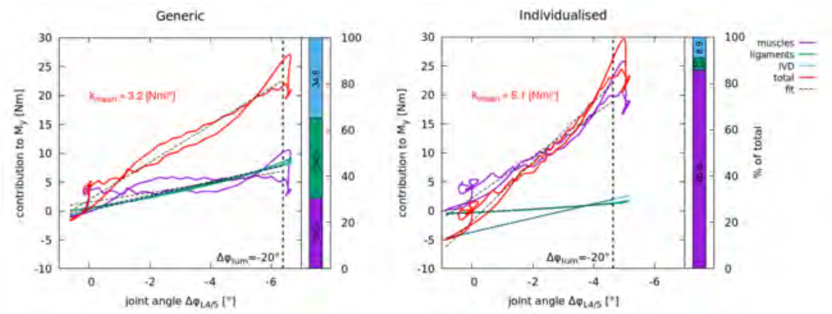

Figure 1: Comparison of load sharing between muscles, ligaments and IVD during flexion-extension movement (up to Δϕlum = 20°) in generic and individualised model. Mean stiffness (kmean) was analysed for both models. [2]

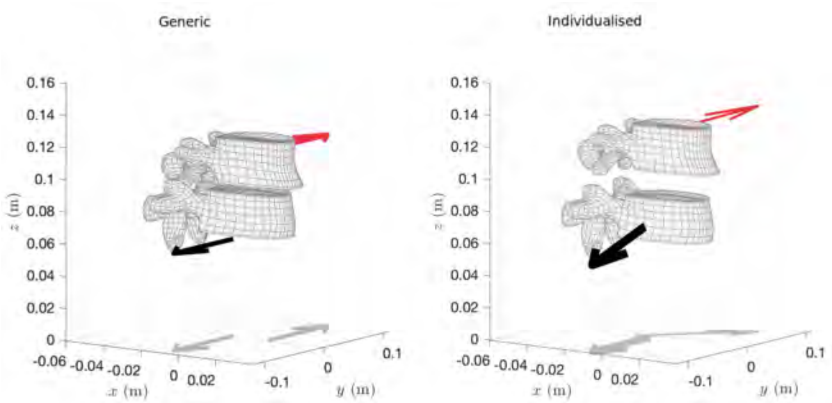

Figure 2: Comparison of mean FHA of L4|5 in generic and individualised spine model during flexion (black) and extension (red) movement (graphic primitives not true to scale).

Comparative evaluation of different spinal stability metrics

Eskandari AH[a], Ghezelbash F[b], Shirazi-Adl A[c], Larivière C[a,d]

[a]*Institut de recherche Robert Sauvé en santé et en sécurité du travail, Montréal, Canada*
[b]*EERS Global, Montreal, Canada*
[c]*Division of Applied Mechanics, Department of Mechanical Engineering, Polytechnique Montréal, Canada*
[d]*Center for Interdisciplinary Research in Rehab. of Greater Montreal (CRIR), Institut universitaire sur la réadaptation en déficience physique de Montréal (IURDPM), Centre intégré universitaire de santé et de services sociaux du Centre-Sud-de-l'Ile-de-Montréal (CCSMTL)*

Stability is a fundamental concept in science and engineering, yet its application in musculoskeletal systems remains uncertain. While the direct in vivo measurement of instability is impossible, it has been estimated using dynamic time series and/or structural analysis. We aim to investigate the differences between dynamic and structural stability measures during dynamic cyclic lifting tasks.

Nineteen healthy controls and 13 participants with chronic low back pain performed repetitive lifts of a crate, 35 cycles, with (4/2.6 kg for males/females) and without weight. EMG signals and 3D kinematics were collected using 12 surface electrodes and 17 inertial sensors. Three dynamical stability measures were computed: short and long maximum Lyapunov exponent (LyE-S and LyE-L); max Floquet multipliers (FM). A dynamic subject-specific EMG-assisted musculoskeletal model was used to quantify four structural stability measures: critical muscle stiffness gain at which spine becomes unstable (q-critical); average spine stiffness (k-spine); minimum and geometric average of Hessian matrix eigenvalues (λ-min and λ-avg).

Dynamical and structural stability outcomes had different trends (Figure 1), LyE-S and all structural stability measures were more impacted by the percentage of cycle (posture factor) than phase (lifting, lowering) or load factors. The effect of all factors were non-significant for FM and LyE-L, except for the posture on LyE-L with a medium effect size (Table 1). Pearson's correlations revealed that dynamical and structural stability measures are generally not correlated ($r \leq .35$, $P > .05$). A few correlations (13 out of 120) reached statistical significance, the highest reaching a moderate magnitude at best (e.g., LyE-S vs q-critical; $r = -0.52$, $P < .001$).

Structural and dynamic stability measures shared small common variance at best. In addition, low sensitivity of dynamic measures to posture and load factors and consideration of the diverse theoretical fundamentals highlight the distinct and independent nature/applicability of these metrics.

Stability outcomes	Metric	Main effects			Interactions			
		LD	PHS	PSR	LD × PHS	LD × PSR	PHS × PSR	LD × PHS × PSR
Lyapunov Exponent	LyE-S	.02 NS	.15 ✸	.21 ✸	.00 NS	.03 ★	.00 NS	.00 NS
	LyE-L	.00 NS	.00 NS	.09 ✸	.00 NS	.00 NS	.00 NS	.00 NS
Max Floquet Multipliers	FM	.01 NS	.01 NS	.00 NS	.00 NS	.00 NS	.00 NS	.01 NS
Structural analysis (EMG-Driven Model)	q-critical	.42 ✸	.00 NS	.88 ✸	.03 ✦	.41 ✸	.00 NS	.03 ✦
	k-spine	.08 ✸	.00 ✦	.77 ✸	.00 NS	.00 NS	.00 ✸	.00 NS
	λ-min	.08 ✸	.00 NS	.90 ✸	.01 ✦	.10 ✸	.00 NS	.01 ✦
	λ-avg	.00 NS	.00 NS	.88 ✸	.00 NS	.01 ★	.00 NS	.00 NS

LD: Load, PHS: Phase; PSR: Posture; Effect sizes of 0.02, 0.13 and 0.26 correspond to small, medium and large effects, respectively; ✦: $p < 0.05$, ★: $p < 0.01$, ✸: $p < 0.001$, NS: not significant

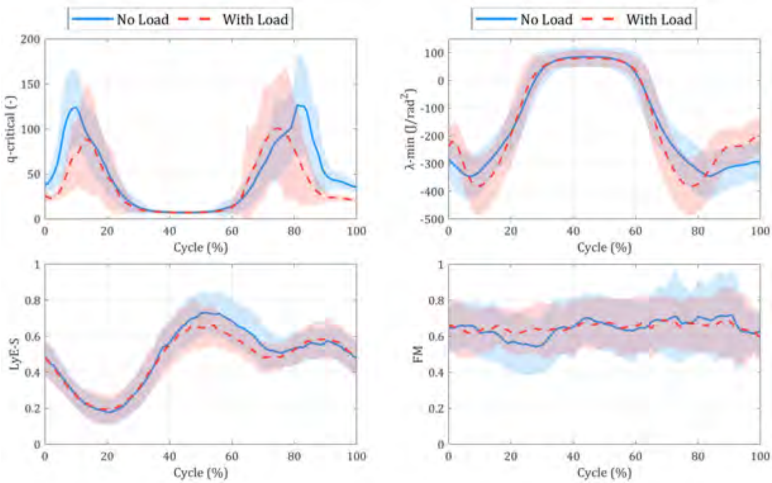

Table 1: Sensitivity of the stability outcomes (effect size and statistical significance) to the Load (with vs without), Phase (flexion vs extension) and Posture (up vs down) main factors and their interactions, as tested with 3-way ANOVAs

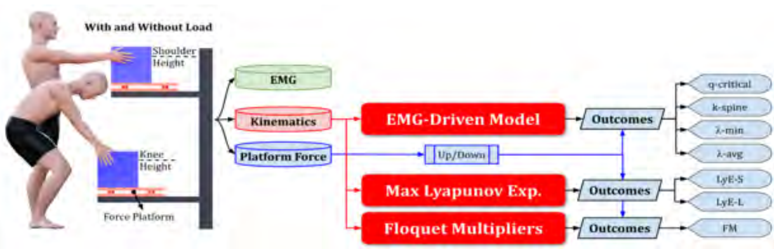

Figure 1: Dynamical and structural stability outcomes at different lifting cycle and loading conditions.

Low-back pain and associated anxiety may increase the gain but reduce the precision of feedback in control of trunk posture and movement.

van Dieën JH, Kistemaker DA

Department of Human Movement Sciences, Vrije Universiteit Amsterdam, Amsterdam, Netherlands

Literature reports paradoxical findings regarding effects of low-back pain (LBP) on trunk motor control. Compared to healthy individuals, patients with LBP, and especially those with high pain-related anxiety, showed stronger trunk extensor reflexes and more resistance against perturbations. On the other hand, LBP patients and especially those with high anxiety showed decreased precision in unperturbed trunk movement and posture. These paradoxical effects might be explained by the finding that arousal, which can be expected to be increased in patients, and especially in the more anxious patients, causes concomitant increases in the average and variance of muscle spindle firing rates. Increased mean and variance of spindle firing rates may both reflect higher reflex gains and would decrease admittance but also decrease precision. We performed a simulation study to test this hypothesis.

We modeled the trunk as a 2D inverted pendulum, stabilized by two antagonistic muscles based on their intrinsic stiffness and damping dependent on constant open-loop muscle activation and through 25ms-delayed velocity feedback. We assessed the effect of velocity feedback gains on precision of trunk orientation in unperturbed and perturbed conditions. We assumed a constant variance in spindle input. Perturbations consisted of low-pass filtered white-noise moment time series.

At low perturbation magnitudes, increasing reflex gains caused a monotonous increase in the variance of spindle afference and of trunk orientation. At larger perturbation magnitudes, increasing reflex gains caused a monotonous decrease in the variance of trunk orientation (Figure 1).

Our results support the notion that LBP and related anxiety cause increased reflex gains, resulting in an increase in the average and variance of spindle afference and resulting in decreased admittance and increased motor noise. This can explain the paradoxical findings described above and suggests that ‘guarded movement’ may protect against perturbations with decreased precision as an adverse side-effect.

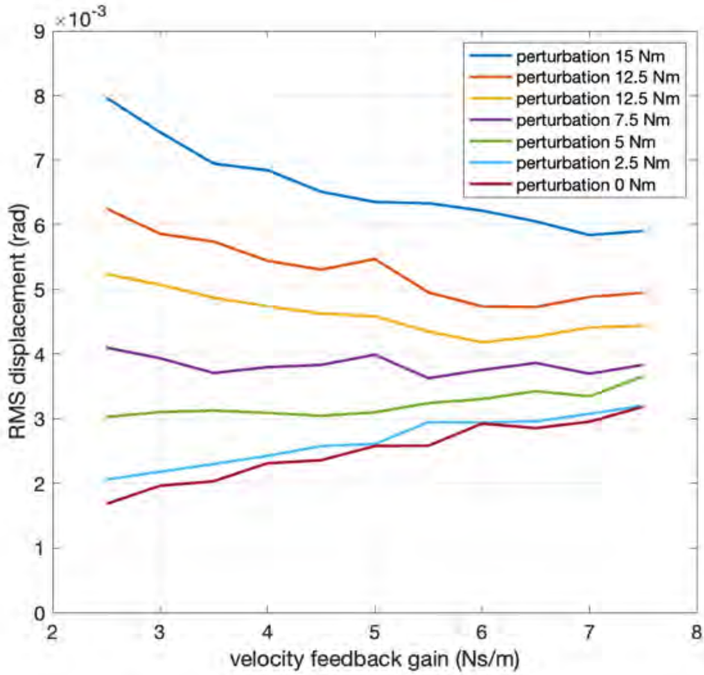

Figure 1: Variance in trunk orientation as a function of velocity feedback gain for different perturbation amplitudes.

Can intermittent changes in muscle length delay back muscle fatigue development?

Brouwer NP[a], Kingma I[a], van Dijk W[b], van Dieën JH[a]

[a]*Department of Human Movement Sciences, Vrije Universiteit Amsterdam, the Netherlands*
[b]*TNO, Leiden, the Netherlands*

Excessive cumulative low back load, for instance due to prolonged static bending [1], is an important risk factor for low back pain[2] and recurrent prolonged contractions may cause muscle and tendon damage[3]. The aim of this study was to evaluate whether changes in back muscle length (i.e. lumbar flexion) during prolonged bending can delay muscle fatigue development. These changes might induce changes in local muscle loading through, for instance, alternating activity between back muscles [4,5].

Nine healthy male participants (no history of low-back pain) completed three trials until exhaustion in 30 degrees trunk inclination in three separate sessions (>7 days between sessions). The lumbar flexion was either: (1) fixed at a self-selected angle; (2) continuously self-selected; or (3) intermittently (every 2 minutes) changed ±5 degrees around a fixed self-selected angle. The order of conditions was counterbalanced. Real-time trunk and pelvis angle feedback was provided using inertial measurement units. Single differential high-density (three 8x8 electrode grids) and conventional surface electromyography (EMG) was measured on the right and left sides of the spine, respectively.

Repeated measures ANOVA revealed a significant effect of condition on endurance time ($F(2,16)=3.983$, $p=0.041$; fig. 1). However, post-hoc pairwise comparisons (Bonferroni corrected) did not reveal significant differences (1-2: $p=1$; 1-3: $p=0.188$; 2-3: $p=0.071$). No significant effect of condition on the linear rate of change in average high-density and conventional EMG-based median frequency was found ($p=0.531$, $p=0.058$, $p=0.209$, $p=0.514$ for high-density EMG and the 3 conventional EMG sites, respectively; fig. 1).

Endurance time results may suggest that muscle fatigue development was delayed due to intermittent back muscle length changes, only when these changes were imposed. The application of such a strategy on the work floor would require real-time postural feedback which could be implemented using wearable sensors or an exoskeleton. However, no support for these findings was found in changes in high-density or conventional EMG spectral content. This could be explained by (1) differences in between-session EMG placement6, (2) cross-talk of the latissimus dorsi and trapezius muscles, or (3) the small sample size.

[1] Hoogendoorn et al. (2000) Spine (Phila Pa 1976);
[2] Coenen et al. (2013) J Occup Rehabil;
[3] Sjøgaard et al. (2000) Eur J Appl Physiol;
[4] van Dieën et al. (1993) Eur J Appl Physiol;
[5] Tucker et al. (2009) J Electromyogr Kinesiol;
[6] Farina et al. (2003) J Electromyogr Kinesiol

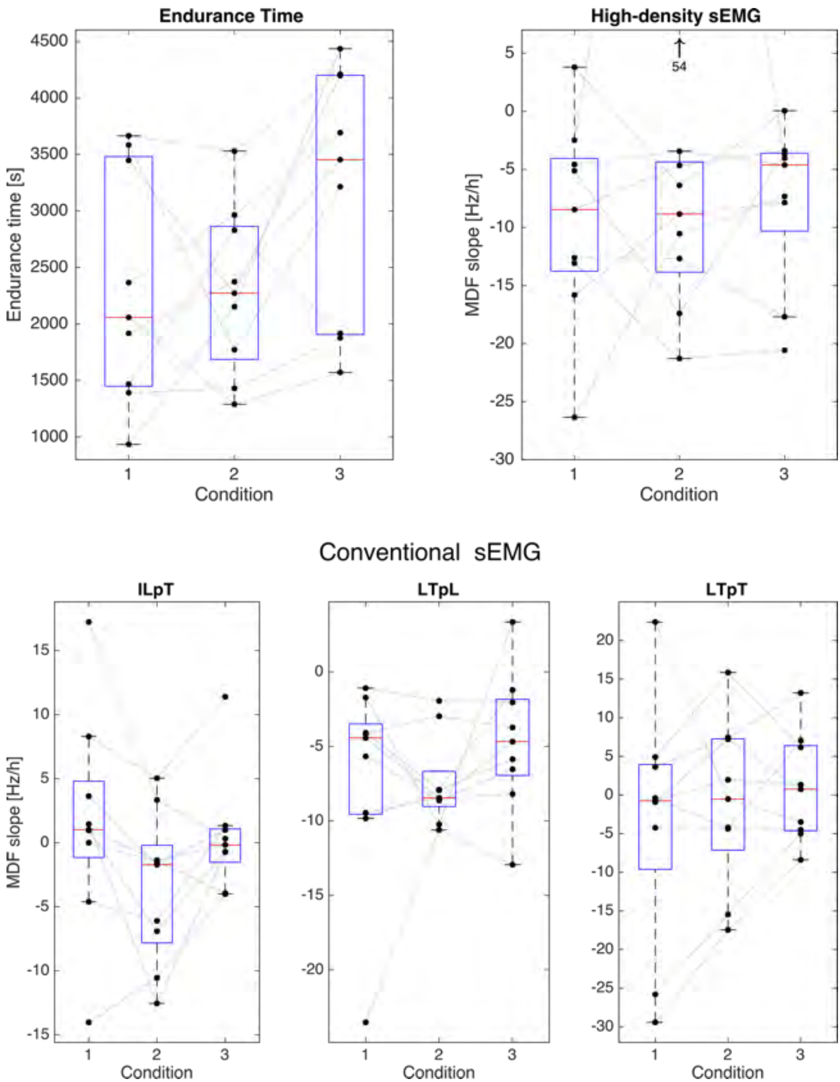

Figure 1: Boxplots of endurance time, linear rate of change in high-density EMG-based median frequency (averaged over 3 8x8 electrode grids) and linear rate of change in conventional EMG-based median frequency obtained over the iliocostalis lumborum pars thoracis (ILpT), longissimus thoracis pars lumborum (LTpL), and longissimus thoracis pars thoracis (LTpT). Individual data points, median, and interquartile range are depicted with black data points, red line, and blue box, respectively. Data points corresponding to each participant are connected by gray lines. Over conditions the lumbar flexion angle was either: (1) fixed at a self-selected angle; (2) continuously self-selected; or (3) intermittently (every 2 minutes) changed ±5 degrees around the self-selected angle.

Can multi-body spine models predict muscle antagonism? A methodological and validation study

Caimi A, Ferguson SJ, Ignasiak D

Institute for Biomechanics, ETH Zurich, Zurich, Switzerland

Musculoskeletal simulations based on optimization methods aim to minimize muscle effort in the system and are therefore considered unable to predict co-contraction. However, under certain conditions [1,2,3], antagonist muscles activity is theoretically expected as a result of satisfying the muscle recruitment objective function. Considering the lack of available comprehensive analysis, the problem of co-contraction simulation remains poorly understood. Therefore, the aims of this study were to demonstrate the influence of individual factors enabling and modulating predicted antagonism and to validate these predictions.

To demonstrate under which conditions inverse-dynamics models can predict muscle antagonism, simple models (2 or 3 rigid bodies) were created to study the problem in 2D vs. 3D, using simple vs. multi-joint muscles. The AnyBody lumbar spine model [4] was used to investigate the effects of modeling intra-abdominal pressure (IAP), linear/cubic and load-/activity-based muscle recruitment criterion on predicted antagonism during several simulated tasks (Table1). The predicted antagonist activations and coactivation were compared to EMG measurements reported in literature.

Using simple models, antagonism was predicted when multi-joint muscles were present (unless symmetrical) or the model was three-dimensional. No antagonism was predicted by a planar model with single-joint muscles only. During simulated forward flexion task, the coactivation was underpredicted for upright and 15° flexed posture, and slightly overpredicted for larger degrees of flexion. Predicted antagonism was mildly influenced by IAP and reduced with a force-based recruitment criterion (Fig.1).

The analysis of simplified models highlighted the conditions needed in multi-body models to predict antagonism: three-dimensionality or multi-joint muscles. The predicted antagonist activations are required to balance 3D moments but do not reflect other physiological phenomena, thus potentially explaining the observed discrepancies between model predictions and experimental data. Nevertheless, the findings suggest overall validity in predicting trunk muscle antagonism and advance the understanding of this methodology for future clinical and ergonomic research.

[1] Herzog and Binding, Math. Biosciences, 111(2), 1992
[2] Jinha et al., Math. Biosciences, 202, 2006.
[3] Stokes and Gardner-Morse, 28(2), 1995.
[4] de Zee et al., J Biomech, 40(6), 2007.

Upright standing	Forward flexion 60°	Lateral bending 30°	Axial rotation 45°

Table 1: Illustrations of the simulated posture and dynamic tasks.

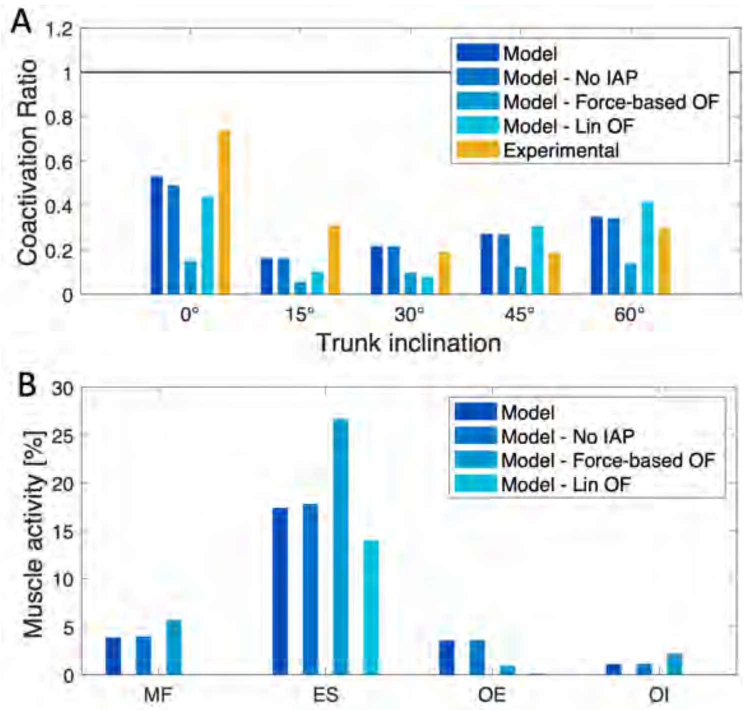

Figure 1: (A) Predicted coactivation ratios (abdominal muscles activity/extensor muscles activity) for various forward flexed positions using cubic activity-based objective function (Model), quadratic force-based objective function (Force-based OF), linear activity-based objective function (Lin OF) and excluding IAP (No IAP). (B) Predicted muscle activation patterns at 30° of trunk forward inclination to gain a more comprehensive understanding of the origin of coactivation levels under various conditions. Muscles: MF – Multifidus, ES – Erector Spinae, OE – Obliquus Externus, OI – Obliquus Internus.

The assessment of paraspinal muscle epimuscular fat in participants with and without low back pain: A case-control study

Rosenstein B[a], Burdick J[a], Roussac A[a], Rye M[a], Naghdi N[a], Valentin S[b], Licka T[c,d], Sean M[e], Tétreault P[e], Elliott J[f], Fortin M[a]

[a]*Department of Health, Kinesiology and Applied Physiology, Concordia University, Montreal, Canada*
[b]*Institute for Clinical Exercise and Health Science, University of the West of Scotland, Glasgow, UK*
[c]*Department of Companion Animals and Horses, University of Veterinary Medicine Vienna, Vienna, Austria*
[d]*Royal (Dick) School of Veterinary Studies, University of Edinburgh, Edinburgh, UK*
[e]*Centre de Recherche du Centre Hospitalier Universitaire de Sherbrooke (CHUS), Department of Anesthesiology, Université de Sherbrooke, Sherbrooke, Canada*
[f]*University of Sydney, School of Heath Science, Department of Medicine and Health, Sydney, Australia*

Measures obtained from conventional radiologic imaging of the lower back are poor predictors of LBP severity and future outcomes but paraspinal muscle characteristics are seldomly explored. This project compared 1) epimuscular fat in participants with and without chronic LBP, and 2) examined whether epimuscular fat is associated with spinal levels, BMI, age, sex and LBP status, duration or severity.

Fat and water lumbosacral MRIs of 50 participants with chronic LBP and 41 controls were used. The presence and extent of epimuscular fat for the paraspinal muscle group (erector spinae and multifidus) from L1-L5 to L5-S1 was assessed using a qualitative score (0-5 scale; 0=no epimuscular fat and 5=epimuscular fat present along the entire muscle) (Fig. 1) and quantitative manual segmentation method. Chi-squared tests evaluated associations between qualitative epimuscular fat and LBP status at each lumbar level. Spearman's correlation assessed relationships between quantitative and qualitative epimuscular fat with participants' characteristics.

Epimuscular fat was more frequent at the L4-L5 ($X2=13.78$, $p=0.017$) and L5-S1 level ($X2=27.82$, $p<0.001$) in participants with LBP as compared to controls (Fig. 2). The total qualitative score (combined from all levels) showed a significant positive correlation with BMI, age, sex (female) and the presence of LBP ($r=0.23-0.55$; $p<0.05$). Similarly, the total area of epimuscular fat (quantitative measure) was significantly correlated with BMI, age and LBP ($r=0.26-0.55$; $p<0.05$). No correlations were found between epimuscular fat and LBP duration or severity.

This is the first study to compare the presence and extent of epimuscular fat in participants with and without LBP. Both our qualitative and quantitative assessments revealed that epimuscular fat is more common in subjects with chronic LBP and associated with age and BMI. Given our findings, the functional and biological implications of epimuscular fat should be further explored and compared to intrafascicular fatty infiltration.

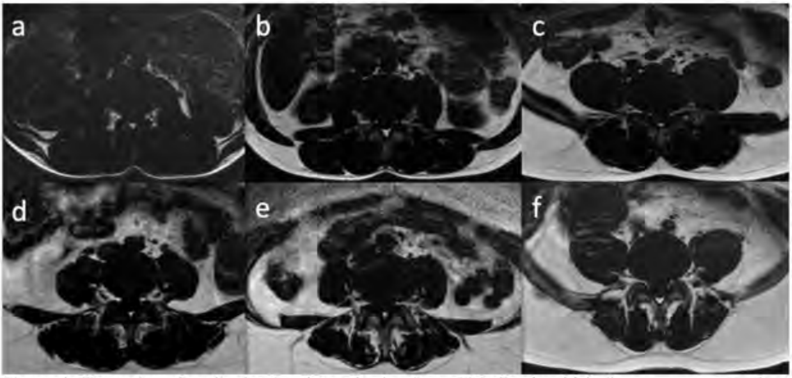

Figure 1. Illustration of qualitative 5-point scale. A rating of 0 indicating (a) indicate no presence of epimuscular fat; for every 25% increase in epimuscular fat along the posterior border of the erector spinae, an additional point was given; (b) qualitative rating of 1, (c) qualitative rating of 2, (d) qualitative rating of 3, and (e) qualitative rating of 4. A score of 5 (f) was given when epimuscular fat was present along the entire posterior border of *both* the erector spinal and multifidus muscle.

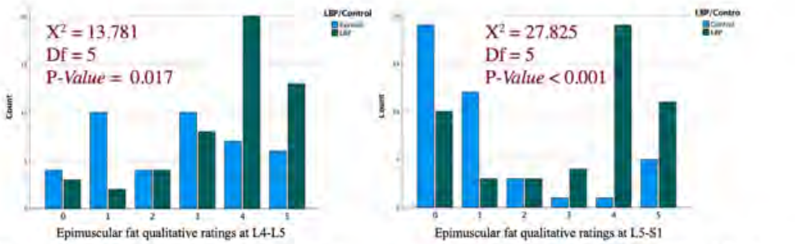

Figure 2. Bar graphs demonstrating the qualitative rating scores (0-5) between controls and LBP at L4-L5 (*left image)* and L5-S1 (*right image*).

The Julius Wolff Institute is located at the Charité Campus Virchow-Klinikum.

Arriving by plane

Airport BER Berlin-Brandenburg: https://ber.berlin-airport.de/en.html
There are different trains from the airport into the city. Find the best way on https://www.vbb.de/fahrinfo/ or
https://ber.berlin-airport.de/en/orientation/getting-here/public-transport.html
and get a connection to S/U-terminal "Westhafen". From there walk 5 minutes across the Putlitzbrücke to the Föhrer Straße.

Arriving by train

Take the train to one of the DB stations - preferably "Zoologischer Garten". Change at "Zoologischer Garten" to the subway U9 (direction "Osloer Straße") and get off at "Amrumer Straße".

Alternatively, you can take from central station ("Hauptbahnhof") the bus 142 (direction "Leopoldplatz") and get off at "Amrumer Straße".

Arriving by car

From the freeway A 100 take the exit Seestraße. Ample parking is available in the public parking garage at Seestraße 4. The garage is always open and costs 1 € for every full/partial hour or maximum 10 € per calendar day. The first 29 minutes are free. Guests who stay at the Virchow-Gästehaus have free parking included here.
On the campus the first 59 minutes are free and every hour afterwards costs 2 €. Disabled parking is available on the campus on Mittelallee.

General Information

Registration
Registration for the workshop is required. Please contact Friedmar Graichen at:
ws2023@spine-biomechanics.com

Registration fee for participants without oral presentation is required
Participation in the workshop, coffee breaks, lunch breaks, happy hour and dinner

Payment and confirmation of payment
An invoice and confirmation of payment will be sent via electronic mail.

Workshop language
The workshop language is English.

WIFI access
Will be provided.

General Guidelines for Authors and Poster Presenters

Submitting your presentation / technical information
Please prepare your presentation in MS Office PowerPoint up to 16:10 aspect ratio. A presentation notebook with Acrobat PDF Reader and PowerPoint 2021 will be provided. The use of personal notebooks will not be accepted, it may interrupt the flow of the program in the lecture hall. A laser pointer will be available at the speaker's podium in the lecture hall. A technical supervisor will help you.

Speaker's preparation
Please hand in your presentation on USB flash drive to our technical staff available in the room where the talk is scheduled, no later than 90 minutes before the beginning of the session. You may view and/or edit your presentation before.

Poster presentation
Panels of 123 cm height and 198 cm width will be available at the foyer for posters. Optimal poster size would be 120 cm height by 85 cm width (A0 portrait) for mounting two posters side by side on one panel. A poster should be self-contained and self-explanatory. Presentations should be kept simple and clearly visible from about 2 meters away with a balanced mix of text and graphics. Posters have to be installed at Thursday, July 6th.
We scheduled the poster session to Friday, July 7th, 10:30-11:30 am.
Presenters are prepared for discussions in front of their posters.

Virchow Guesthouse Charité
Seestraße 4-5, 13353 Berlin, Germany
Phone: +49 30 450 578 062
E-Mail: gaestehaus@charite.de
https://gaestehaus.charite.de

Hotel Axel Springer
Föhrer Straße 14, 13353 Berlin, Germany
Phone: +49 30 450 060
E-Mail: hotel-axel-springer@dhzb.de
https://www.dhzb.de

Mercure Hotel MOA Berlin
Stephanstraße 41,
10559 Berlin,
Germany
Phone: +49 30 3940430
Fax: +49 30 394043997
https://www.accorhotels.com/gb/hotel-A0F7-mercure-hotel-moa-berlin/index.shtml

Supported by

We would like to thank everybody who helped us to make this **4th International Workshop on Spine Loading and Deformation** happen.

Our special thanks to our supporters:

DFG
SCHM 2572/14-1

Deutsche Arthrose-Hilfe e.V.
DAH

JULIUS WOLFF INSTITUT

BIH
Berlin Institute of Health
@Charité

OrtholoadClub
Science for Orthopedics

CHARITÉ
UNIVERSITÄTSMEDIZIN BERLIN

Charité
Verein der Freunde und Förderer der Berliner Charite e.V.

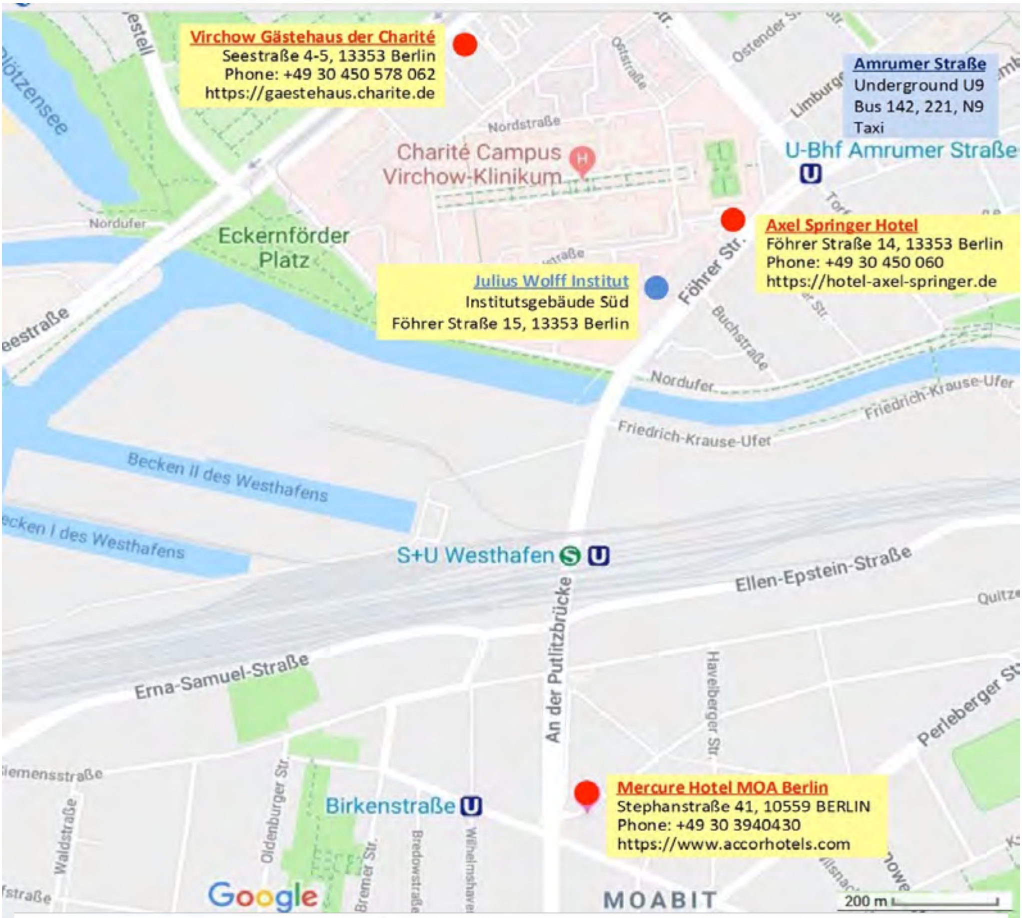

Virchow Gästehaus der Charité
Seestraße 4-5, 13353 Berlin
Phone: +49 30 450 578 062
https://gaestehaus.charite.de
Amrumer Straße
Underground U9
Bus 142, 221, N9
Taxi
U-Bhf Amrumer Straße
Charité Campus Virchow-Klinikum
Axel Springer Hotel
Föhrer Straße 14, 13353 Berlin
Phone: +49 30 450 060
https://hotel-axel-springer.de
Julius Wolff Institut
Institutsgebäude Süd
Föhrer Straße 15, 13353 Berlin
Eckernförder Platz
Nordufer
Nordstraße
Föhrer Str.
Buchstraße
Friedrich-Krause-Ufer
Becken II des Westhafens
Becken I des Westhafens
S+U Westhafen
Ellen-Epstein-Straße
An der Putlitzbrücke
Erna-Samuel-Straße
Havelberger Str.
Perleberger Str.
Birkenstraße
Oldenburger Str.
Waldstraße
Bremer Str.
Bredowstraße
Mercure Hotel MOA Berlin
Stephanstraße 41, 10559 BERLIN
Phone: +49 30 3940430
https://www.accorhotels.com
MOABIT
Google
200 m

Institutsgebäude Süd
Julius Wolff Institute
Ground Floor
1 Registration Desk
2 Lecture Hall
3 Poster Exhibition (Foyer)
4 Coffee Break, Lunch Break, Happy Hour
5 Checkroom
Campus Entrance: Südstraße 2
Street Entrance: Föhrer Straße 15
Föhrer Straße
U9 / Bus 142, 221, N9 [Amrumer Straße]